

Design Report

FEEG6013 Group Design Project

37

Point-of-Care Testing Device

Design of a cheap and accessible point-of-care testing device suitable for both domestic and hospital use.

Project Summary:

Pandemics are a challenge the world faces now and will face again in the future. The mutative characteristics of viruses make them difficult to treat and test for. Human impacts on ecosystems, our agricultural practices, and dense population centers further increase the probability of more viruses crossing species and causing outbreaks. In particular, respiratory viruses are inherently highly transmissible. Efficient and reliable testing for novel viruses is a prerequisite of the effective management of pandemics. Antibody and antigen testing takes time to establish for new viruses, whereas robust DNA analysis can be quickly established using PCR. The device in this project prototypes a safe and automated method for running PCR analysis of saliva samples, in a user-friendly package far smaller than laboratory machines that run equivalent start-to-finish analyses. Additional principles were to seek open instrumentation and alternatives to cleanroom manufacturing as well as minimizing cross-contamination.

Several sub-systems were iteratively designed. Fluid mixing within a complex structure was simulated with CFD and compared to the performance of high-resolution 3-D printed prototypes. The thermal performance of a thermocycler was modeled with COMSOL heat simulations and implemented with PID control. A compact fluorescence detection unit was fabricated and experimentally tested. 3D printed microfluidic chips were designed and tested to validate the components of the microfluidic system.

Interfacing of the sub-systems was modeled in CAD as a consolidated into a cartridge-in-box assembly. The project produced an innovative solution that condenses complex laboratory operations - sample preparation, droplet segmentation, thermocycling, and fluorescence detection- onto one platform.

Group Members:

ID Number	Name
29360714	Jameelah Salahuddin
29204488	Nixshal Nantakumar
28784936	Maria Stamatakis

ID Number	Name
29859565	Hadri Haris
29361249	Keivalin Saringkareekul

Primary Supervisor: Prof. Xize Niu

Co-Supervisors: Dr. Jonathan West

Submitted on: 06/05/2021

Contents

Acknowledgements	1
Introduction	1
Design Brief	2
Background	3
Nucleic acid extraction	4
Fluidics	9
Thermocycler	14
Fluorescence Detector	20
Final Design	26
User Process	27
System Flow Diagram	27
Project Review	27
Future Work	28
Conclusion	29
References	29

Acknowledgements

We would like to thank Prof Xize Niu and Dr Jonathan West for their guidance and continued support throughout the project. We would also like to extend our thanks to Andrew Westerman, Tasos Dimitriou, and Brett Warren for their help in setting up electronics and aiding in power consumption calculations for the thermocycler as well as Dr Simon Lane who helped prototype the micromixer. Liam Carter and Dr Bingyuan Lu are also thanked for their help with consultation of designs, obtaining supplies from the BioLab and 3D printing material for us.

Introduction

Constant global population growth along with the increased global traveling, globalization and highly densely populated cities result in a rise in human interactions [1]. Consequentially, viruses pose one of the greatest threats for the global disease control with the likelihood of pandemics increasing over the past century. Pandemics such as the most recent caused by the virus of SARS-CoV-2, also known as COVID-19, present significant issues for all countries due to their rapid rate of infection and limited world preparation [2].

Prior to analysing the effects of pandemics, it is important to understand how and why pandemics are caused. Scientific consensus is that respiratory viruses are a leading cause of diseases and causing major epidemics and even pandemics [1-3]. They originate from animals and once humans are infected, they can range from asymptomatic to severe. They transfer through respiratory droplets produced by coughing or sneezing and can impact the health of everyone of all ages [4]. The risk of pandemic initiation is higher in densely populated cities due to the increased human contact and undetected spreading. These viruses have ribonucleic acid (RNA) as their genetic material which characterises them as highly transmittable hence the most dangerous group of pathogens [5]. RNA viruses are typically able to mutate at a more rapid rate in comparison to deoxyribonucleic acid (DNA) viruses, thus, they develop drug resistant abilities [6].

Table 1: The number of deaths from influenza and different coronaviruses highlighting the impact of RNA viruses throughout the years.

Virus	Number of infections	Number of deaths
1918 influenza pandemic [7], [8]	Estimated 500,000	Estimated 1,272,300
1968 influenza pandemic [9], [8]	Estimated 500,000	Estimated 86,000
1979-2001 influenza pandemic [10], [8]	Estimated 622,000	47,800
2009 influenza pandemic [11], [8]	Estimated 70,000	Estimated 7,500 - 44,100
2012 MERS-CoV [8]	Estimated 2,580	858
2019 SARS-CoV-2 [12]	153,187,889 (Ongoing)	~3,144,028 (Ongoing)

The effect of pandemics across world are multifaceted. In addition to the health impacts being disastrous (Table 1), the world economic growth along with the healthcare systems have suffered too. Healthcare system requires high human resource and staffing costs to confine the virus infections by tracing the contacts of the contaminated individuals and to isolate them. As the pandemic develops, new facilities are required to manage the infected cases. Therefore, not only new healthcare facilities are needed. Additional testing centres and laboratories are also required to contribute in the diagnosis, prognosis, disease staging and therapeutic drug monitoring [13]. In addition, the demand in equipment such as medical supplies, medications, and protective equipment increases drastically; consequentially, the healthcare costs rise during this time [2]. Furthermore, population management techniques such as lockdown and quarantining – which are necessary to minimise infection spread – inevitably cause economic impacts through closures of non-essential industries, companies, small businesses, and shops. Long-term economic consequences rise as small businesses fail to be supported [14].

Because of the recurrent nature of pandemics throughout history, there has been great progress made globally with regards to preparing and mitigating their impacts. The 2003 pandemic with the avian influenza respiratory virus – where the early cases were not reported on time – galvanised preparations for future pandemics. Hence, the World Health Assembly updated the International Health Regulations to ensure that all member states of the World Health Organisation met specific standards with regards to the detection, reporting, and responding to the pandemic. In addition, international donors started to invest in the improvement of the preparation for pandemics via refining standards and funding for building health capacity [2]. During the most recent pandemic (COVID-19), some countries, such as the UK, created testing kits available for public use resulting in higher testing rates, lower human interaction and gaining a better understanding of the spread of the virus. These testing kits are rapid antigen tests which can detect a high percentage of the symptomatic cases (on average 72%) but lacks in the identification of the asymptomatic (on average 58%) [15]. Despite the improvements that have already occurred throughout the years, pandemics are inevitable, can be sudden and not all countries can support themselves economically or have means of monitoring population infections [16, 17]. Hence, it is important to find a way to be better prepared across all geographic borders in the future.

A potential solution to minimise the effects and being better prepared for future pandemics is to use self-testing [17]. As mentioned, self-testing has been used across a few countries to monitor coronavirus. As a result, the laboratories can focus on their other responsibilities, alleviating workload. However, these self-tests are single - use to avoid cross contamination, resulting in a lot of waste. Also, not all countries can afford to supply their populations. Consequently, we posit that by creating an affordable testing device for households, the monitoring of the public will be more efficient. A device that can be adjusted to different respiratory viruses by altering the chemicals for analysis and that is reusable to some extent make it more adaptable for future use and sustainable.

Design Brief

Our design brief is to produce a prototype of a lab-in-a-box Polymerase Chain Reaction (PCR) microfluidic device that could potentially be delivered to households and care-homes as part of a rental system and enable domestic saliva testing for a respiratory virus. The selected RNA virus to analyse is COVID-19 however the system could be adaptable for future pandemics. The scope of analysis of the device was done for the DNA of COVID-19 alone.

Aims and Objectives

The aim of the project is to create a saliva point-of-care device that can be used by non-specialists for the purpose of reducing the workload of laboratories in the case of a pandemic. Notable objectives to meet the aim are:

- Study the available technologies in market to identify the most suitable route for the project.
- Design our technology of choice capable of sample collection, NA extraction and amplification using the PCR technique and fluorescence detection.
- Design a self-contained, integrated, light weight, small footprint system and low-cost device.
- Manufacture a prototype of the sub-system parts (nucleic-acid extraction and PCR and fluorescence detection).
- Predict and where appropriate evaluate the performance of each individual sub-system.
- Incorporate reusability to some extent (e.g. use of cartridge).

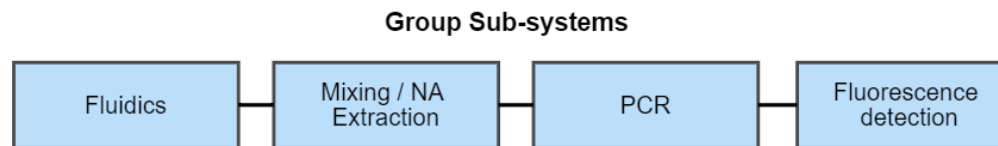


Figure 1: The sub-systems of the project.

Design Criteria

Table 2: Design criteria description

Item	Criteria	Description
A	COST	<ul style="list-style-type: none"> Affordable and accessible by almost every household.
B	EASE OF USE	<ul style="list-style-type: none"> The device requires a low number and complexity of steps to operate and does not require any specialist knowledge. Clarity and simplicity in communicating the results. Can conveniently obtain the sample of the user.
C	EASE OF MAINTENANCE	<ul style="list-style-type: none"> Low downtime.
D	EASE OF MANUFACTURE	<ul style="list-style-type: none"> Minimum number of manufacturing processes.
E	PORTABILITY	<ul style="list-style-type: none"> Lightweight, small in size and self-contained device.
F	RELIABILITY	<ul style="list-style-type: none"> Accuracy in testing and producing results.
G	REUSABILITY	<ul style="list-style-type: none"> The device is to be used by a variety of users, from clinicians to researchers to non-specialists. Minimum waste to prepare for future uses.
H	SAFETY	<ul style="list-style-type: none"> Minimum risk of spillage and cross-contamination between samples. Safe waste disposal system. Suitable for domestic electric supply.

Table 3: Binary weighting matrix used to rank the importance of the design criteria. The highest percentage represents the most important and the lowest the least important. The two most important design criteria are highlighted orange.

	A	B	C	D	E	F	G	H	Total score	Biased score	Normalised score
A	X	0	1	1	1	0	0	0	6	7	15.9%
B	1	X	1	1	1	0	1	0	10	11	25.0%
C	0	0	X	0	1	0	1	0	4	5	11.4%
D	0	0	1	X	1	0	1	0	6	7	15.9%
E	0	0	0	0	X	0	0	0	0	1	2.3%
F	1	1	1	1	1	X	1	0	12	13	29.5%
G	1	0	0	0	1	0	X	0	2	3	6.8%
H	1	1	1	1	1	1	1	X	7	8	18.2%

Based on Table 3, the foremost requirements for the project are ease of use and the reliability of the device. The latter due to university restrictions could not be evaluated. The device performance was assessed based on the sub-systems:

- Practical fluidics testing of chips and partial fit checking of prints relative to the selected tubing.
- Flow simulation for the nucleic acid purification and laboratory mixing test performed by Dr J. West.
- Thermal simulations to evaluate the design of the thermocycler and verification via computing and control application the thermal stability of the thermocycler was tested.
- Iterative design build and test of fluorescence detector setup to ensure repeatability, signal stability and setup which provides the best limit of detection.

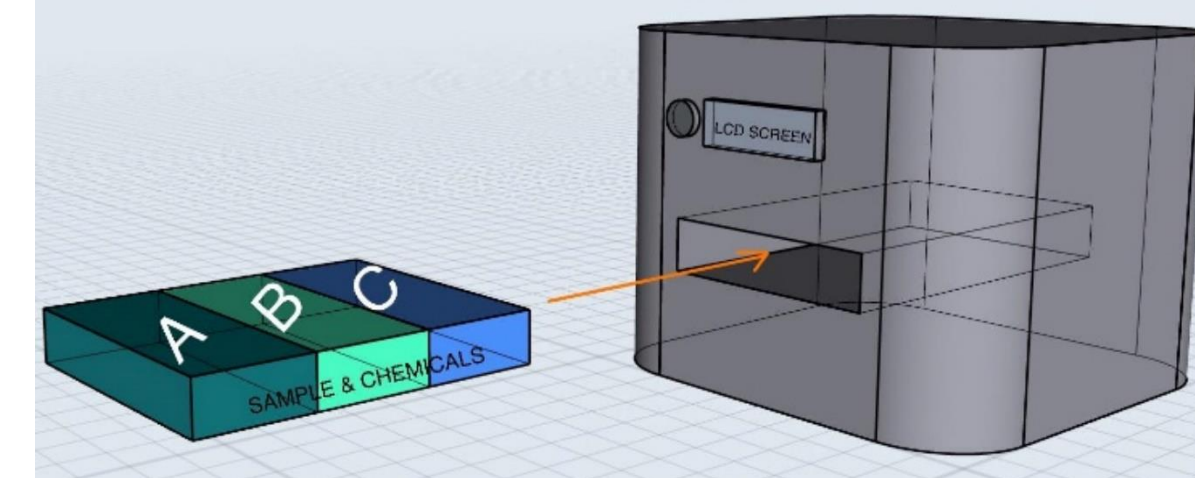


Figure 2: The cartridge with the sample and the chemicals carrying out (A) the purification of the sample, (B) the amplification of the genetic material and (C) the identification of the virus.

A simple representation of the concept of our device can be found above.

Chemical reagents such as master mix required for PCR are a significant cost factor, and sponsorship was secured with [PrimerDesign](#) (Part of the Novacyt Group) who generously contributed approximately £2000 worth of product to our GDP efforts.

Background

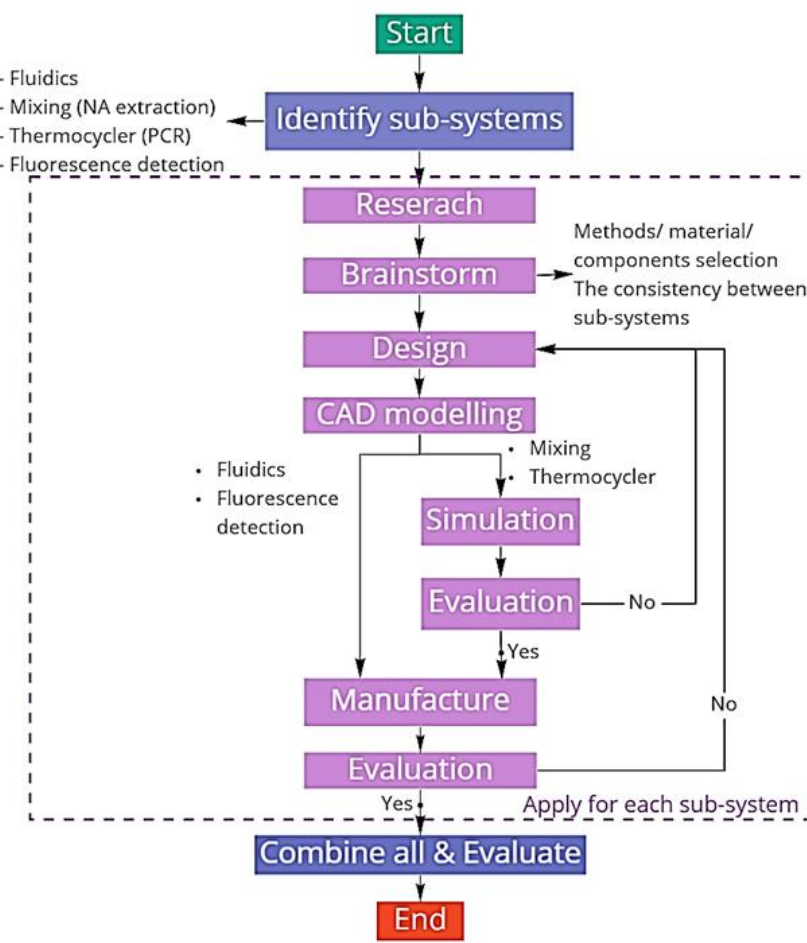


Figure 3: A general system flow diagram.

our design will be mainly incorporating the use of NA amplification methods in determining viral genetic material in a sample.

NA amplification is crucial process in biotechnology, bioengineering, and molecular biology and is a popular tool in various fields such as research and medicine. Advanced methods of amplification such as loop mediated isothermal amplification (LAMP) relies on auto-cycling strand displacement DNA synthesis which is conducted by an enzyme known as DNA polymerase with high strand displacement activity and a set of two inner and outer primers [19]. This is all achieved in an isothermal environment, making this process viable in most settings. Isothermal NA amplification is truly advantageous in cases where thermal cycling is incapable of being performed. Another type of isothermal amplification is rolling circle amplification (RCA) which enables the amplification of both solution and solid phase of a DNA sequence at a single temperature. In RCA, DNA polymerase extends a circle-hybridized primer by continuously progressing around the circular DNA probe of several dozen nucleotides to replicate its sequence over and over again [20]. Although these advanced isothermal NA amplification methods such as LAMP are truly advantageous, they do however still have their limitations. Sahoo et al. [21] describes LAMP as a technique that is unsuitable for cloning or other molecular biology applications due to the final product of LAMP being a large DNA chain. Hence, making LAMP less versatile than the more conventional PCR. The use of multiple primers can also increase the possibility of primer to primer hybridizations which could lead to template-free amplification causing false – positives results [22]. Therefore, LAMP specificity is inferior to that of PCR and positive results from LAMP require confirmation by PCR. Hence, even with these more modern procedures of amplification, polymerase chain reaction (PCR), the first NA amplification method developed, is still ever so popular in the field due to its extremely high specificity and sensitivity [20].

Design Process

The project was divided into four sections fluidics, NA extraction, PCR, and fluorescence detection. Each sub-system went through a process of creating a part of the device ready to be integrated with the rest. For the scope of the project, the integrated device was not manufactured due to the university restrictions.

Testing and Nucleic acid amplification

Diagnostic testing includes methods such as antigen testing and nucleic acid (NA) amplification tests (PCR). Although, quick and simple to conduct, antigen testing does have its limitations. The sensitivity of antigen testing was found to be inferior to that of PCR testing and has limited suitability for determining SARS-CoV-2 infection in patients and regardless of the high specificity of antigen tests, false positive results still occur [18]. NA approaches are much faster to develop for diagnostic applications and therefore,

PCR is performed in a three-step cycle:



Figure 4: The PCR process is shown in this flow chart. First denaturation is where a double stranded DNA template is heat treated at a high temperature to separate the two strands at 95°C, then annealing, where DNA primers bind to the template DNA at 55°C and lastly extension, where the DNA polymerase extends each primer along the template DNA at 72°C.

These three steps are then repeated in a cycle from anywhere between 25 to 35 cycles to amplify the DNA sample.

PCR quickly became the “gold standard” and benchmark in many aspects of diagnostic testing due to its high specificity and sensitivity. PCR is also rapid and can be performed within hours to even minutes depending on the case [23].

Therefore, PCR is widely used in diagnostic tests for detecting pathogens and viruses that causes infectious diseases such as Ebola, African swine fever, and the current SARS-CoV-2 (COVID-19) virus. PCR is also very versatile as advancements such as time RT-PCR, digital PCR, and qPCR are significantly faster and lowers the possibilities of contamination with less errors and remains the most real accurate method available for the detection of COVID-19 [24]. These advancements also increase the sensitivity and specificity issues that PCR faces when compared to methods such as LAMP.

Due to its wide range of advantages and acceptance in diagnostic testing, PCR will be the NA amplification method of choice for our point-of-care testing device. PCR requires a wide range of components from nucleic acid primers to enzymes. Therefore, a PCR master mix will be used as these solutions contain all the necessary chemicals crucial for NA amplification.

PID Controller of the Thermocycler

A PID controller is commonly used in any design/project that requires a specific variable to be controlled. This is done by forcing a feedback to match the desired setpoint. For example, a drone adjusting its horizontal tilt when disturbed to maintain a specific angle. The correction factor can be broken down into three terms/variables (proportional, integral, derivative) that are adjusted or tuned to ensure a functional a controller. Proportional tuning involves only on the difference/error between the set point and the process variable. The proportional term corrects the target set point proportional to this difference. Therefore, the set point is never achieved because as the error approaches zero, the correction factor also becomes zero. The integral tuning attempts to compensate this by summing the error term over time to increase the correction factor. However, the integral term tries to drive cumulative error to zero instead of stopping the feedback when the set point is reached. Therefore, this results in an overshoot. The derivative tuning tries to reduce said overshoot by slowing down the correction factor applied as the set point is approached. The correction factor, $u(t)$ can then be expressed in the Equation (1) below.

$$u(t) = K_p e(t) + K_i \int_0^t e(\tau) d\tau + K_d \frac{de(t)}{dt} \quad (1)$$

Where, K_p is proportional gain, K_i is integral gain, K_d is derivative gain, $e(t)$ is the error between the set point and process variable, t is the instantaneous time, and T is the integration variable (range from time 0 to present time)

Nucleic acid extraction

The DNA and RNA extraction is an important process to assess genetic information of the cells which is then used in biological and medical sciences especially on diseases or molecular diagnostics. In the process, DNA/RNA is isolated from the cells' nucleus by various method physically and/or chemically depending on the application, sources, scale and aimed yield of extracted DNA/RNA. The extraction method have been performed since 1869, yet the scope of extraction is still challenging and needs further development [25]. The main steps of isolation are cell lysis, binding, washing, and elution (Figure 5). In the cell lysis, the cell and its nucleus are broken to release DNA/RNA into a solution which can be done by physical, chemical, or enzymatic methods. The DNA/RNA sometimes binds into a matrix such as a silica membrane or magnetic beads. After that, the debris was washed out by using an ionic solution and alcohol in the precipitation step. The elution buffer then release the clean NA from the solid phase[25]. This process is important because it removes materials which inhibit other downstream analysis steps such as PCR. The mixing of fluid is important in this process so all the fluids can react evenly. It also enhance the reaction of sample and chemical.



Figure 5: The main steps of DNA/RNA extraction.

Design requirements

- Mix chemicals with sample at low Reynolds number and release DNA/RNA
- Ensure there is no leakage
- Can process automatically
- Use chemical resistance material
- Use minimum space
- Less/no contaminations

Current methods of DNA/RNA extraction

The isolation can be done by various techniques so the current NA extraction methods were considered and their advantages and disadvantages were compared [25, 26] (Table 4).

Magnetic Lysis flow (Initial design)

As a result, the magnetic beads were selected for an extraction method. Firstly, the unidirectional continuous flow was considered so there would be a chamber where a chemical reaction occurs with the use of a magnetic trap for keeping DNA/RNA on the beads inside the chamber while waste was flown out to the waste chamber and mixing magnet for mixing the DNA/RNA with chemicals. Another approach is using droplets, there would be only use of a magnetic trap as the droplets contain a small volume of liquid and the sample would mix with magnetic bead and cell lysis rapidly when the droplets were formed. The magnetic field traps a magnetic bead which DNA/RNA attached to its surface and a trend of chemicals would flow pass through it [27-29]. These two approaches require valves to control the flow of waste, magnetic beads after use and the extracted DNA/RNA to PCR section. Therefore the magnetic field, valves position and sensors to detect the flow are very important inside the device.

The droplets system was chosen over continuous flow as an initial design (Figure 22). The system required a smaller amount of chemicals and magnetic tweezers as well as less complexity of valve control system [30]. The channel inside would be rinsed after each test and magnetic beads would be a single use to minimise the complexity of channel and chemicals to rinse them.

The magnetic tweezers consist of two magnetic tips which made of 6-mm-diameter soft iron rod wrapped with a magnetic coil (IMPHU AFK 502) [27, 31]. They would be placed across fluid channel and faced each other. One side of each rod would be shaped similar to a sharp pencil. When the current passes through the magnetic coil, the electromagnetic field would generate and it can be controlled by the applied current. The possible applied currents are 0.23A [27-29]. The advantages of the electromagnetic field is the strength is adjustable and it can be disabled when it is not required by stopping the applied current through a coil.

As the design had been developed, the microfluidic chip and a cartridge idea had been introduced. Therefore, the design was changed so the device consists of main device which contains all electronics and a cartridge where all fluid and reaction occurs (Figure 22). As the magnetic tweezers were outside the fluid channel, the cartridge idea did not affect its location.

Table 4: DNA/RNA extraction methods with advantages and disadvantages.

Extraction techniques	Advantages	Disadvantages
Solution-based system	<ul style="list-style-type: none">• Gold standard• Compatible with either large or small scale• Rapidly denatured and stabilized• High purity and yield	<ul style="list-style-type: none">• May involve hazardous chemicals/waste• Laborious• Difficult to run automatically• May require a centrifuge
Spin columns	<ul style="list-style-type: none">• Fast• Reproducible• Provide a stationary phase and reliable buffer exchange• Some buffer solutions can be minimised	<ul style="list-style-type: none">• Require a centrifuge• Expensive and complex to set up a centrifuge• Difficulty to integrate with microfluidics• Add/remove buffer and waste several times• Purity depends on a pore size of filter and cell lysis
Beads/magnetic beads	<ul style="list-style-type: none">• Process can run automatically and high throughput• No filter involved so no clogging problems• Some type magnetic beads is reusable• Require less space• Compatible with droplets	<ul style="list-style-type: none">• May contain residual magnetic beads• Magnetic field may interrupt other parts within the device• Coating of (magnetic) beads can affect the binding between DNA/RNA and beads

Magnetic beads vs MicroLYSIS

Initial idea of our device was to use magnetic beads in the NA extraction. The process consists of many chemicals to extract and purify DNA/RNA from the sources, e.g. saliva. Therefore the DNA will be purified, and DNA yield can be checked by spectrophotometer. This method involved with sequence of chemicals, magnetic tweezer and valves as the system had to hold the DNA, which is on magnetics bead, in place when the chemicals pass through it and this system need to handle with waste before entering thermocycler section for PCR. The DNA/RNA can be extracted from the cells with only the use of MicroLYSIS which means all main steps were combined into one step (apart from purification). The complexity of mechanic and electronic components of magnetic tweezer and valves as well as waste could be minimised. It should be noted that MicroLYSIS only isolate DNA, so DNA is not purified. The mixture of sample and MicroLYSIS need to be placed in the thermocycler according to the protocol so the thermocycler need to be expanded to accommodate this. The heat enables a specialised detergent within the MicroLYSIS to lyse the cells and capture the non-nucleic acid materials

MicroLYSIS flow

Because of the suggestion of a new chemical, MicroLYSIS, the NA extraction method can focus on the mixing and the cartridge and extraction method were changed. The protocol volume of sample and MicroLYSIS, of 5 and 20 μL then 2 and 18 μL , changed the droplets idea back to continuous flow. In order to minimize the complexity of the device, the passive mixing elements was considered for the cartridge [32]. The sample and MicroLYSIS would be mixed inside the micromixer channel to ensure that the desired mix will be achieved before entering the thermocycler. The possible channel from various studies were compared and the most suitable, Tesla structure was selected according to the Reynolds number, Peclet number and the transition point of interested structure (Table 5). As the mixture is needed to be placed in the thermocycler according to its protocol, the mixing was also enhanced by thermal energy. When the temperature increases, diffusion coefficients also increase therefore the diffusion rate increases. With the use of peristaltic pump, the velocity of 1 mm/s and 9 mm/s of the sample and MicroLYSIS was considered. Our design would use UT5 tube for connecting between each sub-system therefore the sample and MicroLYSIS flow with $Re = 0.5$ and 4.5 respectively.

Table 5: The micromixer of various studies with pros and cons

Channel		Description and comment	Channel		Description and comment
Zigzag channels		<ul style="list-style-type: none"> Li's study showed that the most efficient angle is 60° and transition point is at $Re = 15$. The design is suitable for the flow which Re below 0.5 or greater than 5 [33]. Mengeaud's study suggested the mixing efficiency of 81% could be achieve at $Pe = 2600$ when $0 < Re < 30$ then the mixing efficiency increased when $Re > 30$ [34]. 	Planar asymmetric split-and-recombine (P-SAR) micromixer		<ul style="list-style-type: none"> The mixing index decrease from approximately 0.3 when the Re increase from 0 to 10 provided the transition point at $Re = 10$.
Sinusoidal channels		<ul style="list-style-type: none"> The transition point is about $Re = 5$. The greater ratio of amplitude to wavelength, the better mixing. 	Staggered herringbone structures		<ul style="list-style-type: none"> Enhance chaotic flow at low Re ($0 < Re < 100$) [36] The mixing performance of 90% could be achieved with a suitable design and it increase with the groove width and the number of herringbone structures per mixing unit [37-39]
Square wave channel		<ul style="list-style-type: none"> The transition point is about $Re = 10$. At very low Re, the mixing index decrease from 0.4 to 0.09 in the range of $0 < Re < 10$. It have similar trend as zigzag channels and sinusoidal but the greater mixing performance can be achieve with the same Re [40]. 	Tesla structures		<ul style="list-style-type: none"> Yang's study showed that the 0.2 mm width between each unit provided the highest mixing index up to 97% before the transition point [41]. The transition point is at $Re = 2$ approximately [41] Suitable for $0 < Re < 100$ Coanda effect

CAD Model, simulation, and Final design

After the tesla structure was selected as a micromixer inside the cartridge, the available model was developed and change in dimensions to fit with our cartridge. With the different ratio, the two inlets were considered to have different size while keeping the flow rate constant so that only 1 pump would be used (Figure 6). The different size of inlet channel could increase the complexity of the pump bed and their small dimensions could also be a problem in the fabrication process. Therefore, the design was adjusted. There were two peristaltic pumps to pump sample and MicroLYSIS with different flow rate so the inlet channel size can be similar and the dimension of the two inlets would be similar to the UT5 tube (Figure 7). The CAD model was drawn in SolidWorks (SolidWorks 2020, Dassault Systèmes SOLIDWORKS Corp, USA). The simulation was conducted in SolidWorks as well however there is a limitation so COMSOL (COMSOL 5.5, was used to simulate with the transport of diluted species study. The velocity of 1 mm/s and 9 mm/s of the sample and MicroLYSIS was used according to the mixture ratio and the peristaltic pump limitation. The number of Tesla units were adjusted alongside the simulation until the mixing was achieved. The concentration of DNA/RNA was observed roughly by the 3 linear lines for each run before all slide plot of concentration would be further analysed (Figure 8). As a result, the design was finalised. There were 60 Tesla units which is approximately 60 mm in the total length with the dimension which is shown in Appendix L.

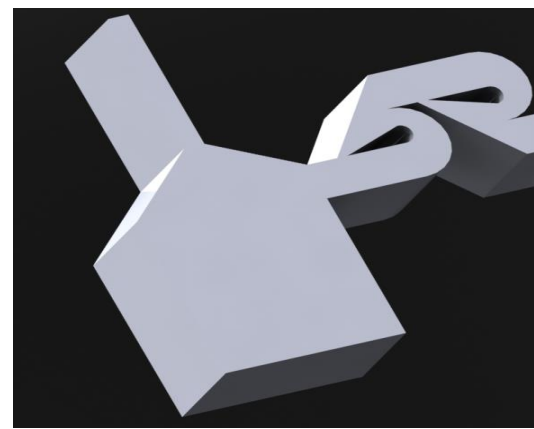


Figure 6: The modified Tesla model with different inlet sizes.

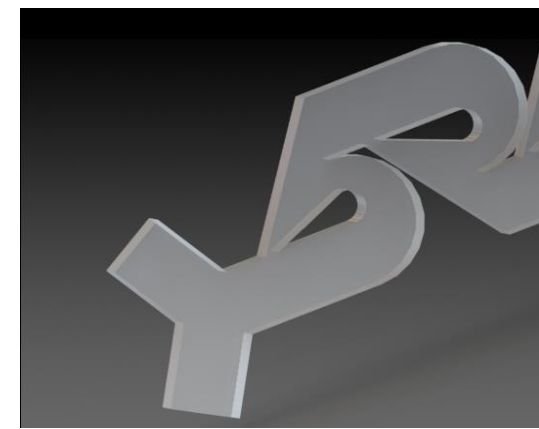


Figure 7: The modified Tesla model with same inlet size.

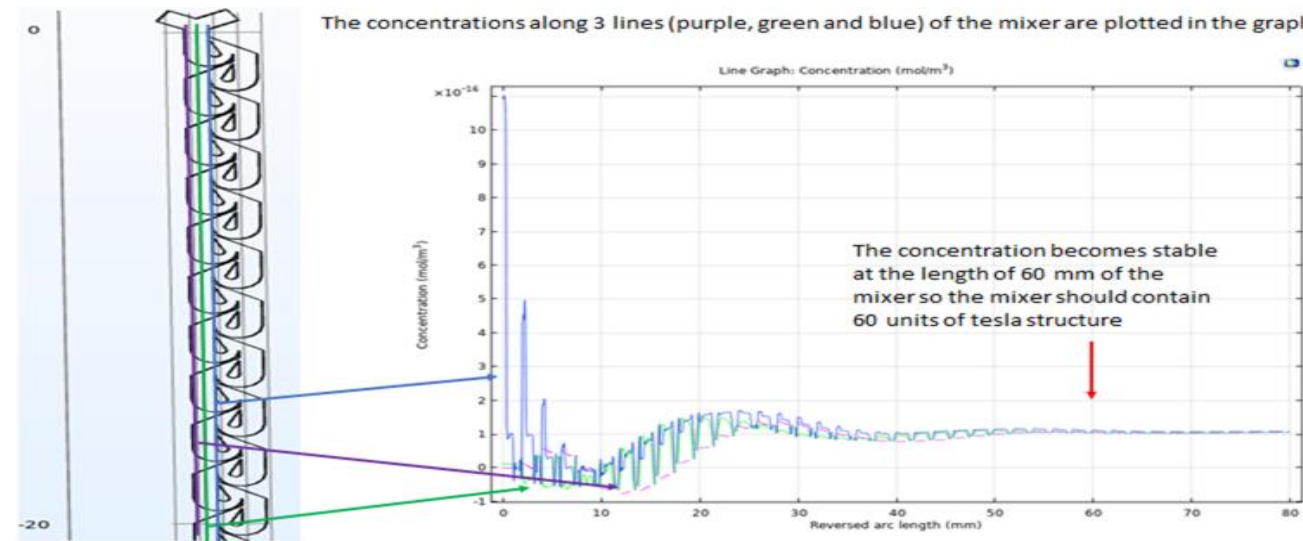


Figure 8: The plot of rough estimation of concentration along the micromixer channel.

Prototype fabrication

After simulations showed that the mixed fluid was achieved within the structure, the CAD model was 3D printed.

PVDF (Polyvinylidene fluoride)

The model was sent to Liam Carter, a Ph.D. student, for PVDF (Polyvinylidene fluoride) printing using Ultimaker 3 (Ultimaker B.V., Utrecht) with a layer resolution of 0.4 mm nozzle: 20 -200 micron [42]. The smallest gap between features of modified Tesla structure is 0.1 mm (100 micron). The Ultimaker 3 could not print the features inside the Tesla structure (Figure 9). The software had shown that there were no features presence in the ideal model, but the features were shown when the model was scaled up to 300% (Figure 10(b)). The dimension of CAD model was changed and simulated further. The larger the gap is, the less fluid being mixed within a unit of Tesla structure (Figure 11). The other materials were then considered for prototyping.



Figure 9: A printed test of the Tesla mixer to observe the small features.

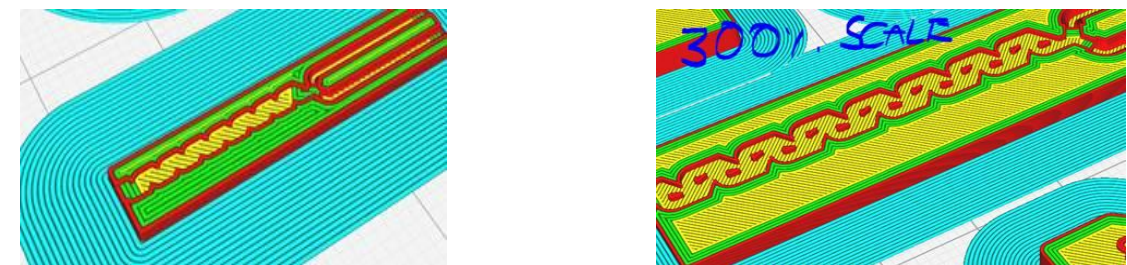


Figure 10: Pre-printed model shown in the Ultimaker printer software. (a) Ideal model (b) 300% scale up.

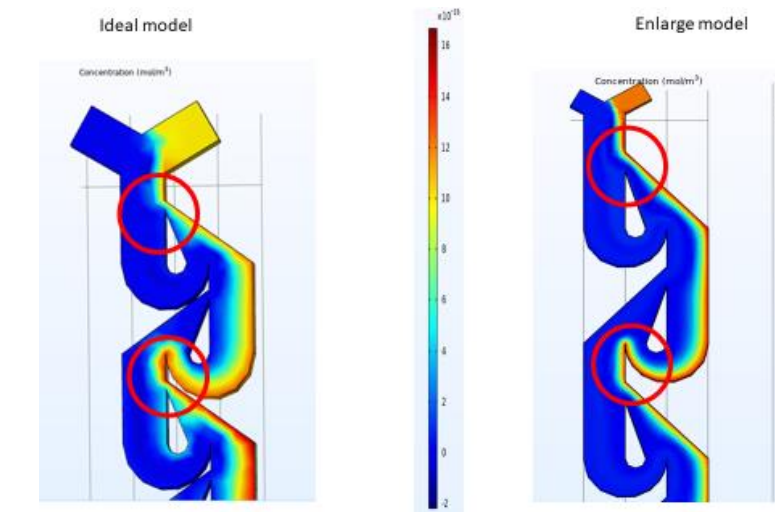


Figure 11: The comparison of simulation between the ideal model and enlarge model.

PDMS

The prototype of the ideal model could be manufactured from the 3D-printed mould and PDMS with the help from Dr West, our supervisor, and Dr Lane (Figure 12). The straight channel was also created. Firstly, the zortrax grey resin was used to print the mould with the post cure under 450 nm light for 15 minutes. 3D mould was thermal cured at 60 °C (e.g. 24 hours), plasma activated using an oxygen-enriched atmosphere at less than 1 mbar for 60 seconds (FEMTO, Diener electronic, Germany) and then submerged in a 1 mL of 1% (v/v) trichloro(1H,1H,2H,2H-perfluoroctyl)silane (Merck) in HFE-7500™ (3M™) at 60 °C for 2 minutes respectively. After that, a nitrogen stream, and 2 minutes bake at 60°C was used to remove solution and dry 3D mould as well as bake-off and residual HFE-7500 and silane.



Figure 12: The 3D-printed mould made of zortrax grey resin.

As the 3D mould was ready, PDMS was prepared from a mixture of pre-polymer and curing agent with the ratio of 10 to 1. PDMS was then degassed and poured over the mould and cured at 60 °C for 2 hours. Cured PDMS were removed from the mould and the inlet and outlet was punched to make holes using a 1-mm-diameter biopsy punch (Miltex). The channel was cleaned by Scotch® Magic™ Tape (3M™, 810) to remove PDMS particulates and any contaminating particulates or fibres. Then the PDMS microchannel was bonded to a glass microscope slide (1 x 75 x 25 mm) using oxygen-enriched plasma treatment for 30 seconds with manually press for 10 seconds. The bonding was also enhanced by a dehydration bake at 60 °C (e.g. 1 hour). By the end, the Tesla micromixer was ready to test. The channel, with 4x magnification, showed that the smooth and sharp edge could not be achieved and the roughness along the mixer wall was identified (Figure 16).

Structure validation

In the design of Tesla structure and simulation, the concentration of sample, DNA, was assumed to be 1×10^{-15} mol/m³. However, it is challenging to observe the mixture of fluid with very low concentration. Therefore, the practical mixing experiment was performed to observe the efficiency of the Tesla micromixer using higher concentration compare to the simulation. The solution of PBS and PBS with 10 μM, 1×10^{-2} mol/m³, FITC (fluorescein isothiocyanate) were used in practical test. FITC would emit light which can be detected so it is useful for further analysis, e.g. the intensity calculation from the image. They were prepared in 2.5 mL syringes (BD) which was connected by sterile polythene tube (ID 0.38; OD 1.09 mm, medical grade to syringe pump (Fusion 200, Chemyx). The fluids were driven into the channels, both straight and Tesla, by at the rates of 1 mm/s and 9 mm/s for PBS and PBS with FITC respectively. It should be noted that our device would use the peristaltic pump and the syringe pump was used for testing purpose only. Another mixing simulations were performed to compare assuming the concentration of sample was same as concentration of FITC. The mixing performance, η , was calculated and compared the results numerically [43]. The flow images from the experiment were recorded on an Olympic IX41 with 4x magnification.

The mixing performance, η , increase significantly for Tesla micromixer in both simulation and practical experiment and become roughly steady when the fluids were beyond the channel length of 20 mm (Figure 13 and Figure 14). The simulation predicted the fluid would be completely mixed, $\eta = 1$, yet the maximum mixing performance from the experiment was approximately 0.9 which is 10 % less than the expectation. A similar trend was also applied to the straight channel with a 10% difference in mixing performance.

Results and discussion

The mixing performance of the channel from the practical results

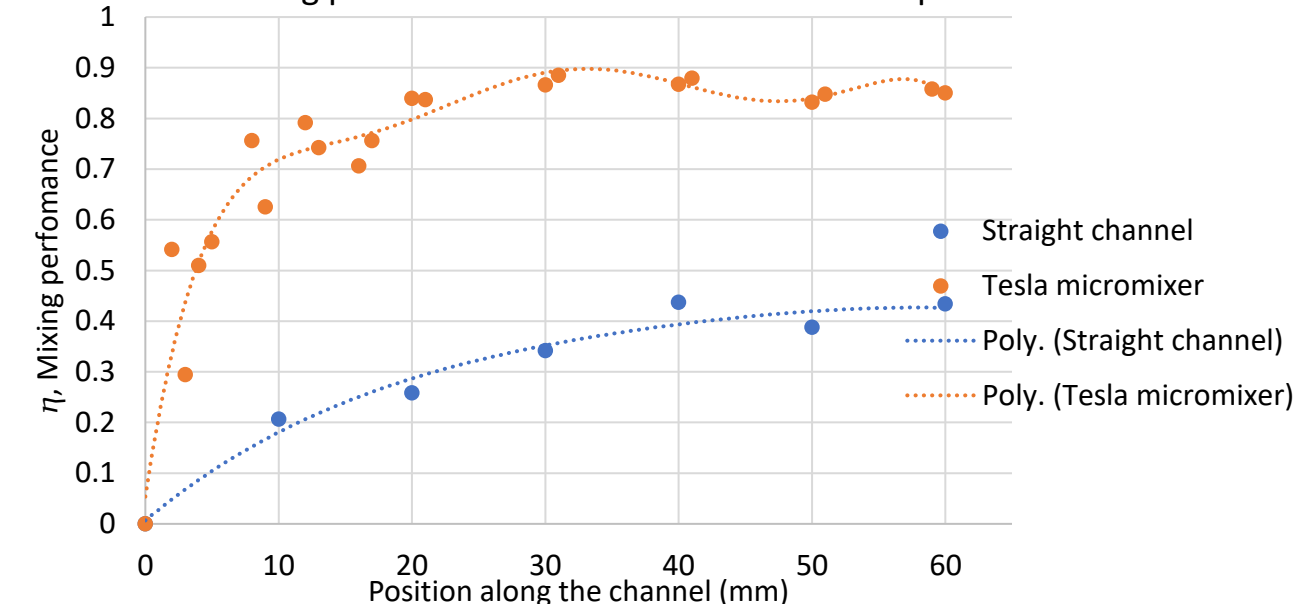


Figure 13: The comparison graph of the mixing performance between Tesla micromixer and the straight channel from the practical test.

The mixing performance of the channel from the simulation results

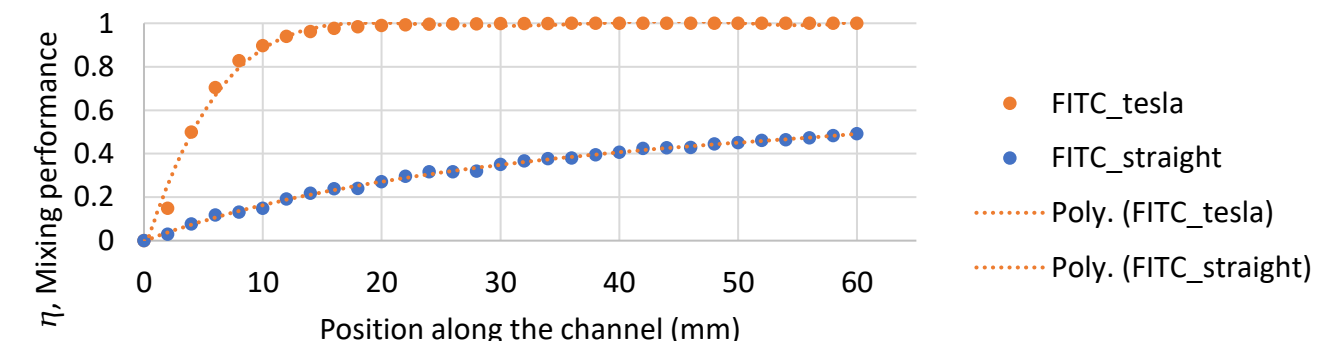


Figure 14: The comparison graph of the mixing performance between Tesla micromixer and the straight channel from the FITC simulation.

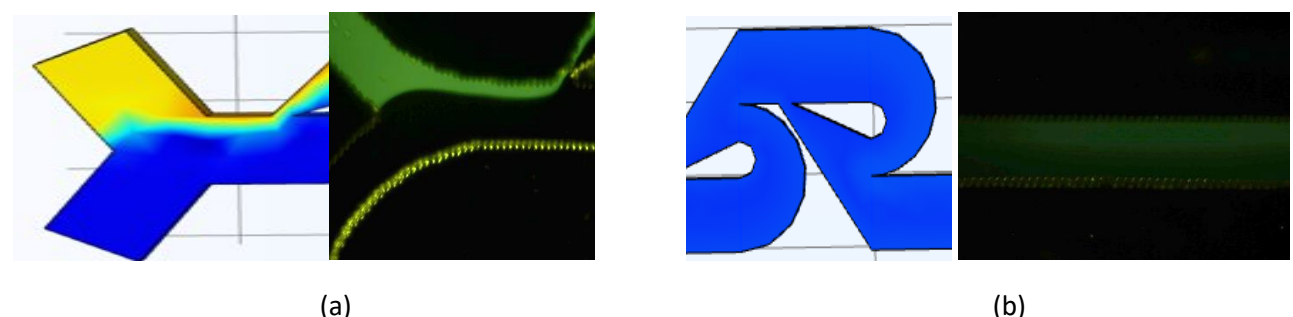


Figure 15: The comparison of mixing profile between simulation and practical test.
(a) Position = 0, (b) Position = 60 and outlet

As a result, it could be confirmed that the Tesla structure provides a better mixing at the same position compared to a straight channel in both scenarios, e.g. $\eta = 0.4$ from simulation compare to $\eta = 0.5$ from practical test at the exit of the straight channel and η is almost 1 from simulation compare to $\eta = 0.85$ from practical test at the exit of the micromixer.

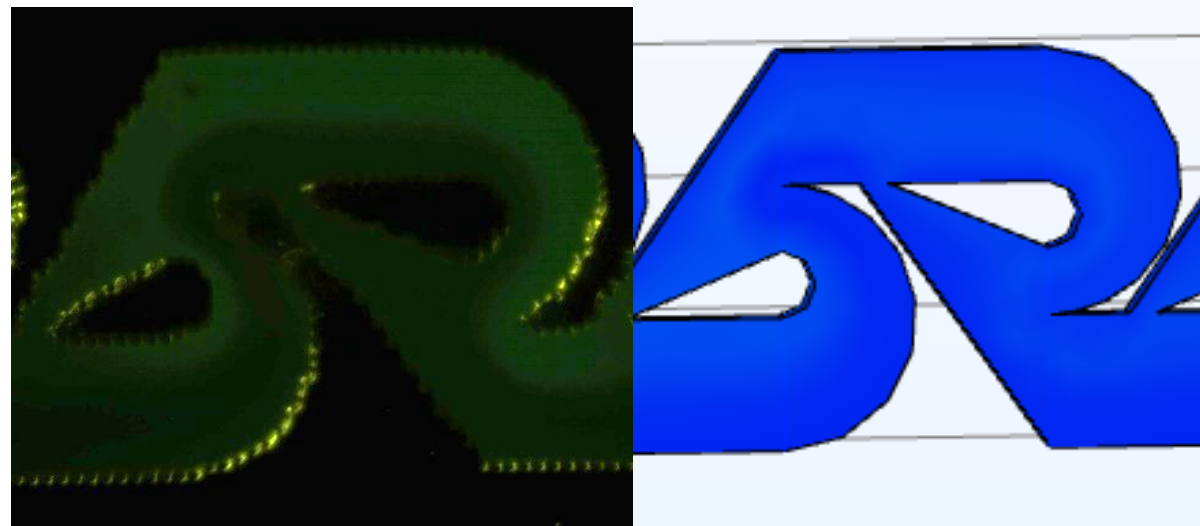


Figure 16: The comparison of the micromixer at position = 50mm.

Even though the mixing performance of the practical test was about 0.9 towards the outlet, the flow profile showed unevenly distributed FITC across the width of the channel (Figure 15(b) and Figure 16). The FITC intensity at the top edge was almost twice the bottom edge. This might be the results of the printed structure as the smooth and sharp edge could not be achieved so the gap of the internal Tesla unit was wider and more curve which affect the flow rate and the flow splitting and recombination when the fluid passes through the section (Figure 11) [41]. In addition, the roughness of the 3D printed mixer wall might not affect the flow at very low Re, e.g. $Re = 4.5$ and $Re = 0.5$ with $Pe = 1100$. The results also confirm that the use of PDMS with the 3D printed technique was sensible for prototyping to observe mixing and compare the mixing trend with the simulation [41, 43].

In reality, the sample and MicroLYSIS might need a longer channel of the Tesla structure, increase the Tesla unit, to achieve the efficient mixed fluid at lower concentration and different diffusion coefficient, e.g. $Pe = 10,000$, compared to the mixing trend from simulation and supported results from the use of FITC (Figure 13,14). More details on the flow simulation can be found in Keivalin's design journal. The diffusion coefficient of the sample, i.e. DNA at $Pe = 10,000$ and FITC at $Pe = 1100$, involves the mixing index thus the length of the micromixer. The mixing depends on the different velocity paths and is controlled by the residence time before the transition position then the transverse flows become a key controller of the mixture when it beyond the transition position [40] As the two flow of different Reynolds number were mixed, i.e. $Re = 0.5$ and $Re = 4.5$, the different velocity paths are important as it would be increase and decrease according to the path inside the Tesla structure. The simulation of 1:1 flow rate was performed to observe the velocity profile at different plane of the channel only (Figure 17). Mostly the Tesla structure are commonly used as a 3D passive micromixer [41, 43]. However, the results suggested that the planar structure of the Tesla units also provide a good mixing (Figure 13,14). In summary, the Tesla micromixer would be a suitable mixer in the cartridge system as it can mix the fluid within a short length and it does not require an active element to enhance the mixing which minimises the complexity of the cartridge and the overall device as well as the cost. PVDF would be used for the micromixer in the real device so the dimension of structure need to be scaled up according to the shrink rate of the materials and it require the higher resolution of the 3D printer than the Ultimaker 3.

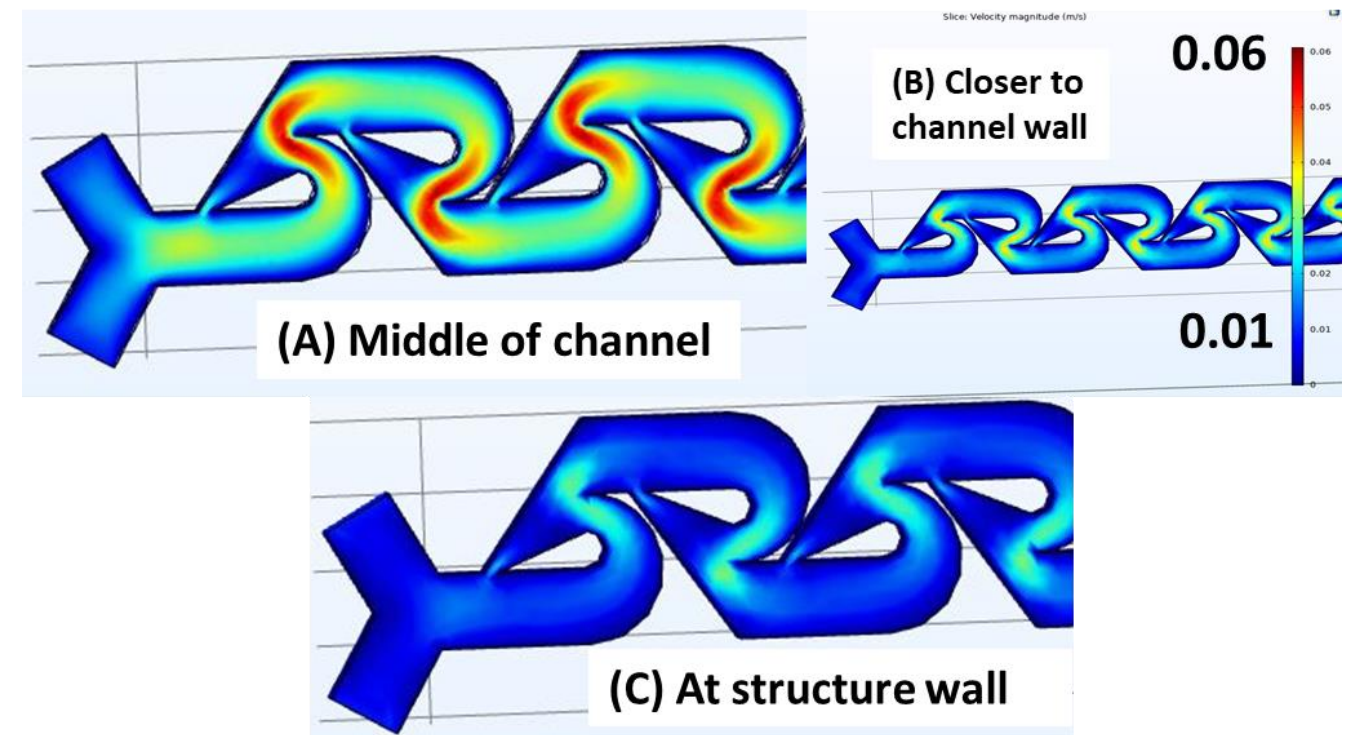


Figure 17: The comparison graph of the mixing performance between Tesla micromixer and the straight channel from the DNA and MicroLYSIS simulation.

Final design

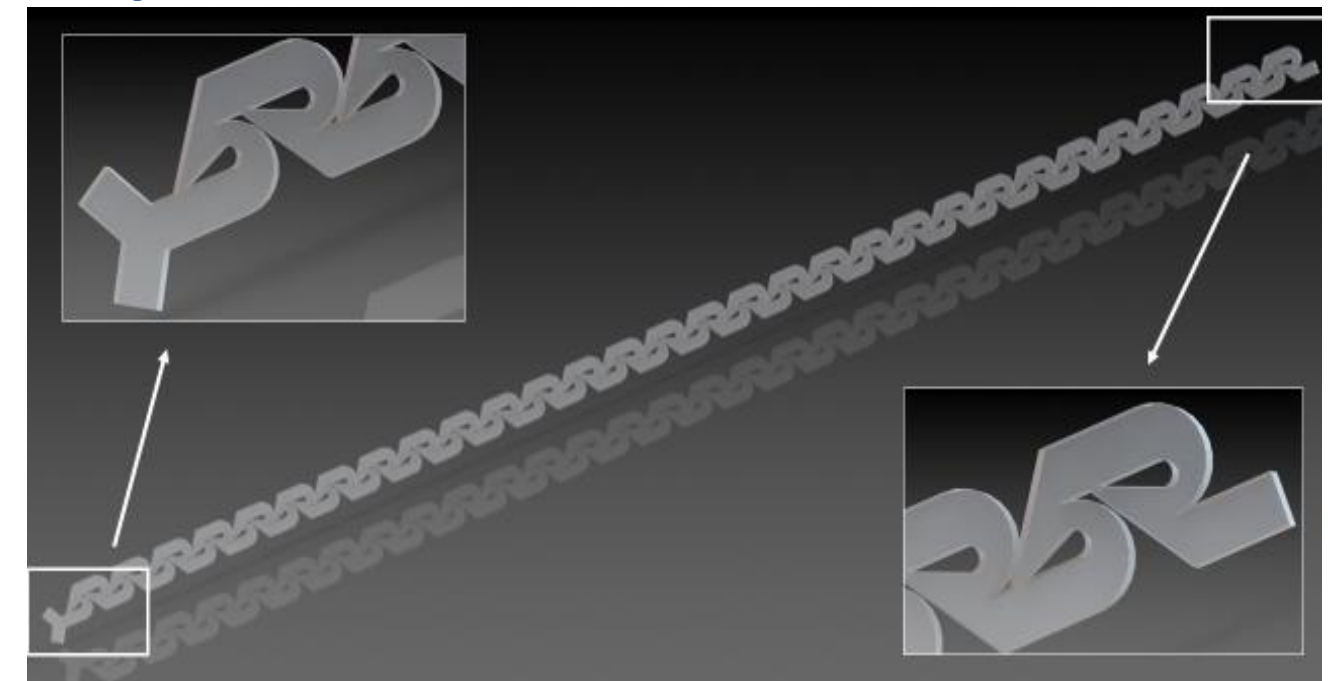


Figure 18: Micromixer design

- Number of Tesla units : 60+
- Fluid : Continuous flow of 1 mm/s and 9 mm/s for sample and MicroLYSIS respectively
- Materials : PVDF
- Manufacturing : 3D printing

Fluidics

The general fluid processing steps established at the start of the project held true for all iterations of the device. These steps are shown below:



Figure 19: Process steps

Microfluidics

Microfluidics is a powerful tool for extending the domain of healthcare and diagnostic devices beyond the laboratory. The strengths microfluidics which validate its use in our project include:

- Enhanced mixing within droplets which are discrete ‘microreactors’ and do not need additional stirring
- Minimal samples loss and Taylor dispersion
- Reduced fluid volumes
- Automation of fluid processing steps
- Smaller systems requiring less power and occupying a smaller footprint
- Portability
- Manufacturable by 3D printing

These characteristics can be exploited to conduct PCR outside the laboratory. Within the scope of this project the ability to 3D print components for the fluidic system was of particularly value as it facilitates rapid prototyping for minimal manufacturing complexity, contrary to the numerous processing steps for making standard microfluidic PDMS chips and other clean room manufacture processes [44].

An important system used as the base for the pumping system in this project came from Prof Niu’s research group and associated company ‘South West Sensor (SWS)’ (Figure 20). This system includes a hall effect sensor and magnets which allow the implementation of control based on rotational orientation reading of the roller.

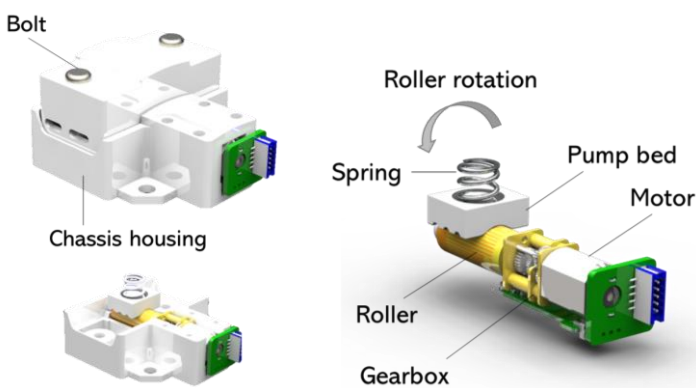


Figure 20: SWS pump components

This pump was used (unchanged) for our testing purposes and is the inherited design which was adapted for our final output. The peristaltic pump generates pulsatile flow by rotation of a roller head, driven by a motor. The grooves on the roller head ‘hardcode’ droplet length for robust generation. The efficacy of an earlier generation of this pump is validated in published works [45] which demonstrate the phased peristaltic pumps deliver “rapid on-demand droplet generation with minimal stabilisation times”.

The requirements of our microfluidic system were as follows:

- Processing with minimum user steps
- Safe and hygienic
- Minimum cross contamination risk
- Minimum power usage/parts
- Recyclable parts where possible
- Facilitate fluid mixing, thermocycling and detection

Magnetic Lysis flow

The first iterations of the fluid flow had 6 input fluids: saliva (from the user), magnetic beads (in solution), washes, elution buffer and PCR master mix. This fluid flow is hereon referred to as the magnetic lysis flow. The key challenges of the magnetic lysis flow were:

- How and where to extract the waste from the NA purification steps i.e., how to remove the supernatant and magnetic beads
- How to recycle the magnetic beads
- When and how to add the elution and master mix
- How to combine droplets chains from separate pumps and time their arrival

The following diagrams show the first 3 iterations for the NA purification steps, all of which use unidirectional pulsatile flow. NA Purification A.1 (Figure 21) would generate a series of consecutive droplets produced at a T-junctions with a separate oil line. These droplets would be driven to the magnetic trap by a pump separate to that which produced the droplet chain. The elution and the master mix would be combined at a Y junction before the droplet-generating T junctions. Similarly, the magnetic beads would be added to the saliva by uniting continuous streams at a Y junction. This design involved all fluid inputs being segmented into droplets at one stage, the main benefit of which is that all fluid stream mixing and segmentation would be contained on one pump, in one key junction and in one area of the device. A very significant challenge and drawback of this design achieving this would be the complexity of the roller features and adapting the grooves on the roller to produce the required ratios (even if both washes were included on a single band of the roller). In addition to the grooves being dimensioned to the correct ratios of fluids, the path length for all inputs would need to be carefully designed to ensure

that every fluid had reached the T junction in perfect succession; this would take considerable tuning. Using a 4-inlet junction point also raised question of viability. To achieve our goal of avoiding clean room conditions and relying mostly on open instrumentation, we had to circumvent the need for PDMS chips. There was not confidence in the capacity to fabricate a complex junction as in NA Purification A.1 (Figure 21) and B.1 (Figure 23) with tubing and a 3D printed connector, including also the potential need to manually cut tubing to precise lengths. These two designs marked the first realization of the NA purification with droplet form but were later enhanced and eventually dismissed when we departed from magnetic lysis flow.

NA PURIFICATION A.1

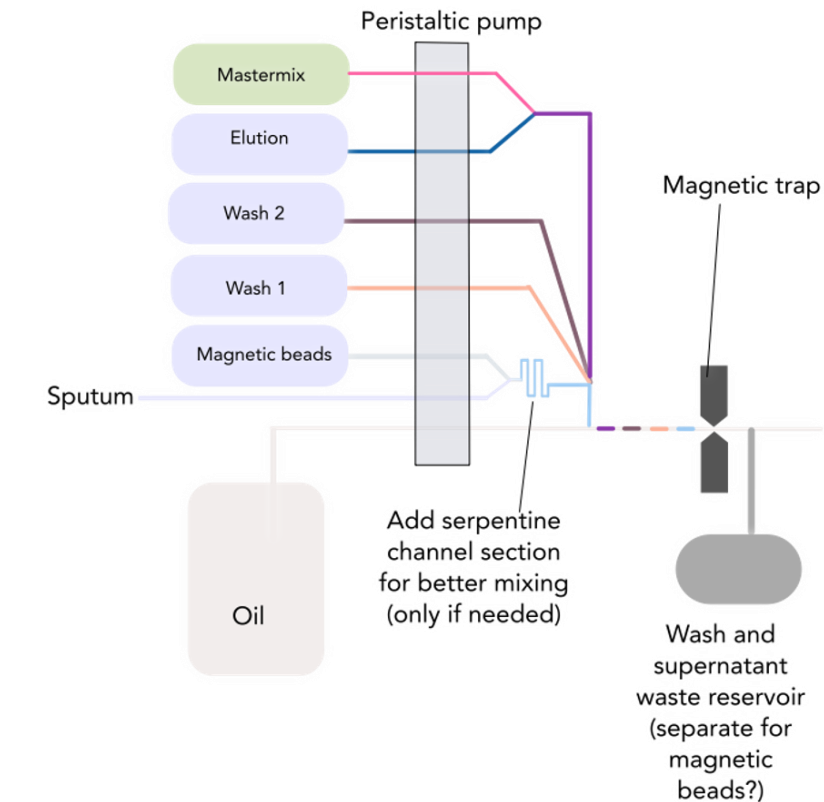


Figure 21: NA Purification A.1 concept with mid-flow waste removal

An important design step visible in NA Purification B.1 (Figure 23) was the addition of a separate oil line, with a designated peristaltic pump, for producing a continuous stream of oil for the purposes of moving the purified droplet chain through the rest of the system (to the right-hand side of the diagram) and secondly for flushing away the waste of the NA purification step. Although the latter purpose was obsolete once magnetic lysis flow was abandoned, the use of an ‘oil only’ pump was included in all subsequent designs. These key advantages of this separate oil line are:

- Simple roller features
- rollers that can have higher fluid throughput per rotation than those used in droplet formation pump
- Simplicity of electronics: a single motor can be used for all the droplet chain ‘moving’. Motor input signal directly changes speed and control is easily implemented with hall effect sensor.
- Only needs one pump on for moving the droplet chain, no need for complex timing or optical detection if oil pump just moves a specific number of turns

NA PURIFICATION B.1

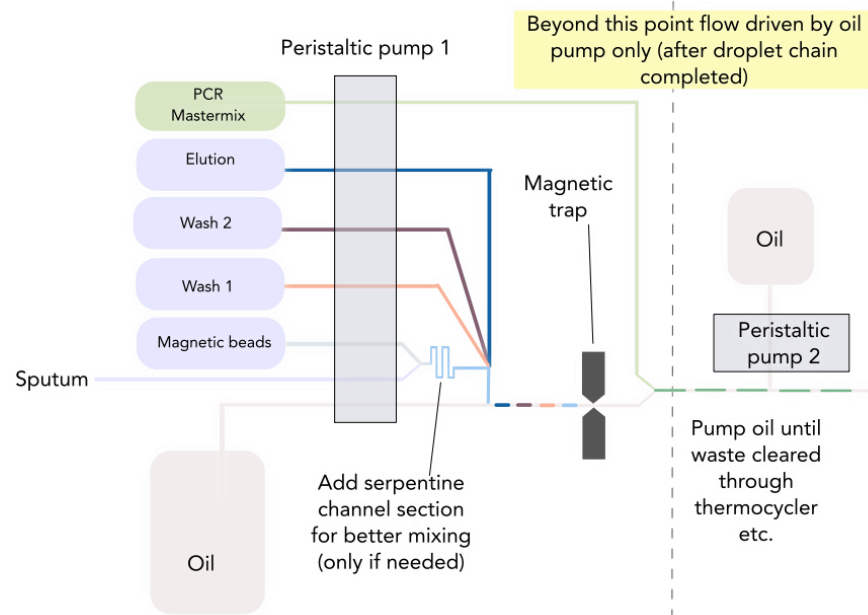


Figure 23: NA Purification B.1 Concept. Includes an oil-only pump line

An important shortcoming of NA purification B.1 (Figure 23) was that even with great tuning of junctions and path lengths the droplet might still arrive at the T-junction at the wrong time. While the magnet beads inherent magnetism would be possible to track, the other colorless fluids were poor candidates for e.g., optical detection, which would contribute the need for more sensors, more cost, and more parts. The complexity of timing needed to ensure the master mix would be added precisely when a droplet arrived (left of the dotted line on diagram) purified NA droplet had arrived would be a significant burden on the prototyping process as well. This issue was present even if we used Y-junctions to simplify and to reduce the manufacturing accuracy needed for the NA purification step as seen in NA Purification C.1 (Figure 24)

By the time iteration NA Purification C.1 (Figure 24) had been designed, it became apparent that the ratios of the droplet sizes needed were of significant range and hence would limit the production of 1 set of ‘ingredient’ droplets to 1 full rotation. This was a limitation on throughput per motor action but not prohibitive. The issue which C.1

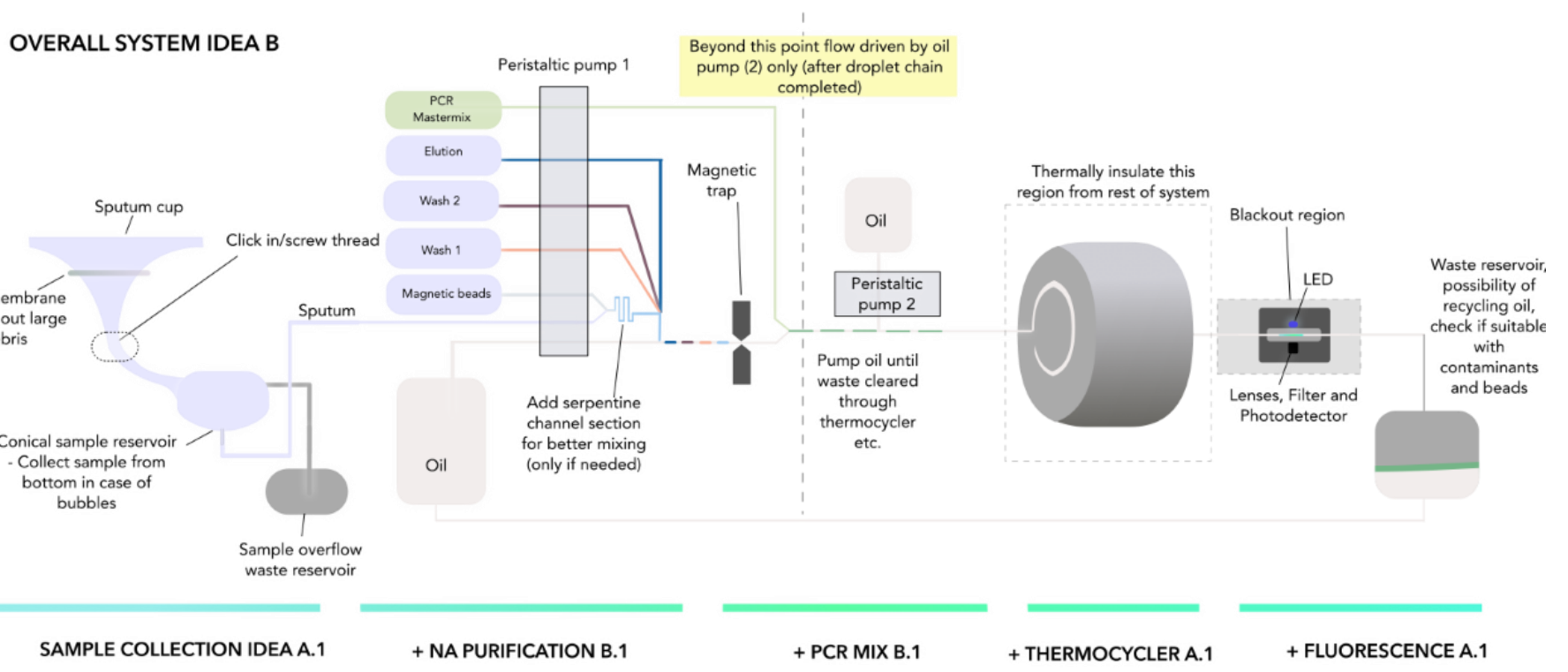


Figure 22: Overall system idea B. After this design Novacyt corrected our team to be using saliva instead of sputum

(Figure 24) did not resolve was that the system was only equipped to produce, purify, and add master mix and move only 1 droplet at a time. This was because after adding the washes the waste needed to be diverted or pushed further down the line.

The easiest conceptual solution we devised was to include an additional diverging line after the magnet trap. With the magnet still on, the oil-pump would first push the waste through to a designated reservoir. This line would then need to be blocked to allow the prepared droplet to proceed to the thermocycler stage. At this stage the greatest barrier to the magnetic lysis flow design was introduced: how to open and shut a line for waste that allowed removal of the waste product and accurately timed the union of a purified droplet with the PCR master mix. We sought a valving function that would allow this, possibly through use of some elastomeric material. After much consideration by the NA purification department and fluidics department, this valving issue remained a very substantial barrier to our design.

FULL CARTRIDGE A.3, NA PURIFICATION C.1

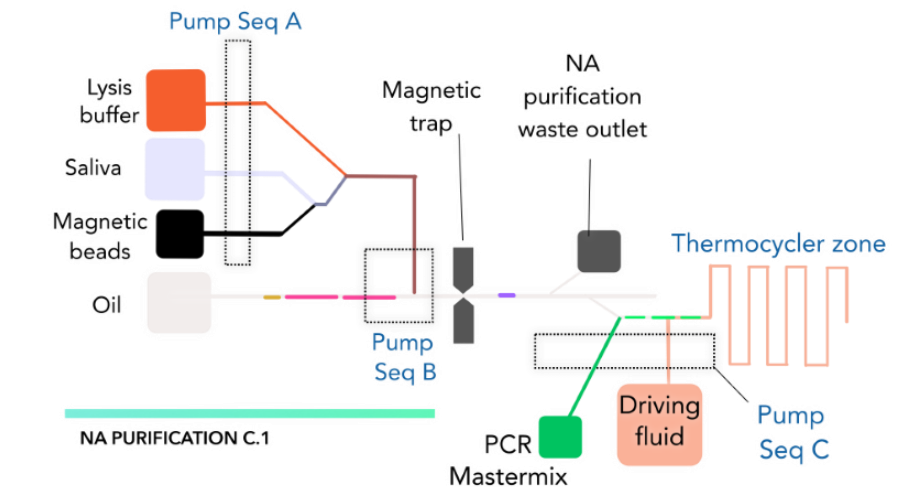


Figure 24: Full cartridge A.3, NA Purification C.1 concepts.

Owing to their expense and nature we also sought to design a method that would allow us to recover and recycle the magnetic beads. Doing so would require the valving system to be used while the magnet was turned off. Because of the challenges of valving and waste, we sought to reduce the complexity of the pumping involved before the magnetic trap. Our main solution was to pre-make the droplets of washes and elution buffer. This would reduce the number of inlets for the first pump (Pump sequence A in C.1, Figure 24), potentially increase the throughput per rotation and make the junction simpler to manufacture. Using sequential Y junction would potentially also reduce

the risk of unintended segmentation due to droplet snagging on the walls of the connectors and tubing.

Concurrent to this shift towards using a pre-made droplet chains was the shift away from using reservoirs of fluid stored on the box, and instead storing reservoirs on a cartridge. The main driver of change here was the need to minimise the risk of contamination. Although not explicitly drawn out, the consensus was that we would design a box into which a user would add their sample. This box would contain all the fluid necessary to prepare and run PCR on the sample, as well as all pumps and tubing. However, to do so the tubing would either need to be sanitized or replaced entirely. Making junctions out of 3D printed connectors into which PTFE tubing could slot would necessitate extremely precise positioning of the replacement tubing. Because of the junctions with more than one inlet, it would not be possible to replace the tubing with one continuous piece. Both factors would make tubing replacement far too complex for our target user and thereby make the device only suitable for one use before needing to be sent back to a skilled manufacturer or designated repurposing plant. The alternative of sanitizing was similarly unfeasible. The diverging tubing pathways and connectors would be difficult to reliably flush and the risk of a viral cross contamination would not be minimized. Additionally, we could not find a standard industry practice for sterilizing tubing. Therefore, despite the environmental benefits of using a non-disposable box and the convenience of housing the fluid on board, we transitioned to an idea of a cartridge in a box.

Overall System idea B.2 (Figure 25) illustrates the joining of the sections in a schematic sense and highlights the pathways which come into contact with the potential viral saliva sample.

OVERALL SYSTEM IDEA B.2

(re-evaluating with a cartridge for the saliva)

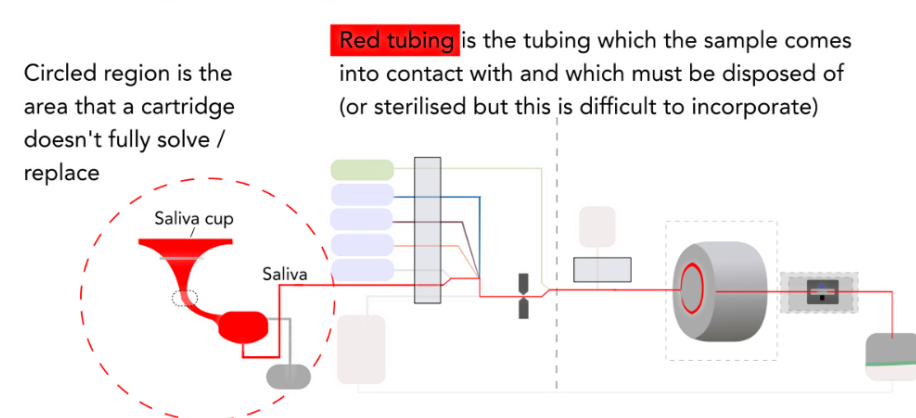


Figure 25: Overall system idea B.2 concept, showing contaminated regions

We had two primary approaches for the cartridge: to design a cartridge containing only the saliva with the beads and fluids needed for preparing the saliva, or to design a cartridge with all ingredients on the cartridge.

SALIVA CARTRIDGE A

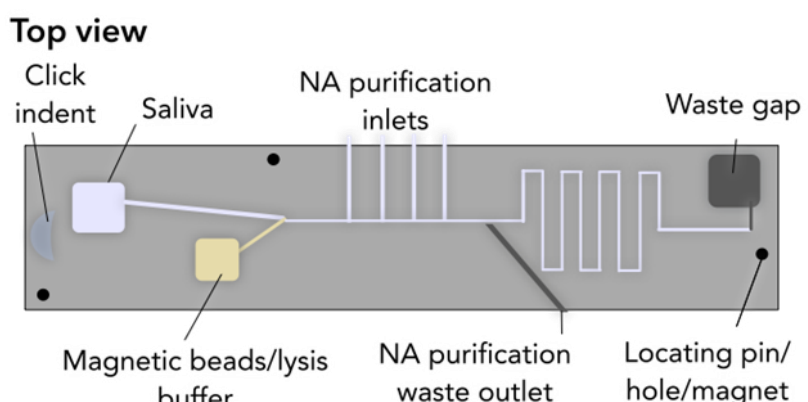


Figure 26: Saliva cartridge A

Using a 'Saliva cartridge' (Figure 26) has some key benefits. Only the parts which contact the saliva are disposed of; fewer onboard reservoirs would reduce the cartridge size and make manufacture simpler; the device box could house large volume of the master mix and therefore be stored in standard vessels; more pump lines could be fixed which would make the system more robust. Note the waste could be stored on or off the cartridge but would be safer if it was disposed immediately after use, i.e., on cartridge.

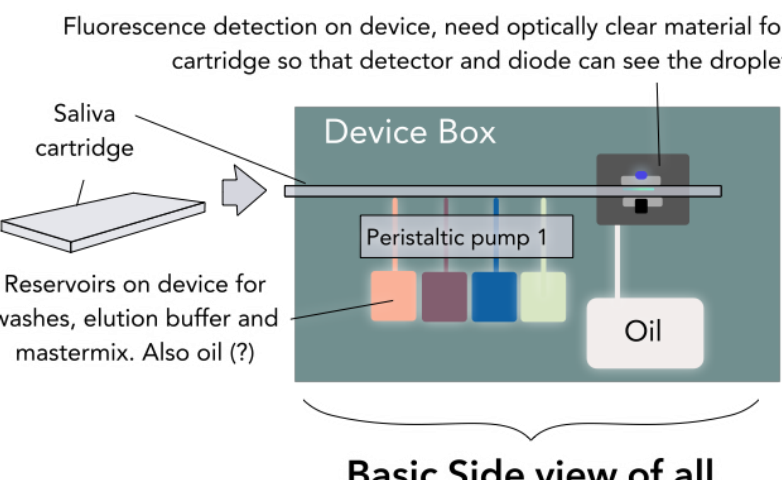


Figure 27: Saliva cartridge concept with side view

This configuration had one extremely significant shortcoming however: the difficulty of interfacing lots of fluidic tubing/channels between box and cartridge. Not only would the cartridge need to be well aligned in the box, a robust, watertight seal would be needed across the connections. At this stage we were considering slotting the cartridge in horizontally, so the fluid inlets would also need connecting in an axis perpendicular to the direction of insertion and could possibly need a valve for each inlet. These challenges led us to reject the saliva cartridge approach.

FULL CARTRIDGE A.2

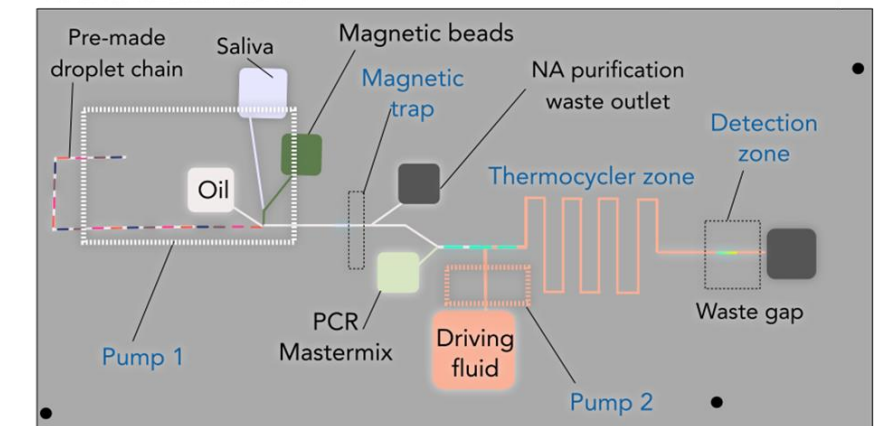


Figure 28: Full cartridge A.2 concept

Therefore, as a group we eventually decided on the 'full' cartridge option' (Figure 28) as it would allow for a fully contained system on each cartridge and is combines user safety, ease of disposal, and minimum cross contamination (as the saliva sample never touches the devices). We also considered using pre-made droplet chain instead of fluid reservoirs on the cartridge. This can be seen in Full cartridge A.2 (Figure 28) whose layout is identical without using droplet chains except for the omission of reservoirs and the additional length of tubing before the saliva junction. Making a chip with droplets already on it minimizes the pumping and segmentation work the device needs to do on as part of operating on the cartridge. However, the manufacture and in-project prototyping of this would be extremely problematic and minor discrepancies in droplet chain positioning would create timing issues elsewhere in the system. We therefore departed from the use of premade droplet chain as the power consumption and pumping advantages were outweighed by the burden or precision of manufacture and difficulty of prototyping.

One additional design flaw with the cartridge which was eventually negated by the use of MicroLYSIS was the potential need to store certain liquids for magnetic lysis flow at subzero temperatures. Our initial solutions for this included either adapting the cartridge for freezing in a domestic freezing appliance and using thermochromic stickers on the cartridge to indicate correct freezing and operational temperature.

MicroLYSIS Cartridge design

The project shift to using MicroLYSIS as part of what is termed here on as 'MicroLYSIS flow' instead of magnetic flow was a milestone change in the project. The removal of the magnetic beads eradicated the need to have a waste outlet mid-cartridge, which has previously restricted our cartridge to using unidirectional flow (as a suitable valve could not be found it would not be safe to reverse the flow). With the possibility of bidirectional and oscillatory flow both the thermocycler portion of the cartridge and the NA purification steps were simplified considerably. The design choice for the thermocycling fluidics section

was to move either the heating elements of the fluids (the latter was not possible with magnetic lysis flow). Oscillating the flow instead of using rotating heaters or other alternatives was found to be the optimal solution due to considerations such as delays in the cartridge heating up to the required temperature if the heaters rotated as well as minimizing the number of moving components

The fluidics process steps became as follows:

- 1) Add sample and MicroLYSIS ratio 1:9
- 2) Heat mixed sample at 75 °C for 5mins, 95 °C for 2mins
- 3) Add heated mixed sample to master mix in 1:1 ratio
- 4) PCR + Fluorescence

The key iteration for the MicroLYSIS flow is shown in Cartridge B.1. (Step 1) (Figure 29) is achieved using a Y junction (mixing is not included here) with continuous fluid stream. 2) and 4 are achieved by pumping the sample-containing fluid over the Peltier blocks and the fluorescence detector. 3) is achieved using a junction whose layout and function will resemble a PDMS chips. Adjustments to this design with further tuning included adding curvature to the tubing in the heat zones to increase the number of sample droplets. An important distinction to make for this design is droplet formation is after NA purification and hence the mixing is done in continuous stream: droplet ‘microreactor’ rapid mixing is not used for combining the saliva with MicroLYSIS.

CARTRIDGE B.1 Stationary heaters, oscillating flow

- 1 Pump1 on, combine micro lysis and sample streams and heat. Begin drawing oil and GenesigMM
- 2 Pump1 on, finish heating and pump blue and pink lines to Y junction to form droplets
- 3 Pump1 on, form droplets
- 4 Pump 1 off but clamped, Pump 2 on, move droplets with oil/air to heating zone and oscillate
- 5 Pump 1 off but clamped, Pump 2 on, move droplets after PCR cycles to fluorescence and waste

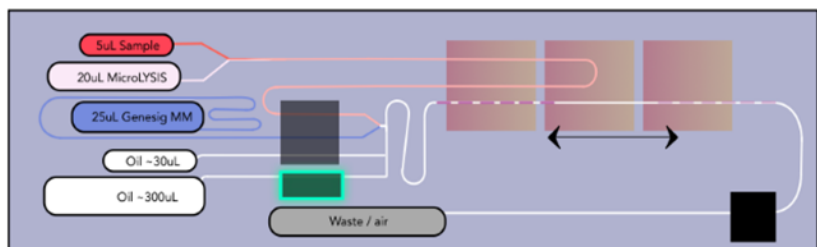


Figure 29: Cartridge B.1 protocol with real top-view diagram of cartridge layout and paths

The rationale for pulling (rather than pushing) the sample and MicroLYSIS with the pump is two-fold; once the path length is correctly optimized, using only one pump ensures that the fluids will reach at a

known point in time without the need for external detection to confirm so. Secondly, by avoiding a 3rd or 4th pump the footprint of the cartridge and the device is smaller and power consumption is lower for fewer pumps. In further iterations however, to ensure an appropriate illiquid interface and good mixing within the tesla mixer with the significant ratio difference (1:9 sample: MicroLYSIS), either two different flow rates or two inlet ratios. The reliability of the pump would be reduced if pulling two inlets of significantly different diameters (may draw out fluid incorrectly) and so to ensure robust pumping, using 2 flow rates was selected.

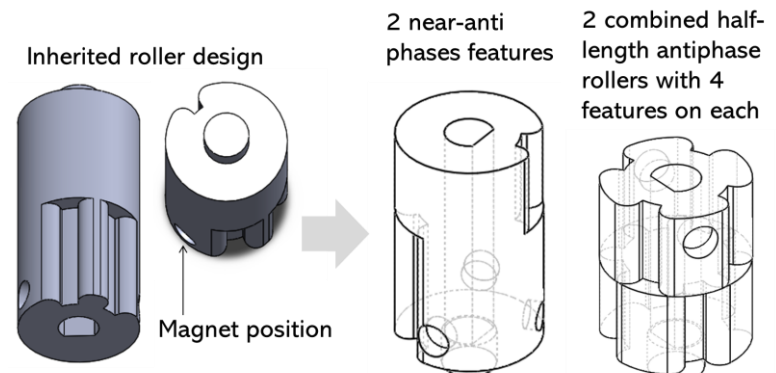


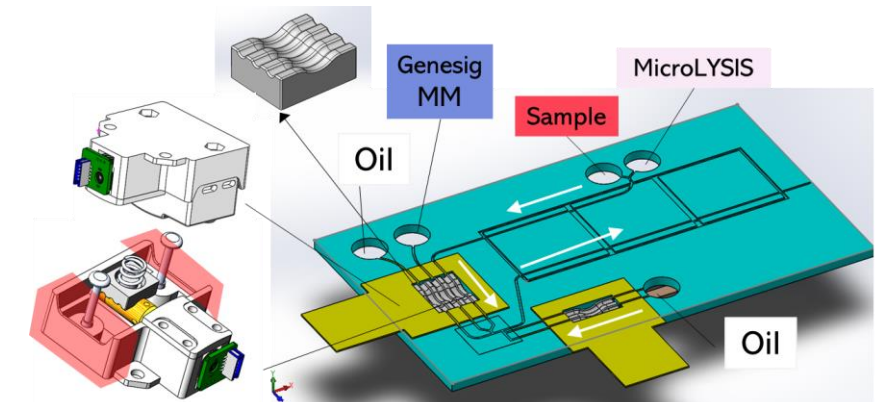
Figure 30: Roller adaptations for droplet segmentation and near continuous flow

The simplest way to do so from the perspective of coding, roller design and motor input was to allocate one pump for each of the sample and MicroLYSIS inlets.

A Y junction after before the Tesla mixer would ensure maximum throughput and a pulsatile flow that more closely resembled continuous flow; having many 4 features per circumference would also increase the throughput. The following rollers were designed for all continuous streams (sample, MicroLYSIS and oil). The right most roller was selected for the final design.

The third iteration of initial CAD for the cartridge is shown below (Figure 31). Eppendorfs were expected to be used instead of reservoirs and the pumps used for basic prototyping would not require adaptation from the inherited SWS sensor. For integration in the cartridge however, the chassis needed significant adaptation.

The inherited pump was set to be effectively laces upside down in the device, and only the pump-beds would be part of the cartridge; everything would be part of the device itself. The green thin feature shows the ‘footprint’ of the pump housing, which constrains how close parts of the cartridge can be to one another and the motor chassis needs to fit in the device. The regions in red, which the SWS design uses to locate the bolts which secure the chassis and compress the spring (compression leads to 40N force) were removed and the shaft length adjusted.



The regions highlighted in red would be removed in modifying the pump to reduce footprint. Thermocycler underneath 3 the 3 Peltier squares on cartridge

Figure 31: Pump positioning and adaption in initial cartridge CAD

The side-by-side comparison of the longer version of the adapted pump shows the direction in which the scale has been increased to reduce. The main difference is the chassis would not include the pumped and the footprint is much smaller and slimmer. The longer shaft allows the motor to be positioned further away from the cartridge and opens scope for positioning the motors near to each other but away further from the tubing areas: this helps with cartridge layout and insertion.

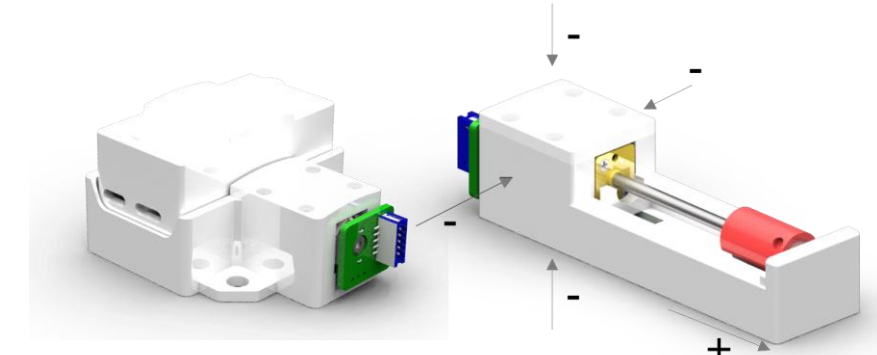


Figure 32: Pump chassis adaptions. Shaft extended, roller exposes, and chassis slimmed

The pump access to the pump bed (on cartridge) was achieved by gluing the compression spring to the cartridge and using a platform and latch to secure the cartridge in place vertically. The image below shows how the pump bed remains connected to the cartridge throughout its compression. The movement along the axis of rotation is constrained by the wall around the pump bed. The requirement to be able to access the inlet and outlets to install the tubing prevents the pump bed itself being better constrained against rotation itself. This was later dealt with indirectly by ensuring good cartridge alignment that would limit movement in plane. FEA of this component and prototyping would have helped us better understand if this potential rotation posed a significant risk, however we were unable to complete this in the project time. The design work completed ensure the pump can interface with the pump beds, without contact with the rest of the cartridge.

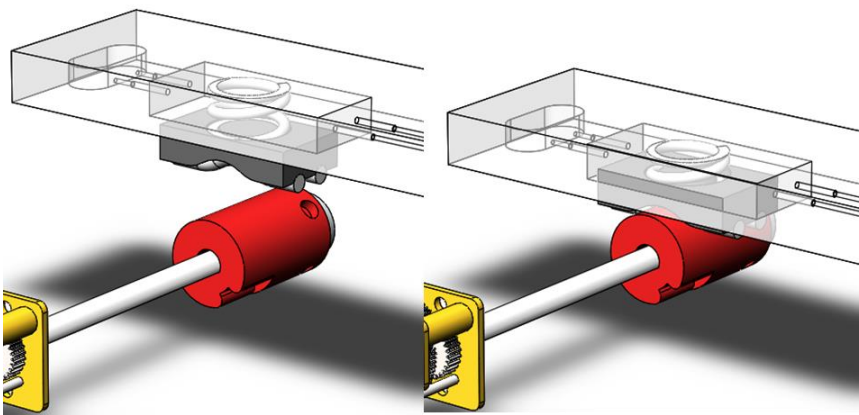


Figure 33: Partial cartridge design showing interfacing between roller and pump beds. The cartridge (translucent) would be pushed down by a platform (not shown here). Roller (red) shaft is fixed and upon compression the pump bed (dark grey) is trapped, causing spring compression and deformation of elastomeric pump lines

Prototyping and validation

Taking inspiration from PDMS chips designed by the Prof Niu's research group, a chip that would take inlets (A) saliva, (B) MicroLYSIS, (C,D) oil and (E) outlet.

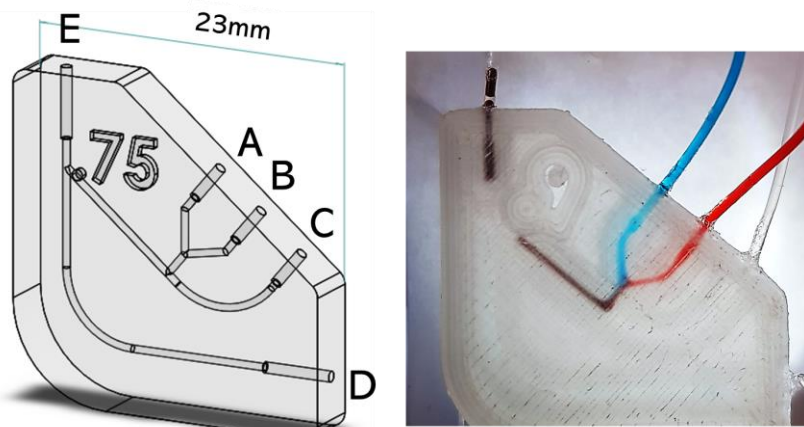


Figure 34: (left) CAD for 4 inlet microfluidic chips, (right) 3-D printed PVDF chips with food dye (A and B) and FC40 oil inlets (C and D).

An iterative process of designing and 3D-printing was completed. Various inlet/outlet diameters were cycled through to find a part dimension which when printed matched UT5 or UT7 tubing. PLA was used for the first prints but the resolution on these prints were poorer and the material was opaque (so droplet formation was hard to observe). The PVDF prints were semi-transparent (Figure 35), had fewer defects and the semi-fluorinated properties of PVDF have a surface chemistry that better supports stable droplet formation. These prints informed our selection of PVDF as our final cartridge material. Although UT5 had OD 0.7, the only viable prints had input print dimensions of 0.8 and 0.9mm diameter inlets. Channel diameters of 0.65mm were used to approximately match the UT5 ID of 0.5mm. This is shown in Figure 35: PVDF (white) and PLA (black) 3D printed chips printed on Ultimaker 3+ by Liam Carter. UT7 (left) and UT5 (right)

tubing shown below. Only 2 chips were viable: On occasion there was unwanted segmentation at the tubing connections (joined by Loctite glue) but these looked to be due to prototyping manufacture issues and residue build up. After validation with experiments to show the PVDF chips were capable of droplet operations and safe to use with oscillating a droplet chain without re-entering the chip, the chips were implemented in our final design.

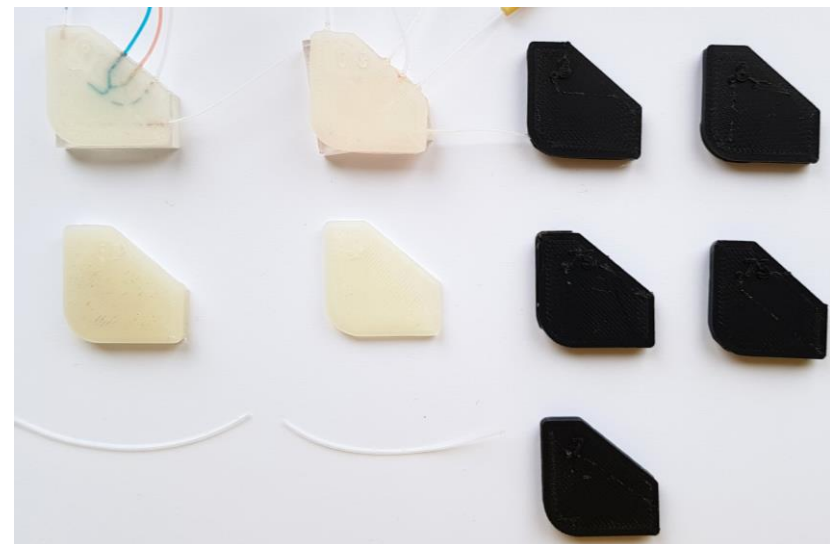


Figure 35: PVDF (white) and PLA (black) 3D printed chips printed on Ultimaker 3+ by Liam Carter. UT7 (left) and UT5 (right) tubing shown below. Only 2 chips were viable:

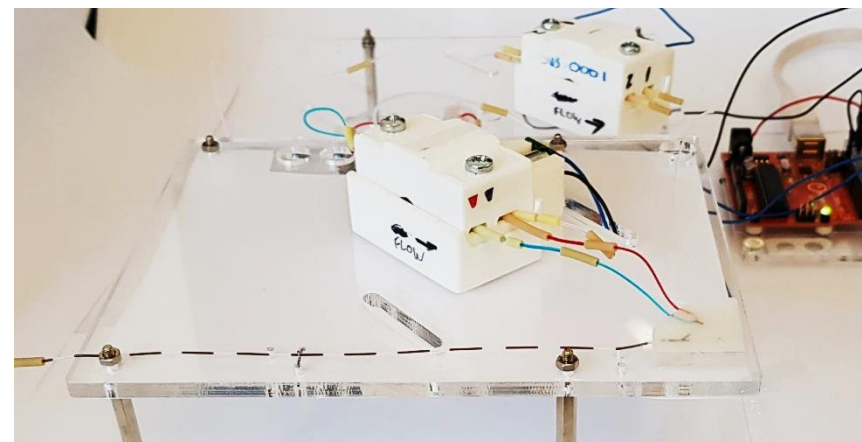


Figure 36: Pump trial and experimental layout for testing droplets. Acrylic test rig drawing in SolidWorks and laser-cut by Dr. Jonathan West

Final iterations

The final iterations of the cartridge design were reached by knitting together the micromixer, thermocycler holder and fluorescence detector together and adjusting path lengths for minimum master mix and MicroLYSIS waste. The final landmark iteration before the final design is shown below. It incorporates all the necessary mixing and space for thermocycler elements to be added, allowing for correct fluid flow, alignment pins and reservoirs. The path lengths were not optimized and tuned, but the serpentine can clearly be added. The

footprint of the cartridge could be significantly reduced. However true layout optimization would be premature here, as factors like reservoir size and volume calculations for every stage would need to be known, which was not the case at our final prototype stage.

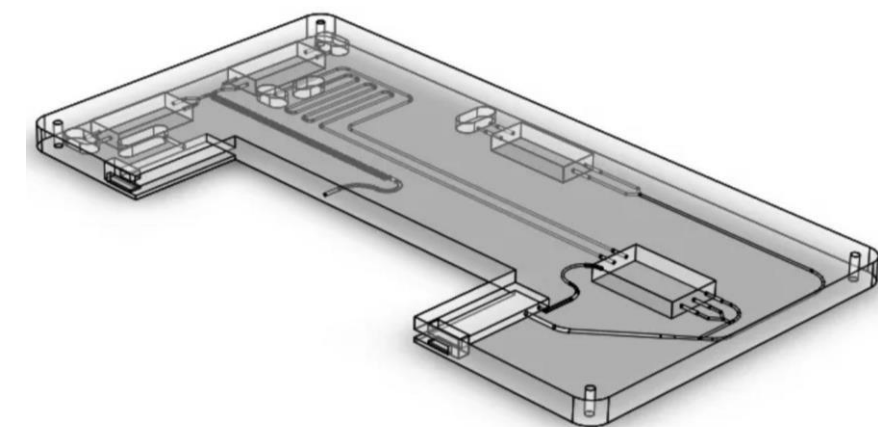


Figure 37: PVDF-only cartridge parts. Pump beds, lines and springs not shown here.

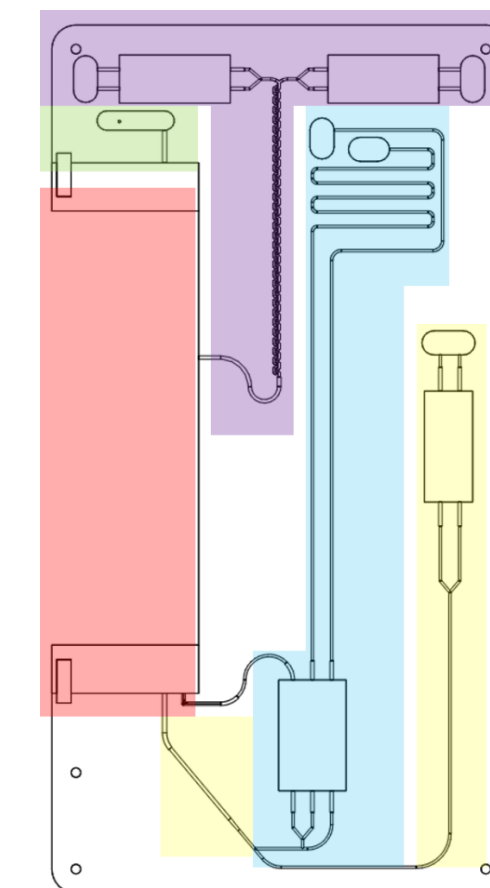


Figure 38: Colour coded PVDF cartridge layout. NA purification (purple), adding master mix and droplet segmentation (blue), oil line (yellow) and thermocycler (red) and waste (green)

Thermocycler

In NA amplification methods such as PCR, the sample needs to be heat treated at different temperatures to allow for successful denaturation, annealing, and extension processes. A thermocycler is what is commonly used in laboratories to achieve these requirements. Thermocyclers are often large and bulky making them unsuitable for portable applications like this project. Therefore, we plan to design a thermocycler that is best suited for miniaturized samples and is also lightweight.

Requirements

The general thermocycler requirements can be viewed in the following table.

Table 6: The thermocycler system requirements.

Thermocycler Specifications	
1.	Create a system that reaches 95°C, 55°C, 72°C and 65°C temperatures. It should be noted that the 65°C is necessary for the MicroLYSIS step.
2.	Ensure thermal uniformity.
3.	Ensure thermal bleeding between zones is minimized.
4.	Temperature change of the heater to be 10 °C / second.
5.	Temperature accuracy at ±2°C.
6.	Have a closed-loop heat cycle (heater, temperature sensor, temperature control, power switch from
8.	Heater is not exposed from the device to ensure not only the failure of other parts but also the safety of the user.

The material requirements are:

Table 7: The material requirements for the thermocycler.

Material Requirements	
1.	Can withstand the temperatures of the thermocycler.
2.	Great insulation will be needed between the thermal zones.
3.	Thermal conductive material is essential to transfer heat where required.
4.	Recyclable material where appropriate.

Component Options

The components to be used for the thermocycler were a heat element and a temperature sensor. The heating element is needed in order to activate the chemicals for the process and amplify the DNA while the sensor is required for the purpose of creating a closed-loop heat cycle and being able to control the temperature of said heat element. For both components there are many options available, nevertheless based on the following criteria the list was narrowed down.

Table 8: The requirements for the heating element and the temperature sensor.

Specifications	
Heater	<ul style="list-style-type: none"> • Can be controlled using an Arduino UNO. • Reach the required temperatures and is reliable. • Relatively cheap (£30-40).
Sensor	<ul style="list-style-type: none"> • Can be used with an Arduino UNO. • Accurate for the required temperature measurements ($\pm 0.5^\circ\text{C}$). • Relatively cheap (around £10).

Based on these criteria, the two heaters considered to be used with the system were a Peltier module and a cartridge heater. The advantages and disadvantages for each option are presented in the following table.

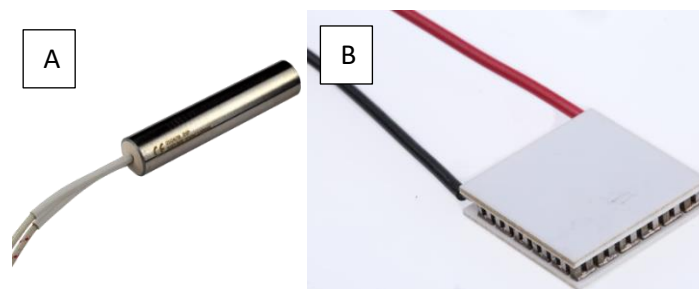


Figure 39: (A) is the cartridge heater presented [46] and (B) is the Peltier module [47]

Table 9: The heater options and their advantages and disadvantages (Appendix M for details)

Heating Element	Advantages	Disadvantages
Peltier modules	<ul style="list-style-type: none"> Can use PID control for controlling the modules with great accuracy. To cool down the system we would need only a heatsink and ventilation (no additional power consumption to the system). Smaller sizes than the cartridge heaters. (from 10x10mm to 60x60mm). 	<ul style="list-style-type: none"> They would require use of external temperature sensors to evaluate. More expensive than cartridge heaters (£20-50)
Cartridge heaters	<ul style="list-style-type: none"> Can have built-in thermocouple sensors. Large variety of sizes. (from 8 mm diameter and length 38-660 mm to 25.0 mm diameter and length 200-1525 mm) Usually cheaper than Peltier modules (about £4-20). 	<ul style="list-style-type: none"> They require a relay to control the temperature which will result in a less accurate heating system in comparison to using Peltier modules. If used potentially a fan would be needed to cool down the system.

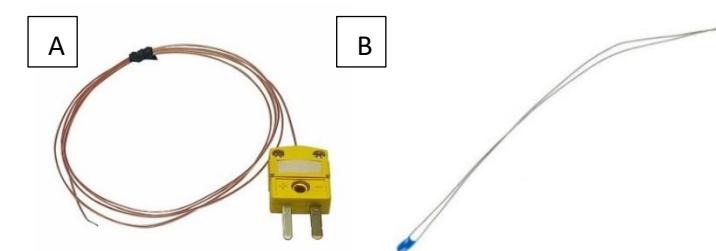


Figure 40: A) is the k-type thermocouple and (B) is the thermistor.

As far as the temperature sensors are concerned, again there is a variety of options however the choices were narrowed down based on our specifications. Hence, the ones considered were the k-type thermocouple and the thermistor.

Table 10 The sensor options and their pros and cons. (Appendix M for details)

Sensor	Advantages	Disadvantages
K-type thermocouple	<ul style="list-style-type: none"> Measures temperature directly. Lower cost than the cost of the thermistor. 	<ul style="list-style-type: none"> Needs amplifier which uses more pins per sensor (accuracy: $\pm 2^\circ\text{C}$ - $\pm 6^\circ\text{C}$). Accuracy: 0.5 to 5°C. Thermal response 0.1-10 s.
NTC Thermistor	<ul style="list-style-type: none"> Connects directly to the Arduino and needs only 1 analogue pin. Greater accuracy ($0.1\text{-}1.5^\circ\text{C}$). Thermal response 0.05 to 2.5 sec. 	<ul style="list-style-type: none"> Measures resistance and not temperature More expensive than the thermocouple.

Initial Designs

Unidirectional Flow

The original plan for the thermocycler position on the cartridge was to design a path for the fluid that allows for unidirectional flow while still ensuring that the fluid is able to have sufficient time to heat up to their desired temperature for PCR. This flow would also need to pass through all three temperature zones for a total of 35 cycles for complete PCR. Therefore, two main options to consider were either creating a cylindrical heating system with the tubing wrapped around it or creating a rectangular heating system with a serpentine pathway.

Cylindrical Heating System

The first design to consider was the cylindrical heating system. In this case, a cylinder would be divided into four sections by an insulation material. Three of which would be heated by cartridge heaters (one for each thermal zone) due to its variety in sizes and its implementation of a temperature sensor. The last section would be a colder transitional zone to allow for the sample's temperature to reduce from the 95°C zone before getting to the 55°C zone and minimise the thermal bleeding between the two temperatures. The tubing would wrap around the whole cylinder 35 times ensuring that the droplets would undergo each PCR cycle and the pump would stop to allow for the droplets to be at each temperature zone for the required time. The droplets would travel from the first zone (95°C) to the transition zone, then to the 55°C and lastly to the 72°C zone to complete one PCR cycle. Once all 35 cycles are completed, the droplets would move to the fluorescent detection. The cylinder dimensions would be 135 mm height and around 64mm radius.

All cylinder parts would be manufactured out of aluminium due to its good thermal conductivity (237 W/mK). However, a lot of material would be required for this design (around 4.5 kg) which would make the thermocycler not only heavy and expensive but also not portable. In addition, cutting and rejoining the parts would be an expensive and a complex method of manufacture. Lastly, the direction of the project changed to the use cartridge in order to eliminate cross-contamination, hence, this design was not feasible.

Serpentine Rectangular Heating System

To accommodate the use of the cartridge, a second design plan was created which implemented a rectangular heating system with the design of a full serpentine pathway that covers all three zones. The heaters for this design would be the Peltier modules and one would be used for each thermal zone. It was considered best to use the Peltier modules for heaters for easier implementation to rest of the

device. In the figure below, the sample would enter the 95°C zone (bottom right of the figure highlighted red) and remain in that zone for the extent of the initial extended denaturation stage. The sample will then continue to flow to the left most section (55°C zone) highlighted in blue, for the annealing stage and then to the middle section – yellow (the 72°C zone) for the extension stage. The reason why the sample will travel in such peculiar path (from the left to the right and then to the middle) is because there is a high temperature difference between the 95°C zone and the 55°C zone and there would be significant thermal bleeding between both temperature zones. The cycling continues for the length of the cartridge or for 35 cycles. At the end of the serpentine, there is an extended path that remains in the 72°C zone for an extended extension stage to ensure that the final cycle is complete before leaving to the fluorescent detection. For this design, the time spent in each zone is decided by the length of the path in that zone as the flow speed is constant. There are also air gaps (Figure 42(a)) to minimise thermal bleeding in between zones so that heat is not lost, and each zone can achieve the desired temperature. The serpentine pathway previously shown would then sit on the Peltier modules attached to a holder for easy removal (Figure 42(b)).

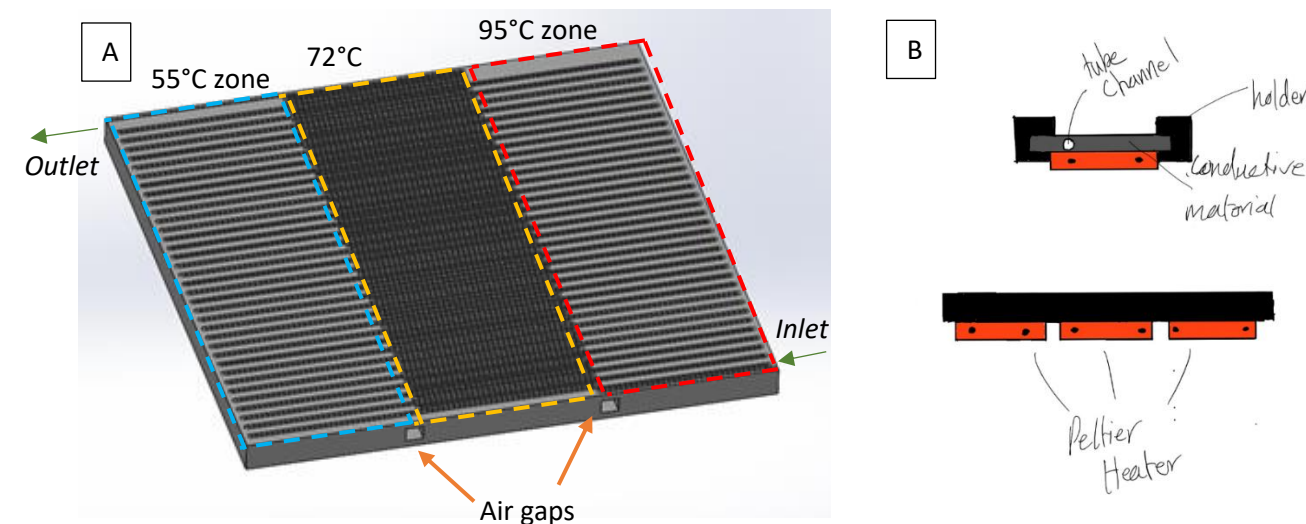


Figure 42 (A) A side view of the overall design with highlighted each thermal zone and air gaps separating each zone, and (B) a draft drawing of the holder of the tube channel.

A SolidWorks static simulation was run to evaluate the design's performance. The size of the Peltier modules (30x30 mm) in relation to the overall cartridge design is big (150x150 mm) hence the heating was not enough for the zones to reach the required temperatures resulting in a non-functioning PCR process.

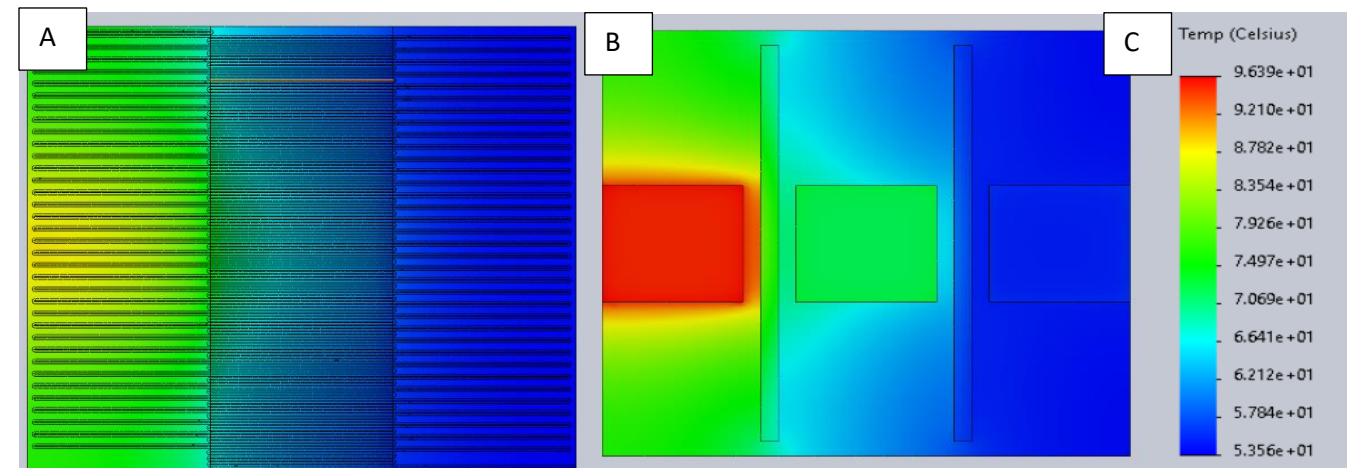


Figure 43: The thermal simulation of the serpentine rectangular heating system with (A) being the top view, (B) being the bottom view and (C) being the temperature gradient.

Bidirectional flow

After implementing the MicroLYSIS process for nucleic acid purification instead of magnetic beads, the use of bidirectional flow was decided instead of unidirectional flow. This allows for the overall size of not only the cartridge and thermocycler but also the whole device to be reduced. As a result, the thermocycler size and mass became smaller and the subsystem could be more easily implemented to the rest of the device.

Thermocycler Cartridge

The cartridge that is to be placed on top of the thermocycler must have two paths, one for the tube for the droplets that need to go through the PCR process and another path for the tube with the continuous flow of the MicroLYSIS process. That is because the MicroLYSIS process requires thermal treatment, hence the additional path allows for the sample and MicroLYSIS reagents to flow. The path for the PCR process was simplified into just a straight line across all zones. The sample would enter the 95°C zone and the flow would stop, allowing the sample droplets to reach the desired temperature and repeating this step in the 55°C and 72°C zones. Once it reaches the end, the cycle is complete, and the flow would switch causing the sample to return to the first zone (95°C zone). This repeats for 35 cycles for PCR (Figure 45(A))

For the PCR path, there was a trade-off between having small thermal zones (20mm length) and having enough space for a sufficient droplet chain. Hence, the implementation of a serpentine path was included which was to allow for more droplets to fit in each zone. At this point as well, the fluorescent detection was also implemented with the thermocycler to gather data for each cycle of PCR. Therefore, a hole from the side of the cartridge was created to allow for direct sight from the LED to the droplets and tubing (Figure 45(B)). This allows for the thermocycling process to be complete once sufficient fluorescence is detected.

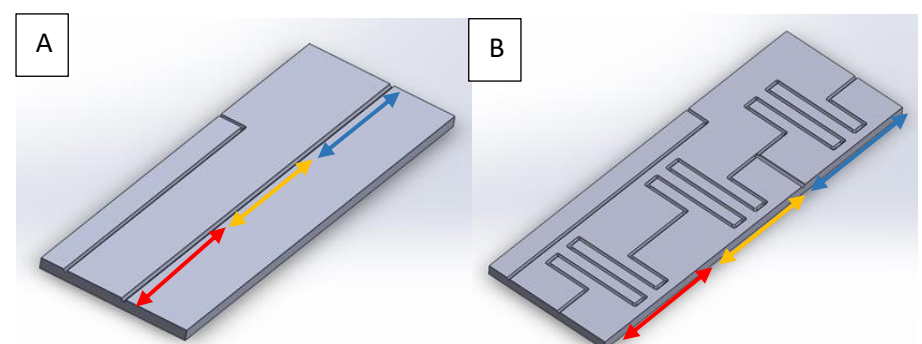


Figure 44: (A) The simple cartridge version with the PCR tube being in a straight line, (B) the cartridge with the serpentine PCR line.

allows for excited fluorophores/light to reach the sensor for fluorescent data collection of each cycle. The top and bottom half are just mirror images of each other.

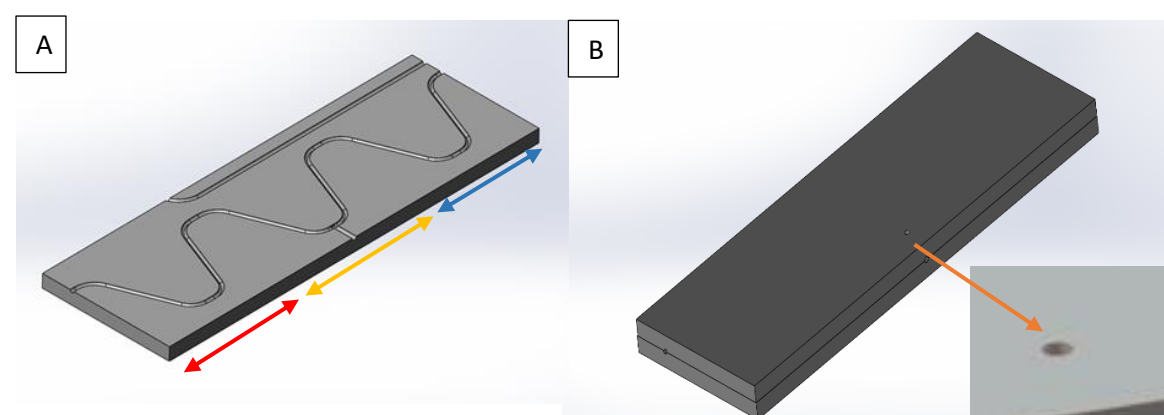


Figure 46: The top of the cartridge (B) the cartridge assembly with an arrow pointing at the hole of the fluorescence detection and showing a zoomed in version.

Final Designs of the System

After designing the cartridge portion of the thermocycler, the housing for which the components would sit in could be designed. The design consisted of three Peltier modules attached on heat sinks (Aluminium alloy 1100) to release unnecessary heat. The components were then enclosed in a housing to ensure thermal isolation from its surroundings. The Peltier modules at the top of the housing would also be surrounded by an insulating sheet to reduce heat transfer between the zones.

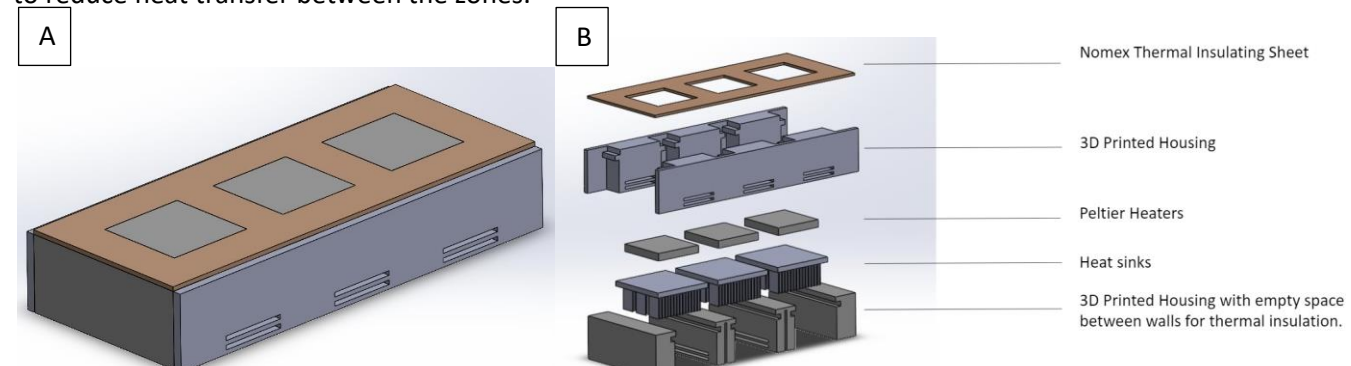


Figure 47: A) Fully assembled view of the thermocycler and (B) an exploded view of showing its components.

For the purpose of evaluating the current design a static thermal simulation was conducted with a simple cartridge on top of the thermocycler to verify if the cartridge would reach the desired temperatures. The results of the thermal analysis indicate that the cartridge did in fact reach the desired temperatures, but the housing would overheat which is not ideal. Temperatures of the housing would reach up to approximately 80°C and it was clear that this design needed to be more exposed to the air to provide sufficient ventilation.

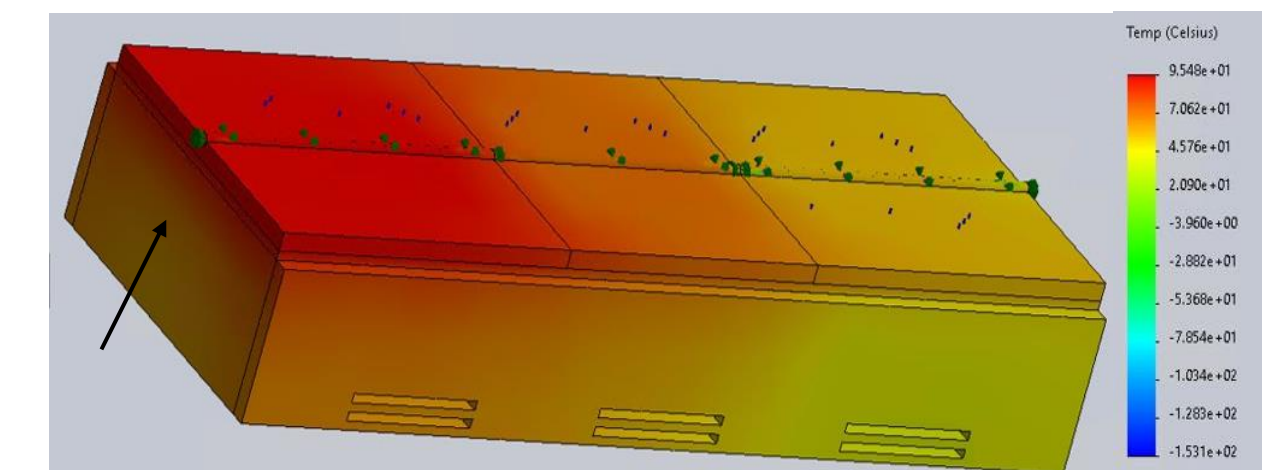


Figure 45: Thermal analysis results of the entire thermocycler. Arrow points to areas that the temperatures of the housing reaching dangerously high levels.

Therefore, the final thermocycler design was changed to the following. The design was more exposed to the air to allow for the 3D printed housing to be thermally isolated from the heaters as much as possible. A layer of aluminium alloy 1060 plates (with each having dimensions 30x29x1.5 mm) was also added to allow for a more even distribution of the heat across the cartridge rather than a concentrated hot spot in the centre. This plate also houses the sensor that reads temperature with a hole on the side for insertion and it allows readings to be taken for the feedback control (PID). The final overall size of the thermocycler was 90x30x22 mm and analysis was carried out in this size however due to last minute changes to the overall device casing, the dimensions of the thermocycler were adjusted to 90x30x17.45 mm.

The performance of the design had to be evaluated prior to designing the cartridge part in more detail. Hence, a final static thermal analysis was conducted.

The results of this thermal analysis were more promising as the cartridge on top was not only reaching the desired temperatures, but the housing of the components was also much cooler than before (approximately 60 – 70°C). These results were satisfactory hence this became the final thermocycler design.

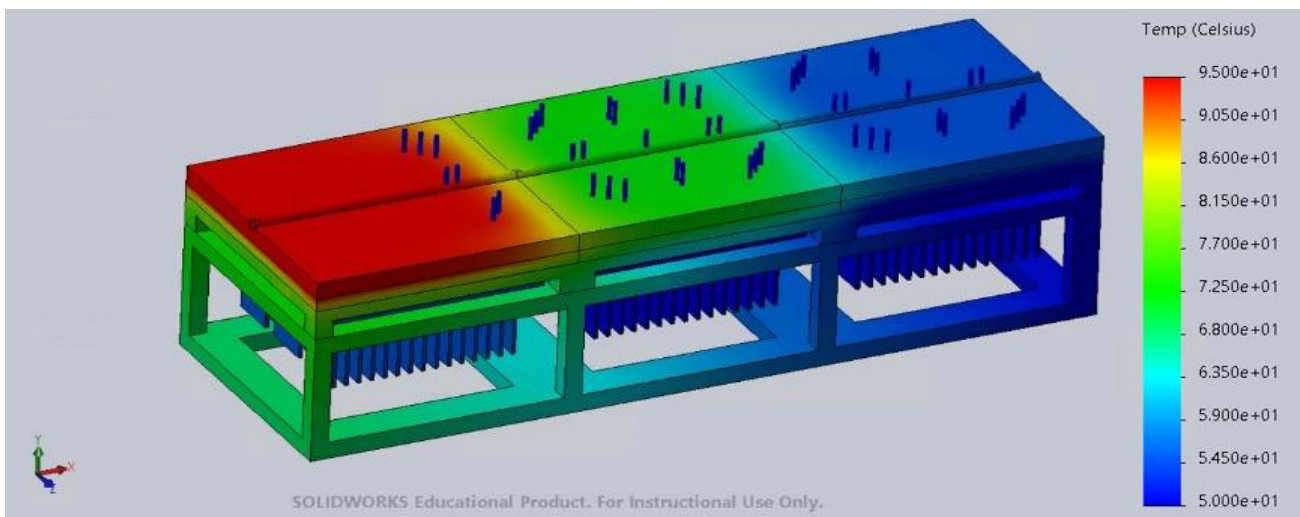


Figure 48: Thermal analysis of the entire thermocycler

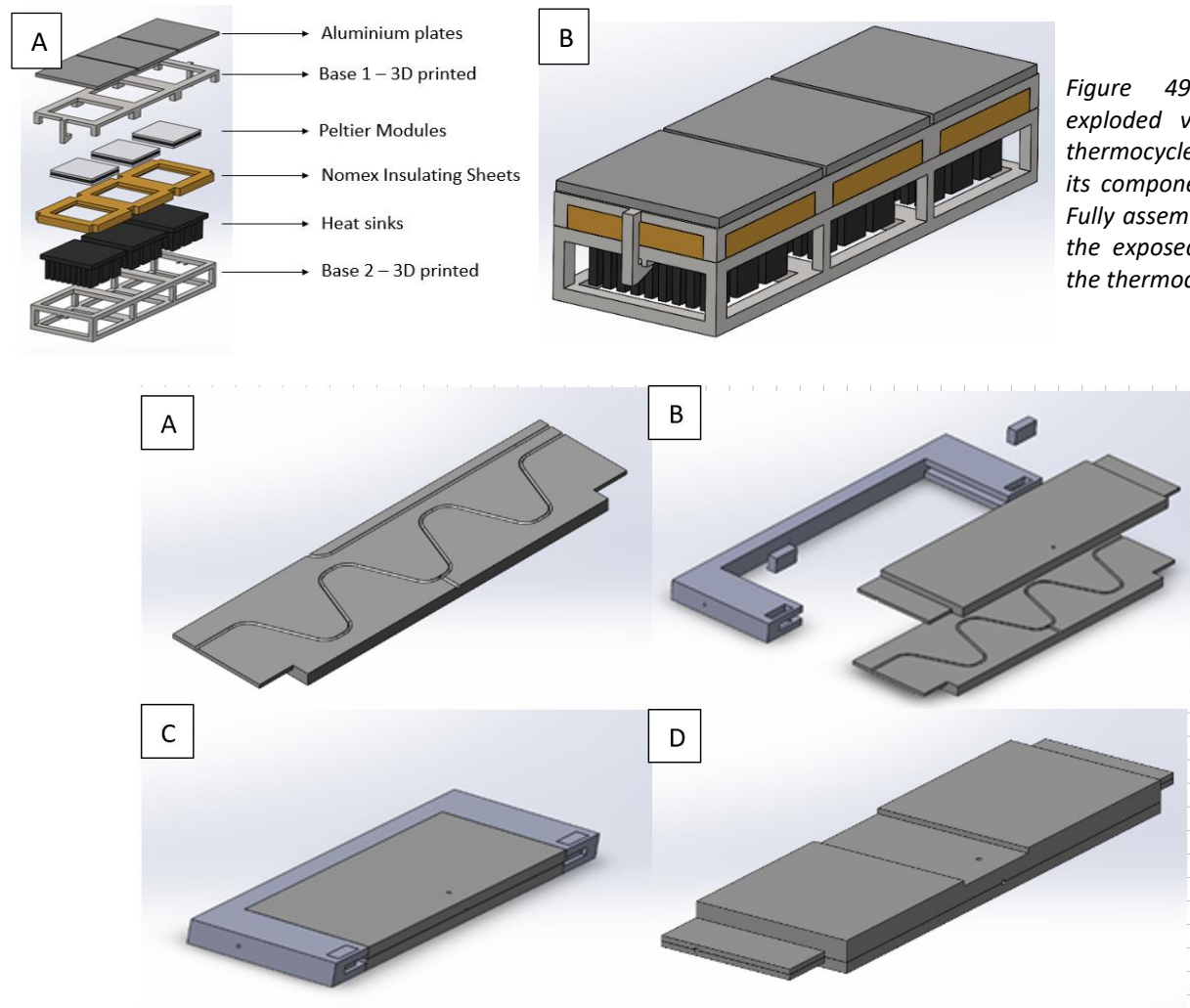


Figure 49: (A) an exploded view of the thermocycler showing its components and (B) Fully assembled view of the exposed version of the thermocycler.

Figure 50: (A) The bottom half of cartridge with extended "wings". (B) Exploded view showing all components (C) Fully assembled cartridge holder. (D) Final changes to the cartridge

Thermocycler integration to cartridge

Now that the general design was created, it was essential to be integrated with the rest of the cartridge. For that, the length of the thermocycler portion of the cartridge needed to be slightly longer. The total dimensions of both the top and bottom part together that was once 90x30x6mm has been changed to 110x30.45x6mm. The design is shown below. The “wings” of the design are meant to slide into the holder (Figure 50(B)) as a tight fit. Two stubs/blocks fit into their designated hole in a tight fit to ensure that the two thermocycler parts cannot move in any direction and holds it in place.

Final changes were made to the cartridge seen in (Figure 50(D)) to accommodate the fluorescent detector. A slot was made in the cartridge to allow for the fluorescent detector to sit at for an optimum position for the detection. Thickness of the top part was increased, and the bottom part decreased but the overall thickness of the cartridge remains 6mm. These changes in dimensions were to allow for better fitting in the final cartridge design.

Materials and Manufacturing

Thermal Insulator

Based on the design, thermal insulators are needed to separate the heaters but also to isolate the body of the thermocycler from the rest of the device for the purpose of limiting the heat transfer. For the body of the thermocycler, as mentioned in Table 7 the main requirements are for the material to withstand the high temperatures of the device and be a good thermal insulator. Ideally, that material could be recyclable in case of creating waste during initial manufacture. Therefore, thermoplastic polymers can fulfil such criteria.

Based on analysis carried out using EduPack (Ansys Granta EduPack, Cambridge), the selective laser sintering is the most economic considering the batch size for our thermocycler is small. However, due to the limited resources and the university restrictions, Mr. Liam Carter who possesses an Ultimaker 3D printer manufactured the body of the thermocycler. For the identification of the most thermoplastic to use for that process, the glass temperature had to be over 95°C to ensure the material would be rigid throughout the operation of the thermocycler. PEEK (Polyetheretherketone), PTFE (Polytetrafluoroethylene) and PI (Polyimide) are the most suitable with PI being the most heat resistant material making it the ideal option. Nevertheless, Mr. Carter had PVDF available which despite the limitation of material availability in the software (EduPack) considered it is a thermoplastic that begins deflecting at 158°C – much higher than the operating temperatures [48].

As far as the isolation between the heating elements is concerned, a thin layer of material was needed between the 3D printed body. Initially, Armaflex sheet was considered as it exists in many forms and is highly used in pipe thermal insulation applications with thermal conductivity 0.042 W/mK [48]. Nonetheless, in the sheet form it can be bought only in square meters therefore a lot of material would be wasted. Hence, the other option was to use Nomex sheet which is highly used in electrical insulation with thermal conductivity being 0.139 W/mK [49]. It was bought in the form of A4 sheets which was ideal.

Thermal Conductor

The thermal conducting material was needed for the cartridge to maximise the heat transfer between the heating elements and the cartridge and to ensure thermal uniformity for each zone. Hence, metal would be the ideal option. Based on the metals’ thermal conductivity and considering their cost, a non-age-hardening aluminium would be the most suitable option. In the case of our cartridge we used aluminium 1060 due to its low cost (around 1.1 GBP/kg) and high thermal conductivity (237 W/mK) [50].

The manufactured thermocycler system can be viewed in figure below.

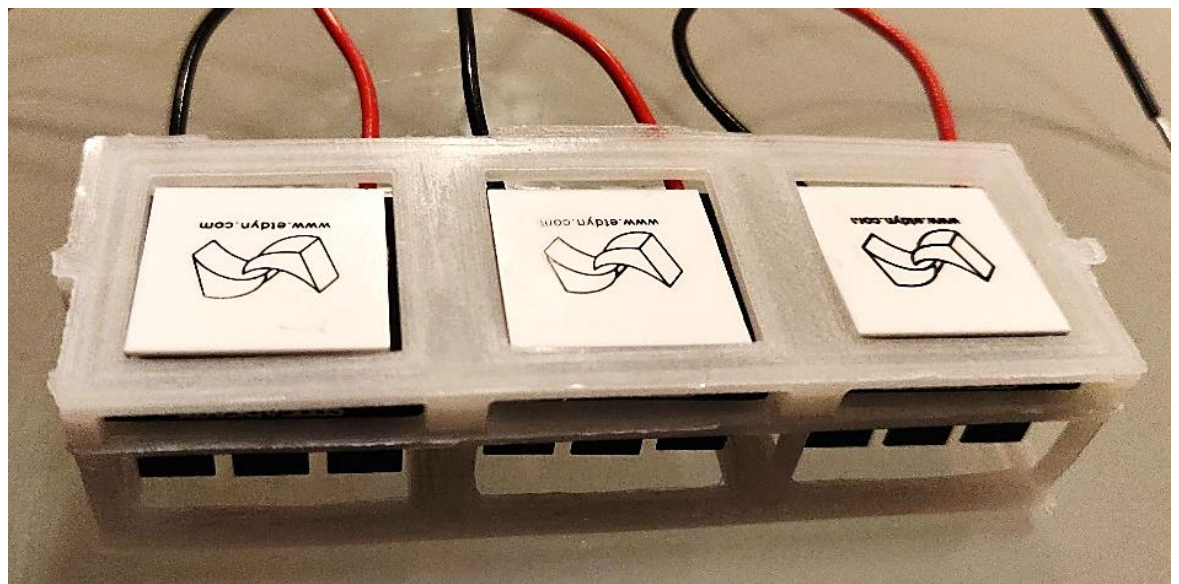


Figure 51: Fully assembled thermocycler.

Electronics

Component performance evaluation

The Peltier modules' performance evaluation was conducted by connecting each Peltier to a power supply and supplying the modules with a constant current and voltage. With the aid of a PID system, the temperature across the modules' surface was measured and recorded using a TENMA 72-823 IR Thermometer. The temperatures differ approximately 0.3°C from the centre to the edges of the elements.

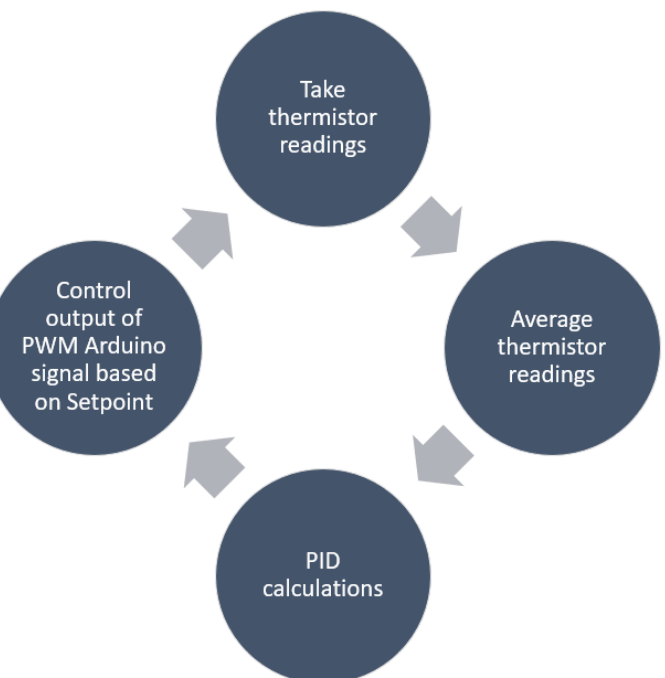
For the evaluation of the accuracy of the thermistor, the abovementioned thermometer was once again used. Tests involved measuring the temperature of the table using the thermistor and then the thermometer. The result of the thermistor was on average 0.25 °C lower than the temperature measurement taken with the thermometer.

Electronic circuit

The electronics circuit consists of 6 small circuits, *Figure 52 Feedback control chart*

three for the heating elements and three for the temperature sensors and all connected in parallel. Circuit diagrams were created in Fritzing.

A commonly used technique to drive a load is to use a MOSFET such as an N-type MOSFET. The gate of a Logic-level MOSFET is connected to the PWM pin on the Arduino with the drain and source connections on the MOSFET connected to the Peltier modules and ground respectively. The working principle is as follows, when a voltage is applied from the PWM output pin (gate) to the ground (source), current is allowed to flow between the Peltier modules (drain) to the ground. MOSFETs are essentially variable resistors controlled by voltage and therefore, depending on the voltage applied to the gate and source, the resistance of the drain and source will vary. With low voltages at the gate, the resistance at the drain is very high. As the voltage increases at the gate,



a threshold voltage is surpassed and the resistance at the drain decreases rapidly allowing current to flow. By adjusting the PWM output, the current allowed to flow through the Peltier modules can be controlled and therefore, the temperature of the Peltier modules is also controlled. There is also a pull-down resistor before the gate to keep the gate at zero volts if the Arduino pin is not configured for output. In other words, the MOSFET is kept off when the processor is booting and has not yet set the pins correctly.

For the sensor circuit, a 10kΩ thermistor was used. Thermistors work by measuring resistance, but the Arduino UNO cannot read the resistance hence, it reads the voltage via the analogue-to-digital-converter. In the case of the presented system, a 10kΩ resistor is used. The resistor was connected to the voltage supply from the Arduino and the other end was connected to the thermistor pin and the other to the thermistor ground. The Arduino voltage used was the 3.3V instead of the 5V as when using the analogue pins of the microcontroller the results are 'noisier'. Hence, by using the 3.3V, a secondary filter is activated in the Arduino ensuring most of the time better readings. The 3.3V is connecting it to the analogue reference (AREF) of the microcontroller so that it can be used as the Vcc voltage (is set in the code). Then by taking many readings in a row for the thermistor and averaging them, better results can be achieved, and the 'noise' is reduced.

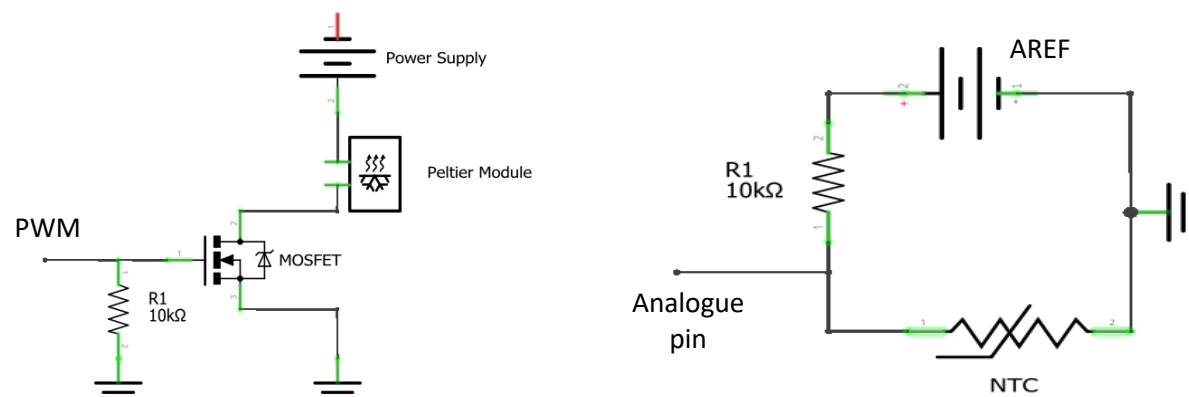


Figure 53 Peltier module driving

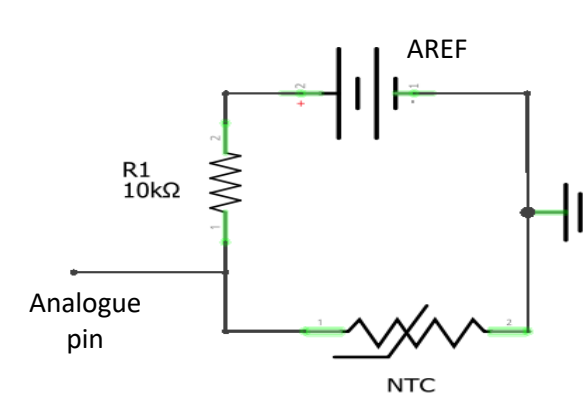


Figure 54 Thermistor sensor circuit.

The final circuit diagram, that fully integrates all three Peltier modules and thermistors can be viewed in Appendix E.

Final Thermocycler Evaluation

PID

To control the temperature of the Peltier modules, the principle of PID previously mentioned (in background section) was programmed using Arduino. The cycle shown below explains the process for our PID controller.

Tests for PID were conducted with just the Peltier modules and thermistors assembled with no surrounding insulation except for air. They were set 10 mm apart in order to be similar to the final thermocycler design. The temperature change over time was also recorded and the results of the PID implementation to achieve three set temperatures (95°C, 55°C, and 72°C) are shown in the graph below.

The results indicate that for the set temperatures of the 55°C and 72°C, the time taken for the Peltier modules to stabilize at said temperatures are approximately 40 seconds. The 95°C set point took longer, about 150 seconds to stabilize. This is because at high temperatures, the temperature difference of the Peltier modules to the surrounding air is very high and therefore, more heat is lost to the environment and the Peltier modules tend to cool down. Hence, the PID takes a longer time to stabilize at 95°C. It is expected that a better result would be seen once the fully manufactured and assembled thermocycler was tested. Note that this analysis was conducted using four 18650 3.7V 20A lithium ion batteries in series as the power supply.

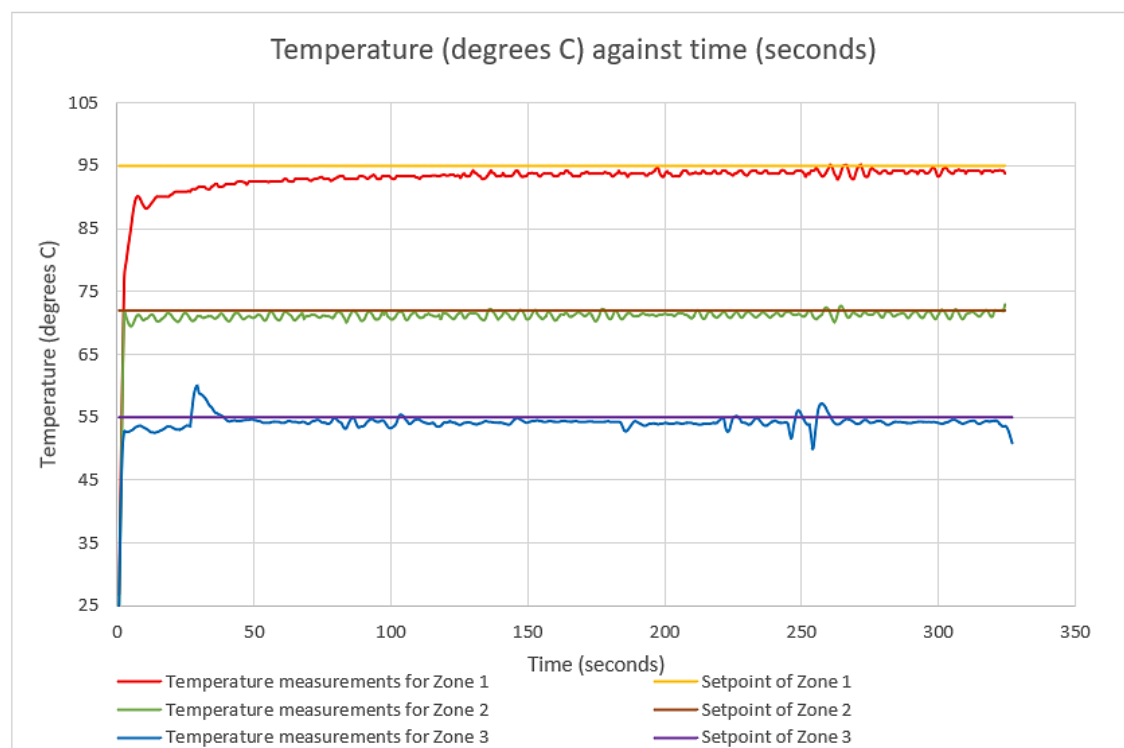


Figure 55: Temperature of the Peltier modules over time using a PID controller.

Thermal Analysis

Time-dependent thermal analysis was conducted in COMSOL on the thermocycler design setup to evaluate any shortcomings of the design. The thermal analysis was set up so that only heat transfer through solids was considered. This means that no surrounding ambient fluid like air was modelled and taken into consideration. The Peltier modules were modelled as a heat source with an initial temperature already at the desired value (95°C, 72°C, 55°C) meaning that this analysis assumes that the Peltier modules have already reached their desired temperature and only solves the time it takes for the cartridge at the top to heat up. The tubing and fluid in the cartridge are assumed to be negligible and geometries such as the “wings” of the cartridge are removed for a simplified model. The results are shown in the figures below.

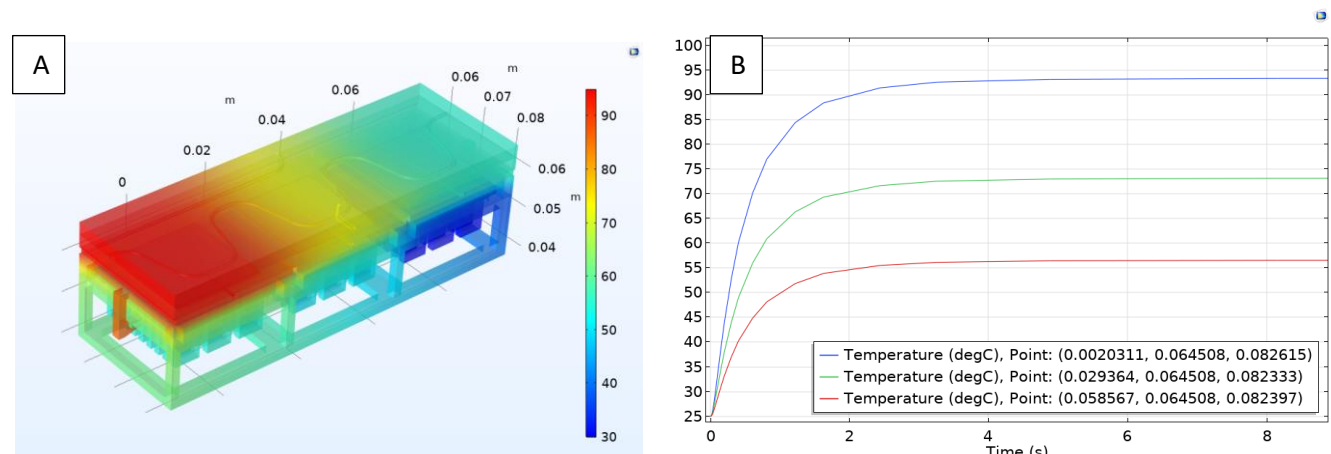


Figure 56 (A) COMSOL thermal analysis results of the thermocycler and (B) the graph of temperature of the cartridge on top over time.

Three locations on the cartridge representing each zone was probed to understand how their temperature changes over time. As can be seen in the graph, the probes take approximately 6 seconds to reach the set temperature. Their final temperatures are also $\pm 1^{\circ}\text{C}$ of the set temperature but still remain in the safe range for

a successful PCR and proves at least in simulations that this design is viable. Unfortunately, due to university restrictions and time constraints, the thermocycler could not be manufactured and tested in real-world situations.

After running both tests for PID and the COMSOL thermal analysis, it can be concluded that the total time taken for all three temperature zones to be reach its' final temperatures is approximately 156 seconds (150 seconds from PID and 6 seconds from thermal analysis). It should be noted however, that these tests were conducted under non-final design setups (PID tests) and in an ideal environment (thermal analysis). Therefore, tests in real world conditions are crucial in realizing the potential of this design and should be conducted in the future.

Power consumption

The theoretical calculation for the power consumption of the thermocycler was completed. The system as mentioned consists of two parts, the thermistors circuits, and the Peltier modules circuits. The thermistor power consumption is calculated considering that the resistance (R) for each thermistor is $10\text{k}\Omega$ and the voltage (V) flowing through each of them is the 3.3V from the Arduino UNO. By using Ohm's law, the current, I can be found:

$$I = \frac{V}{R} \quad (2)$$

Hence, the power consumed by each thermistor is simply

$$P = V \times I \quad (3)$$

And gives $1.089 \times 10^{-3} \text{ W}$, hence all thermistors use $3.267 \times 10^{-3} \text{ W}$.

The theoretical power consumed by the Peltier modules is calculated considering the resistance of the Peltier modules which based on the datasheet is $0.65\Omega \pm 15\%$ for each, the voltage of the battery which is 11.1V and the voltage of the drain of the MOSFET based on the PWM signal. The current was calculated using Ohm's law again. Hence, the power consumption of each Peltier module depends on the PWM. In comparison to the thermistor, each Peltier uses a lot more current thus its impact on the system is negligible.

PWM (%)	Power (W)
0	0
50	33.08
100	46.92

Table 11: Theoretical values of power consumption.

Temperature	Power (W)
95	24.52
72	17.69
55	16.68

Table 12: Experimental values of power consumption.

The experimental method conducted in understanding and calculating the power consumption was to drive the Peltier to a certain temperature and let the PID maintain the Peltier at said temperature. The readings of the PWM output (0 – 255) of the Arduino UNO were noted over the course of a set amount of time (60 sec). Then, the average of 30 readings was calculated and recorded following the temperature stabilisation. That way the average percentage of the PWM used was identified and the power was calculated for each thermal zone using the same procedure as for the theoretical power consumption. The steps were then repeated for other temperature zones to understand the power consumption of the thermocycler as a heating system and the test was repeated twice to check the difference over time. The results are shown below.

More power is consumed when the temperature of the heater is at 95 °C due to the difficulty that the system has in maintaining the temperature. As a result, the PWM turns off once the setpoint temperature is reached and due to the high temperature difference between the Peltier and the ambient temperature, the overall temperature at that point decreases by 1.5-2°C. Then, the PWM turns back on and it is necessary to remain on for a longer period to reach the setpoint again. As a result, depending on the ambient temperature the power consumed changes, thus, to get a better idea of the actual power consumed, further testing needs to take place at various ambient temperatures.

Fluorescence Detector

Background

A fluorophore is a fluorescent chemical compound that can emit light upon exposure to an excitation light. Fluorescence is instantaneous, emitting light when the excitation light is absorbed and ceasing this emission as soon as the excitation light source is removed.

The basic process of fluorescence involves the excitation, excitation state lifetime, and subsequent fluorescent light emission. The absorption of light energy (photons) is absorbed by orbital electrons of the fluorophore compound. This absorption causes the energy levels of these electrons to rise from their ground state to an unstable, excited state. When these excited electrons return to their stable ground state (in a matter of nanoseconds), some energy is lost and is emitted as another photon that has less energy than the absorbed photon. The emitted photon is what forms the fluorescent light. The transition between these different energy states can be described by a Jablonski diagram (Figure 57) [51]

A major tenet of PCR is the link between the amplification of the viral DNA to fluorescent light levels produced, where fluorescent compounds such as SYBR Green I present in the master mix intercalate with the double helix of DNA during the mixing stage. Fluorescence detection is used in PCR to continuously detect the fluorescent levels of the analyte in real time. In the context of our device which is used in a point of care setting, with microfluidic principles applied along with the PCR method, fluorescence detection is integral to diagnose the status of the patient by determining if they have a large concentration of viral DNA present in their sample. The use of droplets within the device lends well to fluorescence detection as it can detect minute quantities of biomolecules in these droplets, allowing for less reagents to be used overall [52].

Design requirements

Table 13: Summary of design requirements for a fluorescence detection unit in device.

Index	Design Requirement
1	Construct a stable housing for detectors' essential components
2	Ensure detector can reliably distinguish between different concentrations of fluorescein/viral DNA
3	Data from fluorescence detection to be transmitted to microcontroller for processing
4	Ensure detector fits the design context of the whole device as a low-cost, miniaturized device.
5	Ensure environmental conditions (dark/stable temperature) in the detector's vicinity is controlled

The overall design of the fluorescence detector in this project is directed by factors such as cost, power consumption and the relatively small footprint of the detector when compared to commercial options.

Material/Component Selection

Detector housing & layout

Fluorescence detector layouts fall into two general categories [53]:

1. Conventional spectrometer types: which employ devices such as monochromators (mirrors) to remove the excitation wavelengths and collect the emission wavelengths

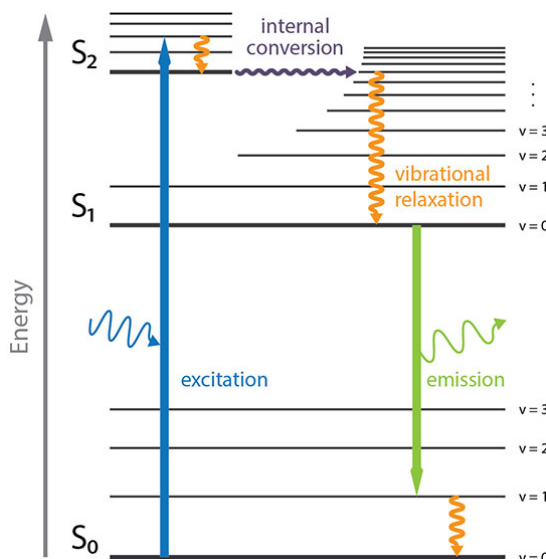


Figure 57: A simplified Jablonski diagram. Blue represents the electron rising in energy levels as a photon is absorbed, and the subsequent emission of fluorescent light. S_0 and S_1 represent the ground state and lowest excited state respectively. Reproduced from Enzo Life Sciences

2. Fluorometer types: Similar in setup to spectrometers, except optical filters are used instead of wavelengths selection devices.

Complex spectrometer designs are not suitable as the cost and size profile defeats the purpose of a small, low cost device for point of care applications. Fluorometer-type setups on the other hand, with cheap optical filters and clever design can be miniaturized. Some designs use a dichroic mirror which serves 2 purposes: to reflect the excitation light onto the sample and act as a filter to only allow the desired emission light spectrum to the detector[54]. However, a dichroic mirror can be excluded entirely when only a single point of detection is concerned [55], as the detector remains static and measures the fluorescent levels of droplets passing through the tube.

An orthogonal layout (Figure 58) was chosen as the most suitable solution for the device, as it allows for the smallest possible system by eliminating the need for a dichroic mirror.

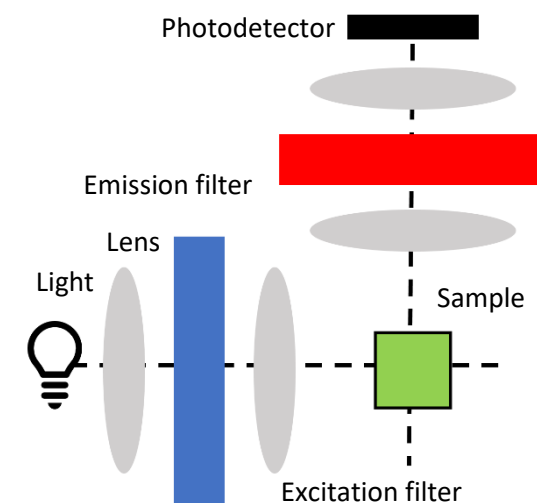


Figure 58: Schematic of a fluorescence detector with an orthogonal layout

Light Source

To observe fluorescence, the fluorophore passing under the detector must be excited by an appropriate excitation light source. Laser excitation remains the gold standard for its ability to produce a focused, high-intensity light beam and is widely used in commercial fluorescence detectors as the narrow wavelength of light emitted from the laser make highly sensitive measurements simple to perform [56]. However, in the context of an easily portable device operated by non-specialists: the high-power consumption, running cost and relatively larger laser system bring more disadvantages than advantages [53].

Recent advancements in light emitting diodes (LED's) have been utilized as the excitation light source in microfluidic applications [57, 58]. LED's present advantages over laser-based excitation with high power efficiency, remarkably low cost, size, working lifetime and a large selection of wavelengths[53].

The main issue with LED's is the broad emission spectrum which introduces noise into the data. To circumvent this, additional optical filters are needed to be added into the orthogonal layout. Compared to a laser, the beam of a LED is much larger. For detecting flow inside a small droplet tube, a compromise was reached by using a simple pinhole cutout to restrict the size of the beam that would reach the tube.

The fluorophore of interest in this device is FITC (fluorescein isothiocyanate) (ThermoFisher Scientific, UK) with a peak emission wavelength of 525nm and a peak excitation wavelength of 490 nm [59].

A 470nm LED (Broadcom, United Kingdom) [60] was used as the excitation light source as it was readily available and close to the peak excitation wavelength of FITC. Using a wavelength lower than the peak excitation wavelength prevents overlap with the fluorescent light while remaining within range of the fluorescein excitation peak.

Optics

The purpose of optical elements within a fluorescence detector setup to ensure only selected excitation/emission wavelengths reach the intended target. As the device is only concerned with detecting one pair of wavelengths from the FITC, the use of 1 low pass filter to include only the emission light wavelength and 1 short pass filter to include only the excitation light wavelength was sufficient for this application. The optical filters considered for a specific application also need to have their cost, size, and performance balanced.

A 510nm long pass acrylic filter (Knight Optics, United Kingdom) was chosen to filter out the excitation light above the pass wavelength and only allow the emission light from the fluorescence too. Similarly, a 500nm short pass acrylic filter (Knight Optics, United Kingdom) was slotted between the LED and the tube carrying droplets to avoid the spectrum of light from the LED being reflected on the tube to the detector. A value of 500nm was chosen for the SPF to reduce the LED light spectrum near the peak FITC excitation wavelength while excluding most of the overlap between the excitation light and fluorescence spectra. Acrylic filters were chosen on the grounds of price and ease of handling as both the filters cost under 50 GBP and could be cut into smaller pieces with a laser cutter.

Sensor

There are a multitude of sensor options for fluorescence detection, and the appropriate sensor must be fit for purpose when factoring in the specific application. Sensor types include photomultiplier tubes (PMT), photodiode (PD), charge-coupled device (CCD), and avalanche photodiodes (APD).

The ideal requirements for a sensor for fluorescence detection in a point of care application is low cost, low power consumption and of a compact size, while not sacrificing its sensitivity. In this device, the parameter measured by the sensor is the intensity of the fluorescent light. Sensors such as CCD's, APD's and PMT's are offer high sensitivity, but must be rejected based on the complexity and significant cost factor involved.

A commonly used photodiode (TSL257LF, ams AG, Austria) [61] (Figure 59) was selected as the sensor owing to its high sensitivity, price (< 1.5 GBP) and physical size. Additionally, stability over a wide temperature range (0 – 85 °C) and low power consumption (similar to LED used; no additional power supply is needed) make it the ideal sensor for this device.

Control & Electronics

An Arduino NANO microcontroller was used for control of the electronic components for the detector. No specialist power supplies were needed as the components used for the detector can be powered from the 5V pin of the Arduino itself, where the digital pins were used to control the LED turning on/off and the analog pin feeding data from the sensor into the Arduino. A MATLAB (The MathWorks Inc, Natick, MA, USA, version: R2019b, platform: Windows 10) script was written to process the voltage signals from sensor, plot it in real time and save it to a spreadsheet for further processing. A button was added to the circuit to ease the collection of data during testing (Appendix C,D) Note: the detector was tested in its own test rig independently of other components that form the device.

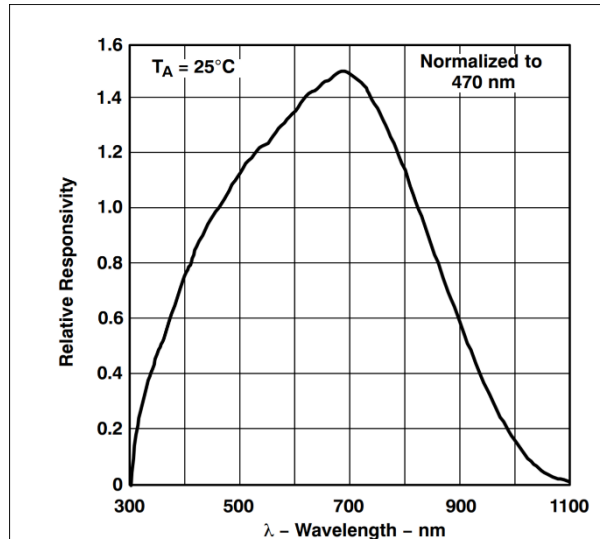


Figure 59: TSL257LF photodiode spectral responsivity, showing good response for wavelengths in the fluorescein spectrum. Image from TSL257LF datasheet.

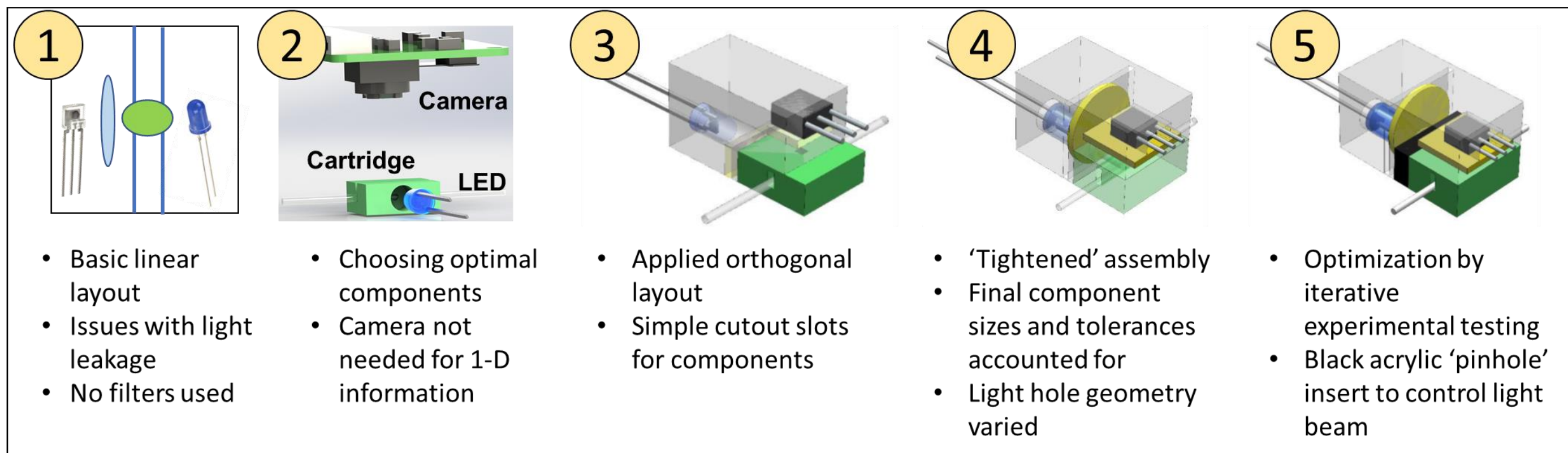


Figure 60: Graphic showing the iterative changes to the fluorescence detector from the initial design to the final design. The green cartridge and tube are not part of the fluorescence detector itself but is shown here as this is how it would interface with the droplet flowing through the tube in the cartridge.

Design Process

Initial Design

Initial designs of the fluorescence detector took inspiration from DIY/open source projects [62] which have established the possibilities for low cost detection of small viral samples using fluorescent techniques. The first concept used a simple approach with the 4 major components of detection: light source, fluorophore, optics, and sensor all aligned consecutively [63].

While effective in some commercial detectors, this in-line layout tends to produce incorrect outputs as too much excitation light may shine directly onto the sensor. This approach was discarded in favor of the orthogonal layout which has the light source and detector perpendicular to each other. At this stage, a CMOS camera was also suggested for detection instead of a photodiode. After consultation with supervisors and further research, a photodiode was chosen as the detection device for its lower cost, reduced complexity, and the fact that only 1 dimensional data would need to be collected.

Development and iteration of the detector

Due to limited access to laboratories throughout the year, the earlier development of the detector focused on proper design to ensure meaningful results could be extracted from the setup, and fewer trial and error iterations to be carried out. The first design applied the orthogonal detection layout with the minimal number of components required. This was done by integrating all the components required for detection into its own housing within the device. The aim of the housing is reliably ensuring the detection apparatus will be in the correct position and orientation as the cartridge is slid into the device. The housing is L shaped with an LED placed at the lower side which has a line of sight to the tube via a hole present at the side of the cartridge. The emission light from the fluorophores is then to be captured by the sensor which has line of sight with the tube via a hole present vertically above the tube. Optical filters are placed after the LED and before the sensor to ensure only the light in the desired wavelength is reaching the fluorophores and sensor respectively.

After a design advice session from Dr Bingyuan Lu who is experienced with fluorescence detection, several adjustments were made to ‘tighten’ the detector assembly by reducing distances and creating a more optimized footprint with less empty space compared to the previous design. Delivery of components such as the short pass filter which was in a different expected shape (circular instead of square) resulted in redesigns of the cutout for the slots for optics. As the SPF was already small and thin, it was decided not to laser cut it to fit the original design dimensions to not alter its optical filtering properties. An adjusted cartridge height from other aspects of the project also required changes to the geometry of the housing, where additional changes were made to the light hole and slot sizes to reflect tolerances when the housing would be 3D printed by Mr Liam Carter..

Initial tests with the previous setup had issues with tolerances of the 3D printed housing such that the components did not fit well into the housing. Furthermore, the light hole responsible for limiting the amount of light entering the tube in cartridge from the LED was too big and resulted in a large amount of excitation light being reflected off the tube into the sensor. The light hole issue was down to the resolution of the 3D printer which could only print holes of a certain size before reaching the limits of its resolution and not printing a proper hole at all. To that end, a ‘pinhole’ was trialed using small holes in the center of a piece of black acrylic cut by a laser cutter by Dr Jonathan West, with much better accuracy than that achieved by the 3D printer. Two designs were tested (Figure 61) with the main idea of using the small pinhole to allow excitation light from the LED, past the short pass filter to reach the tube in a thin, focused beam. To prevent multiple trips to the 3D printer, a variation of pinhole sizes, geometry changes to the housing and light hole geometries were changed to experiment with mix-and-match setups to determine an optimal fit for the final version.

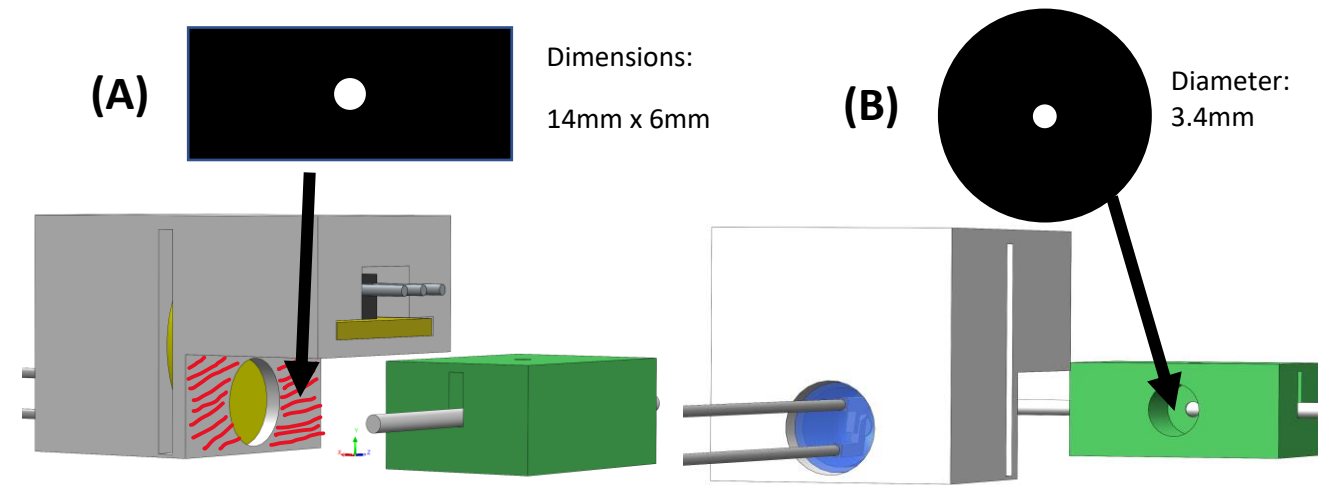


Figure 61: Pinhole geometries tested by laser cutting small holes in the centre of a piece of 3mm thick black acrylic. Design (A) uses a rectangular piece which is sandwiched between the cartridge and the detector housing. The top of the detector is extended by the thickness of the acrylic piece. Design (B) uses a circular cut-out intended to be placed in the circular hole already present in the cartridge for the excitation light to enter.

Final Design

The final design consists of a 3D printed housing with slots for the LPF & SPF filters, LED, and photodiode. The rectangular design for the pinhole acrylic was chosen with a pinhole diameter of 0.3mm (chosen after trial and error).

Design validation

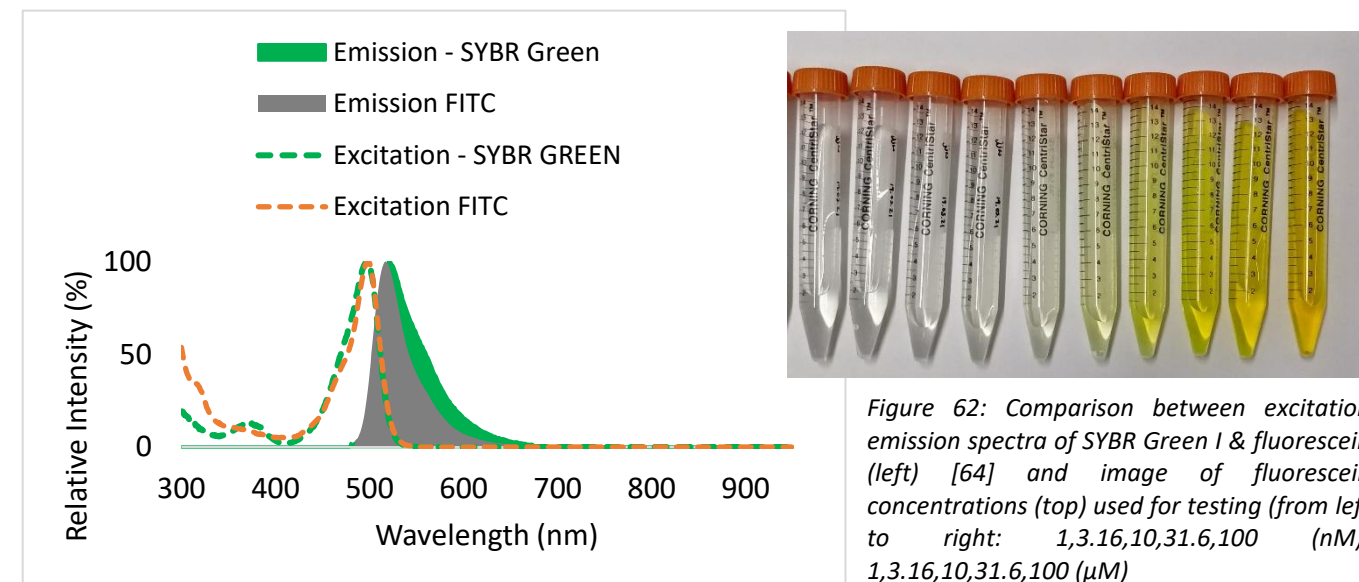


Figure 62: Comparison between excitation emission spectra of SYBR Green I & fluorescein (left) [64] and image of fluorescein concentrations (top) used for testing (from left to right: 1, 3.16, 10, 31.6, 100 (nM), 1, 3.16, 10, 31.6, 100 (μM))

Method

The final design had to be validated for its effectiveness in measuring and distinguishing between different concentrations of viral DNA. Ideally the design would be validated against a viral sample intercalated with fluorophores present from the master mix. However, university closures did not allow for this to be done easily and a fluorescein dye (FITC) comparable to a DNA + intercalator (SYBR Green I) was used instead as it was easier to handle for testing at home. A series of 10-fold dilutions of FITC in 1x phosphate buffered saline (pH 7.4) was prepared by Dr Jonathan West producing 10 concentrations to work with: 1, 3.16, 10, 31.6, 100 in both nanomolar (nM) and micromolar (μM) concentrations

Round 1

Using the final design, a first round of testing was carried out. The main structures of the detector, the housing, pinhole, and cartridge (a piece was 3D printed to simulate part of the cartridge) were put together and held by tape for easy assembly/disassembly. The short pass filter was then carefully slotted in and upon ensuring it was in place, the sides of the hole were covered with tape too. A simple cardboard piece with a cutout the same footprint as the detectors' served as a steady base during experimentation. The LED, long pass filter and photodiode were inserted into their respective slots, with the photodiode being supported by a cap to ensure the sensor on it is horizontal and not at angle to the filter. The tube (0.5mm ID x 0.35mm wall, silicone, Hilltop Products UK) was then carefully inserted into the cartridge channel.

Once the tube was in place, the lights were turned off and a syringe with a needle attachment was used to take a small volume (approximately 0.3ml) of FITC. The MATLAB script was started, and FITC solution was passed through the tube by pushing the plunger of the syringe at a slow, consistent speed. Once the plunger was fully depressed, the MATLAB script was halted by the push of a button and data collection stopped.

The tube was extracted and washed by passing water through it via a syringe and dried. The process was then repeated for fluorescein of different concentrations. Concentrations in the nanomolar range were not used, as the detector could not discern them from background noise during initial setup and testing.

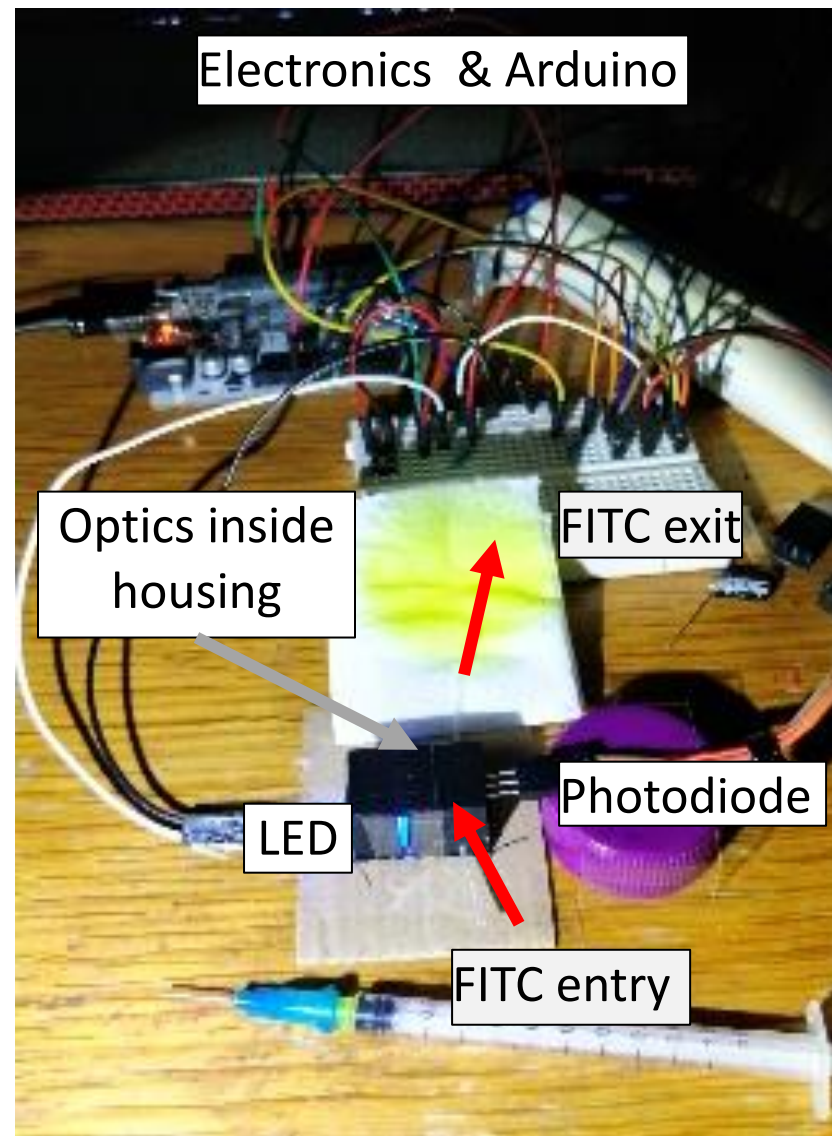


Figure 63: Testing setup used for Rounds 1 and 2. Syringe was used to push fluid through the detector.

Round 3

A droplet maker provided by Prof Niu's research group was used to verify and analyze the detector's capabilities of measuring fluorescence levels in droplet flows. A syringe was used to pull FC40 oil and selected concentrations (10, 31.6, 100 μM) of FITC through the detector.

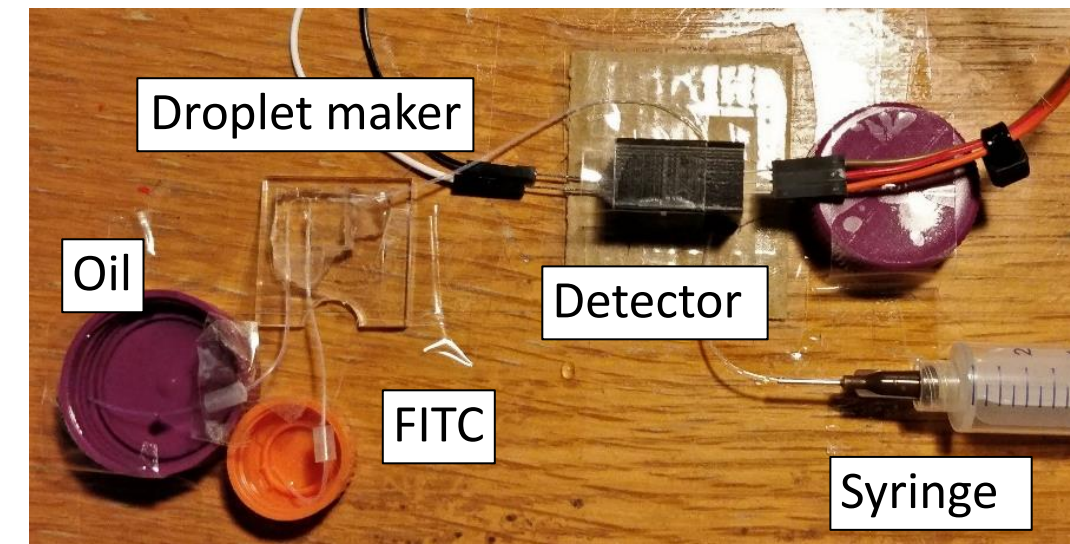


Figure 64: Testing setup used for Round 3. Note the droplet maker. Syringe was used to pull oil and FITC through the droplet maker.

Results

Round 1

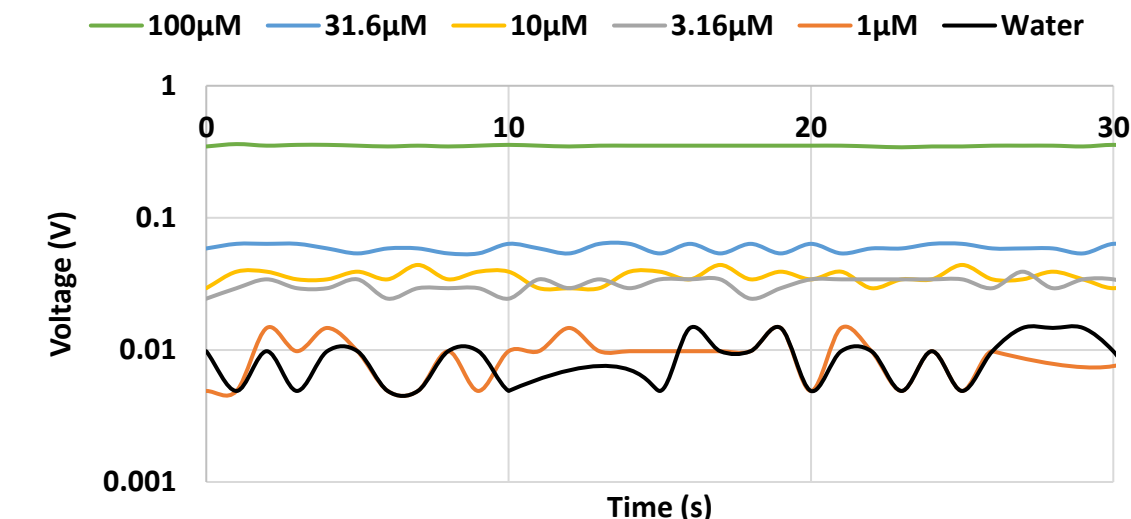


Figure 65: Plot of voltage against time for 5 different concentrations of fluorescein from Round 1 data.

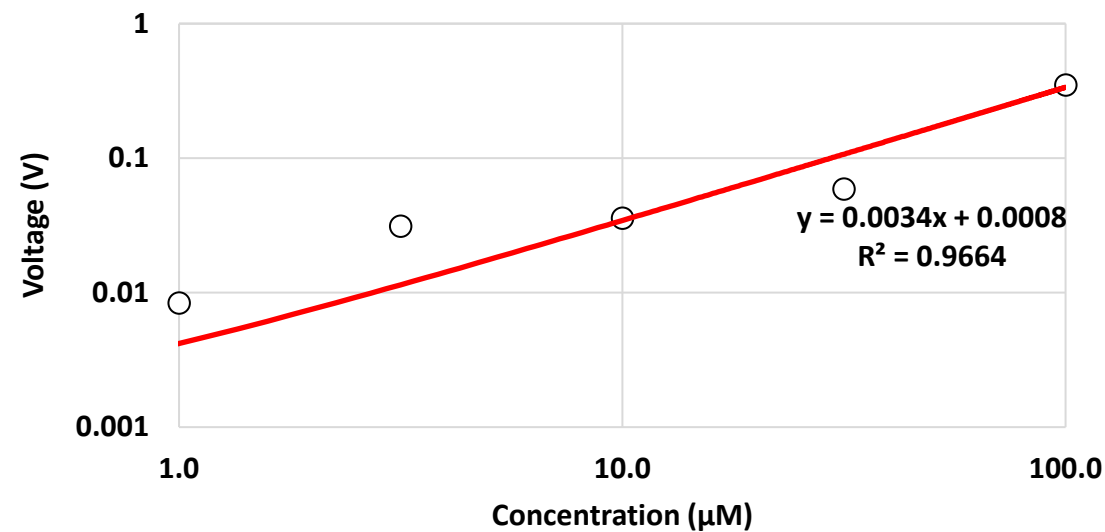


Figure 66: Plot of voltage against concentration for Round 1 data. A best fit linear relationship is shown.

Results from continuous flow experiments in Round 1 show the differences in voltage for each concentration recorded over a period of time (Figure 65) and the linearity of the relationship between voltage and concentration (Figure 66).

Round 2

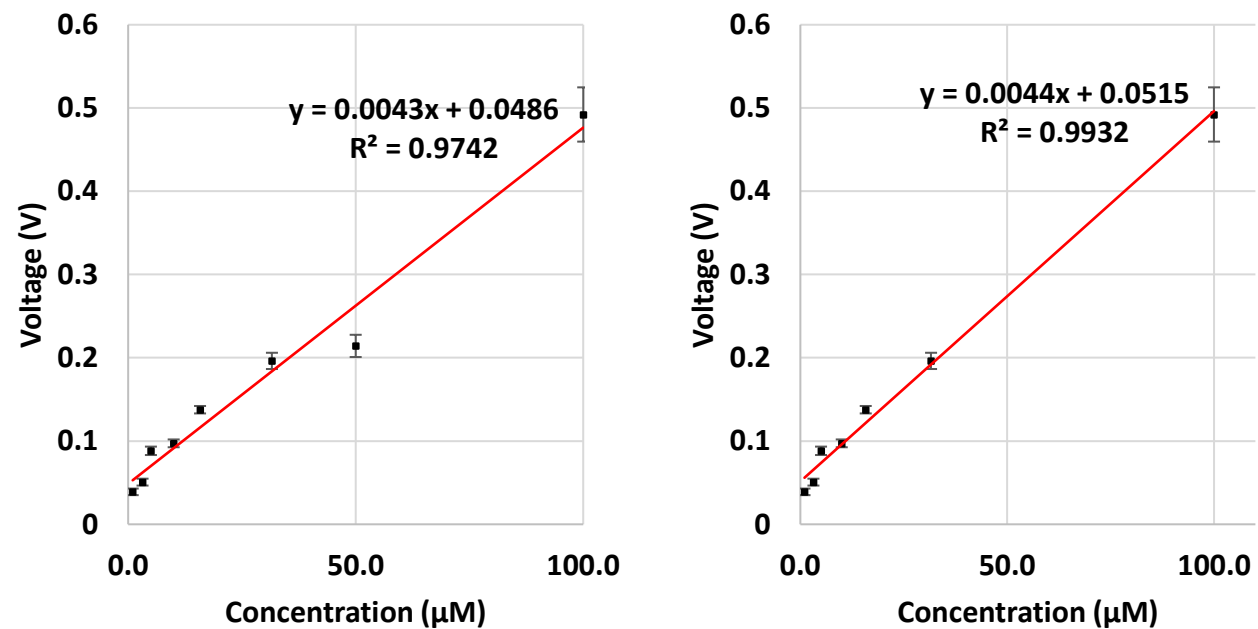


Figure 67: Round 2 data with (left) plot of voltage against concentration for all concentrations and (right) with the 50 μ M concentration removed.

In Figure 67 the 3 repetitions for each concentration tested are GROUPED, with mean shown and standard deviation as the error bars. Concentration of 50 μ M was removed, showing the change in R^2 from 0.9742 to 0.9932.

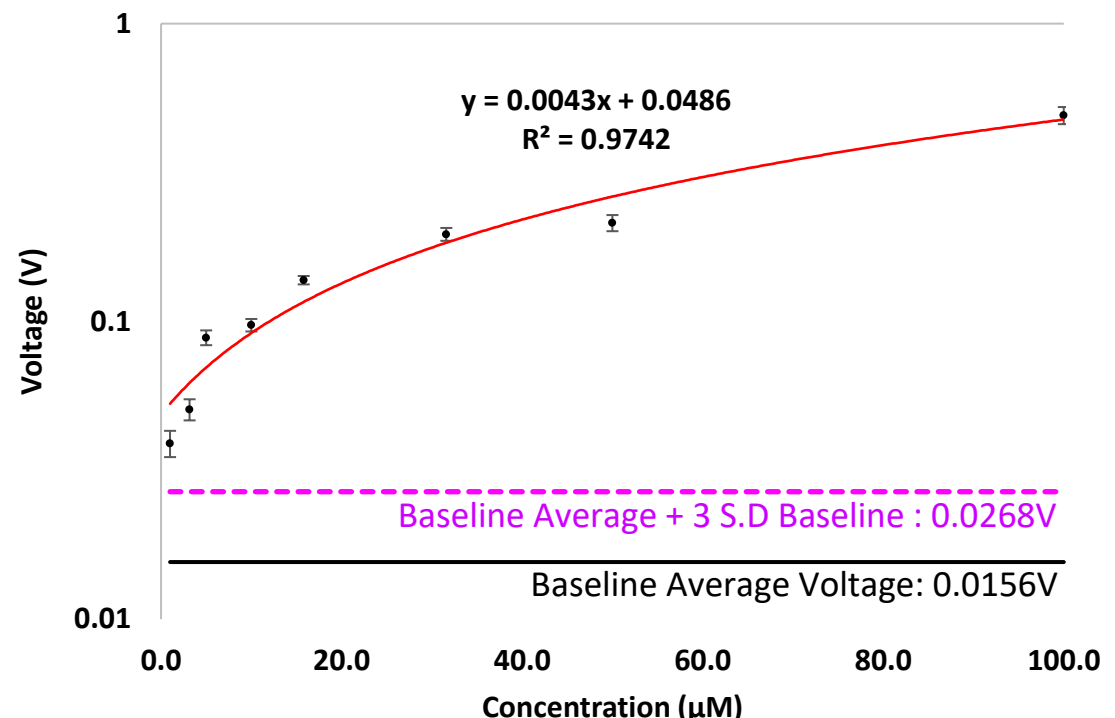


Figure 68: Round 2 data (all concentrations) shown with a log Y axis. Baseline mean ($n=3$) : 0.0156V; Baseline standard deviation : 0.00375, Baseline SD \times 3 : 0.01125. Pink dashed line represents mean of baseline + 3 standard deviations from the baseline

Limit of detection (LoD) for the detector was calculated using Equation (4) [65], which gave a limit of detection of 0.0268V, which when plugged into the linear equation in Figure 68 to obtain the fluorescein concentration results in an LoD of 0.05 μ M to 4 decimal places.

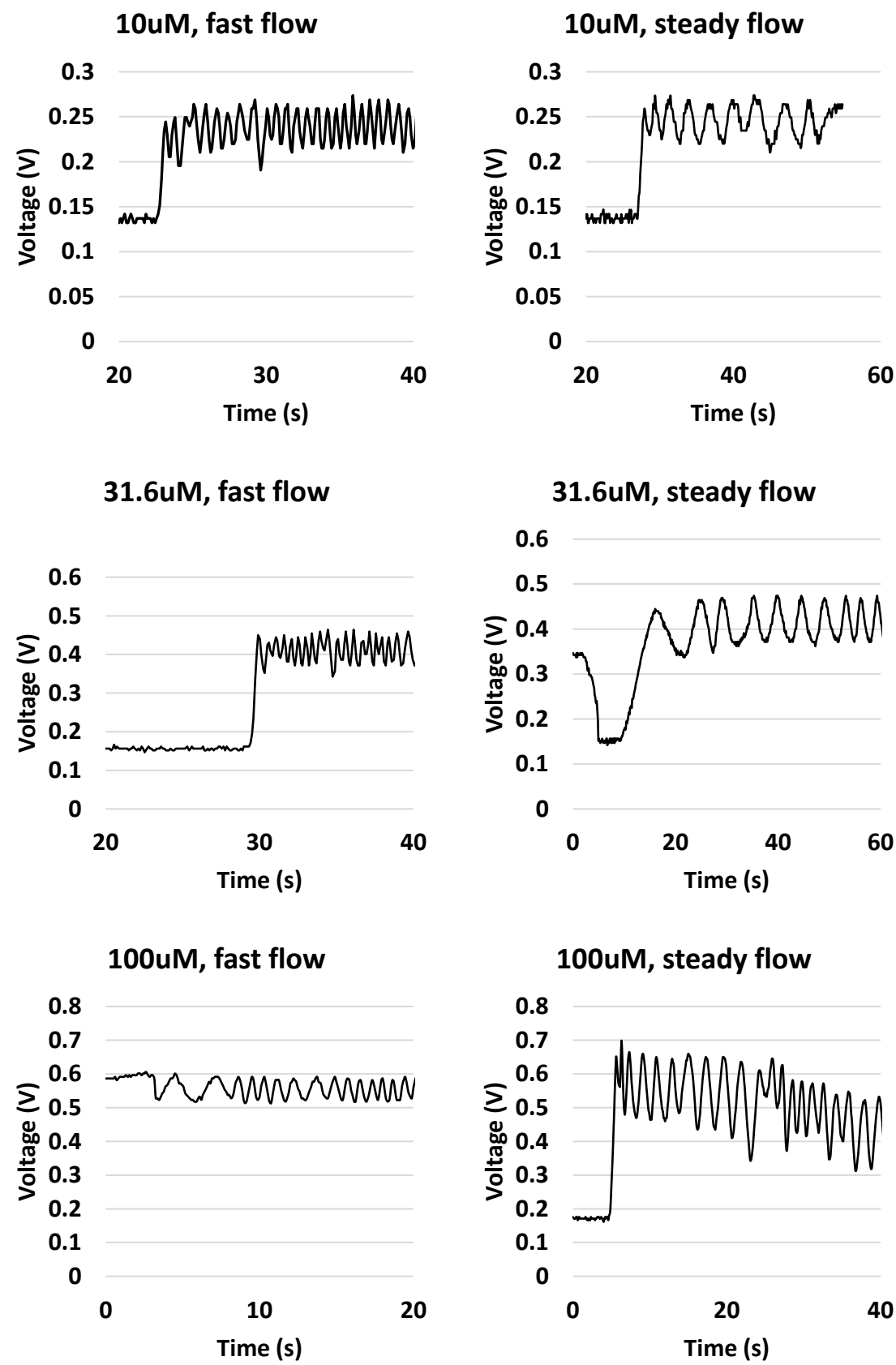
$$LoD = \text{Mean Voltage}_{\text{Blank Sample}} + 3 \times SD_{\text{Blank Sample}} \quad (4)$$

Round 3

The frequency of the change in voltage increased when the flow of droplets through the detector was fast. Results are shown for a fast flow of droplets and a steady flow of droplets, where this flow rate was manually controlled by pressure applied on the syringe.



Figure 69: Image showing droplets flowing from droplet maker into the detector.



Discussion of fluorescence results

A fluorescence detector was designed, built, and tested for use in a miniaturized setting for POCT applications. The design tested in this study shows some promise with a high linearity ($R^2 = 0.9932$ if erroneous measurement is discarded) for continuous flow. The response of this detector does not match those found in the literature ($R^2 > 0.995$) [55, 66, 67], most likely due to the ad hoc setup of the detector. The concentration of 50 μM had to be removed, as it skewed the results too much due to a dilution error in the during at-home testing.

The limit of detection was calculated to be 0.05 μM but should approached with caution as the full range of the sensor's voltage was not utilized (0 – 5 V), and a small range of the y axis could have contributed to this linearity. When compared to those found in literature it did not have high levels of detection as more expensive components such as high sensitivity sensors were used [68]. The cost of these lasers, sensors and advanced optics stray away from the concept of a small, cheap miniaturized device. Despite the current not being currently able to reach detection limits, it does show that it can get close to it, and further iterations in a proper lab setting are required enhance the detector's performance. Additionally, as costs and sizes of the more advanced sensors such as APD's decrease over time, a miniaturized detector with high sensitivity could be achieved with the current design.

The detector was also tested for its ability to detect droplet flows, by making use of a droplet chip and oil to create fluorescein droplets. Droplets were not uniformly spaced (due to issues with the droplet chip, it was an old spare with some defects in the inner tubing) but data obtained clearly shows the detector registering individual droplets with the up/down spike of voltage readings for both fast flow of droplets and a more steady, controlled flow when the pressure on the syringe was manipulated. The tight spacing of the droplets (Figure 69) also added noise to the signal and prevented the signal from going to the baseline after detecting a single droplet as the next incoming droplet was too close and would start to fluoresce (Figure 71). The use of a pump and good droplet chip could have controlled the separation between droplets better and provide a consistent flow rate compared to a syringe. However, this does not pose a significant issue when it comes to the performance of the detector, as a similar number of DNA molecules would be expected to be present in each droplet and the readings would be averaged (or only peak readings taken) for analysis.

Due to university closures, all parts of this fluorescence detector was constructed at home with available material and limited manufacturing resources. Additional items such as a lens to focus the light onto the sensor were not tested owing to limited manufacturing opportunities. The use of relatively cheap components could have also affected the results provided by the detector, e.g. acrylic low pass and short pass filters could have been replaced with higher quality glass filters, though this is expected to hit a cost ceiling as well. Little design wiggle room was left to test alternate design philosophies such as different sensor angles with the increased lead time between getting a design out and testing the final component.

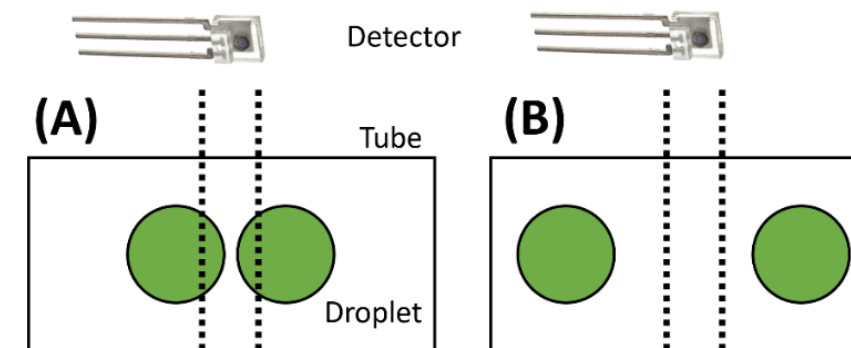


Figure 71 Graphic showing how a tight spacing of droplets (A) excites the incoming droplet as soon as the outgoing droplet leaves the detection area, preventing the signal from hitting baseline values. (B) shows an optimal droplet spacing

Figure 70: Round 3 data with droplet flow for select concentrations at steady/fast flow rates. Baseline voltage approximately 0.15 V.

Final Design

The device is essentially two parts: a cartridge and a box/housing for components and electronics. The cartridge is where the sample of the user is processed.

Cartridge

The 3D printed PVDF cartridge is 180×95×6mm in size and contains channels that allow for the sample fluid to flow by using a total of four pump beds. The pump beds have a compression spring attached to them that is used to engage the pump beds on motor heads to begin fluid flow. These pump beds can be seen and are exposed on the bottom side of the cartridge. On the top side, a blue sticker covers the sample collection reservoir hole where the user deposits their sample.

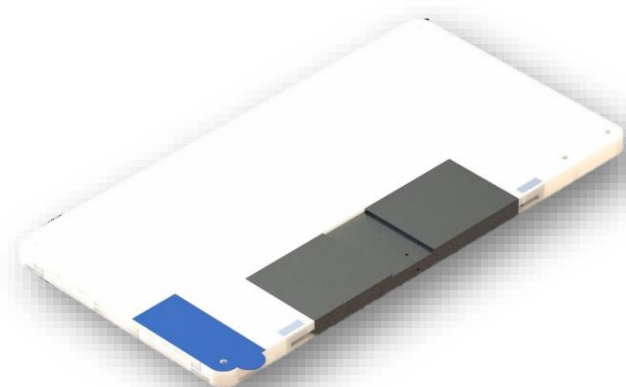


Figure 72: Cartridge

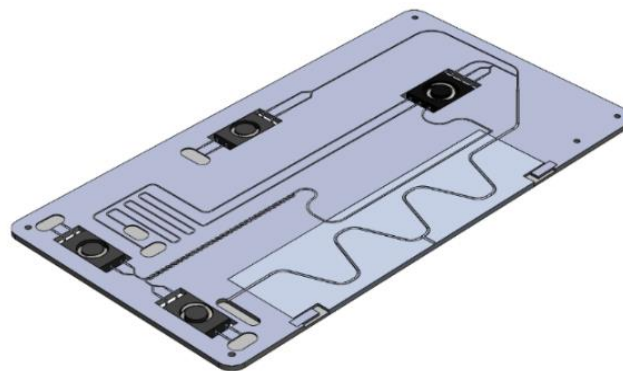


Figure 73: Cross section of cartridge

This reservoir connects to a pump bed and the samples and MicroLYSIS solution are driven to individual Y-junctions before they enter a Y junction which mixes the two fluids. This mixture then flows into the micromixer to ensure that the sample and MicroLYSIS solution are completely mixed and enters the thermally conductive material of the cartridge for heat treatment. The fluid continues to another pump bed and junction where the heat-treated solution is mixed with the PCR master mix and segmented into droplets by interspersing with oil. The droplets then re-enter the thermally conductive material to begin the process of PCR. The droplets oscillate throughout this section of the cartridge for 35 cycles. A hole on the side and top of the cartridge (Figure 72) is for fluorescent detection. After PCR, the fluid then enters the waste reservoir. The cartridge also consists of five alignment pin holes that are fitted to their corresponding pins on the device to ensure that the cartridge can only be inserted in one orientation, which minimizes the possibility of improper user insertion. The way the cartridge is designed and manufactured, and by placing more expensive components in the casing, makes the cartridge cheap and disposable.

Casing/box

Our final design of the casing of the device can be split into two halves; the lid and the base made out of PPSU (Polyphenylsulfone) and manufactured via injection moulding. PPSU is not only high-temperature resistance but is also a dimensionally stable material with high toughness. PPSU is commonly used in medical instrument component applications making it ideal for our project. The lid consists of the LCD touchscreen that the user will use to interact with the device. The lid also houses the fluorescent detection components. The lid, for the most part, is hollow with aluminium beams spreading across the surface area of the lid providing structural integrity and preventing any flexing of material that could damage components and/or the device casing. The aluminium beams and any exposed wiring from the fluorescent detector and LCD touchscreen are covered by a layer of plastic fitted by screws in each corner of the lid, protecting the wires from the possibility of damage. The wires are fed into the base via a cable protector located in the corner of the device. The base is where electronics such as the thermocycler, motors for pumping, and microcontroller are located. The four motors and thermocycler are strategically placed within the base to match the placement of the pump beds and conductive material (for PCR) on the cartridge. The extruded parts

at the bottom of the base (Figure 74) are 3D printed using PVDF upwards on the PPSU base where it merges with components such as the thermocycler's PVDF frame. The five alignment pins can also be found in the base. On the back of the base locates the power switch that activates the device and a vent to allow cool air to enter the base to cool down the thermocycler. The microcontroller fitted in the corner of the base away from any moving parts and radiating heat from the thermocycler. Beneath the abovementioned components, sit a battery pack that powers the device. This battery pack consists of four 18650 3.7V 20A lithium-ion batteries in series. The reason for a battery pack is so that the device is more suitable and capable for remote testing scenarios. A hole is then cut out from the ceiling of the battery pack cell through the floor of the base to allow wire connections between the batteries and the power switch. This battery pack cell can be easily accessed on the side of the device by removing two screws and removing the cover. This allows the batteries to be removed to be recharged or replaced.

Similar to the lid, the components in the base are covered by plastic. A cut-out of the cartridge shape, holes of the alignment pins, thermocycler, and motor heads are made in this plastic to allow the cartridge to be in direct contact with the components and ensure the cartridge can be placed flush with the surface. The lid and base are connected by two torque hinges rated for a torque range up to 1.5kgf/cm each. This prevents the lid from slamming down and possibly hurting the user or damaging the device. These torque hinges also allow for the lid to stay open while the user places the cartridge into the device. As the lid shuts, the lid is held closed by two toggle latches on either side of the device. These toggle latches attach to the catch plates fitted on the lid and are able to withstand tensions up to 25kg of force. With the lid closed and secured, the cartridge is pushed down onto the thermocycler and motor heads causing the springs in the cartridge to be compressed and the pump beds to be engaged. The fluorescent detector sits along the length of the cartridge. When the diagnosing process is completed, the user is notified on the LCD touchscreen and the user has to simply unlatch the lid, remove, and dispose of the cartridge. The total dimensions of the entirety of the device casing is 250×172×65mm (smaller than A4 paper) making it significantly smaller than conventional PCR machines while still able to integrate extraction and detection method.



Figure 72: Exposed view of box



Figure 75: Closed box

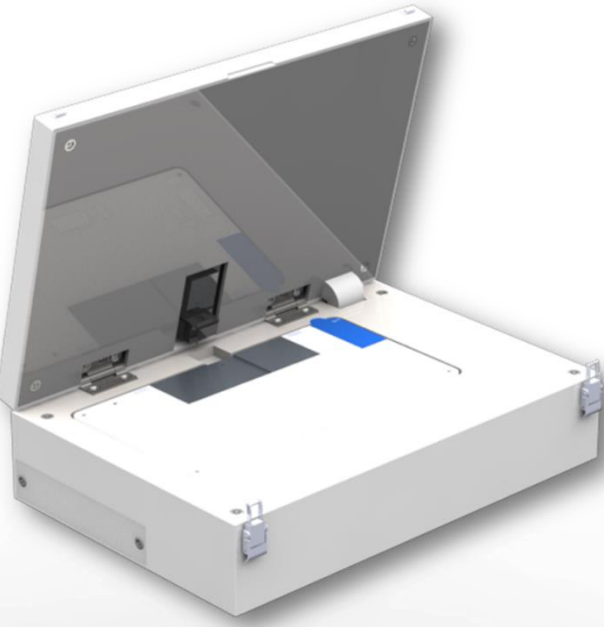


Figure 76: Open box with cartridge

User Process

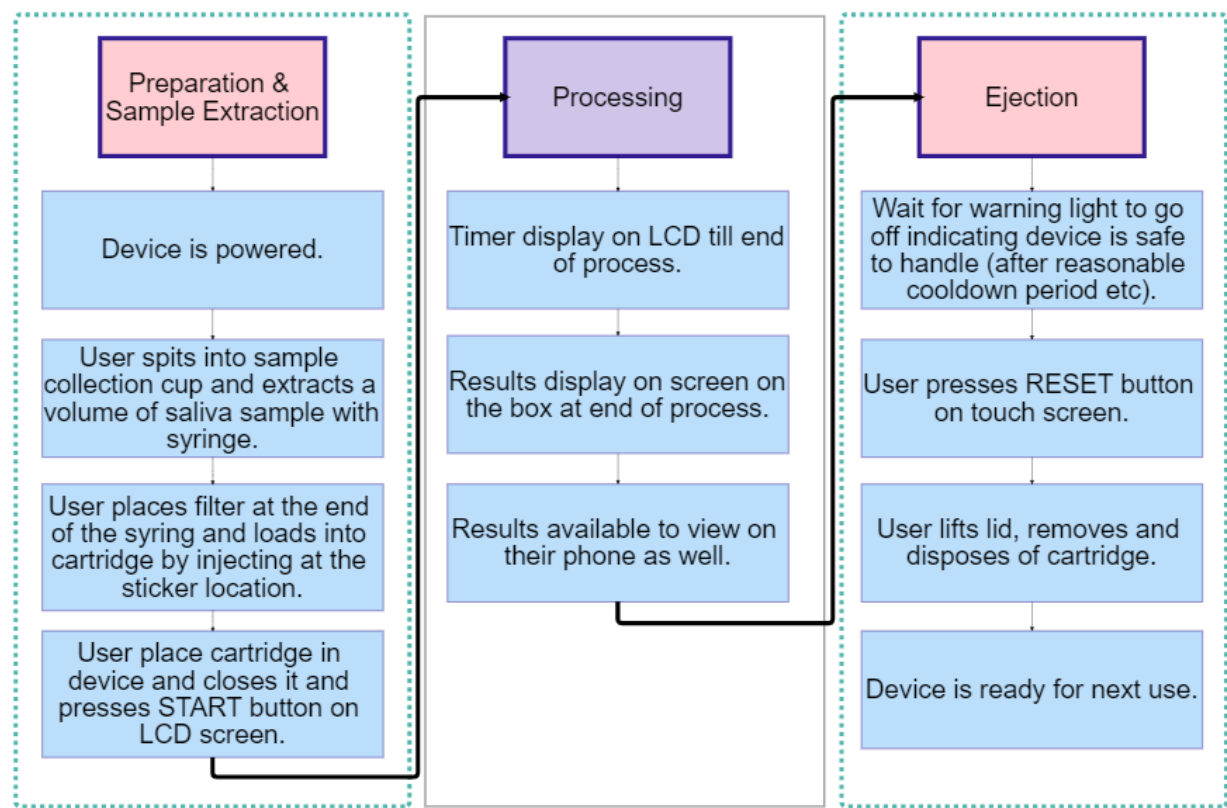


Figure 73: User process flow diagram

The user process can be divided into 3 main steps: Preparation and sample extraction, processing, and ejection (Figure 77). Firstly, the users prepare their sample into a cartridge and place the cartridge in the device for further analysis. During device processing, the user can see the process within the device from the LCD display. Once the warning light is off, the users remove the cartridge and the device is ready for the next use.

System Flow Diagram

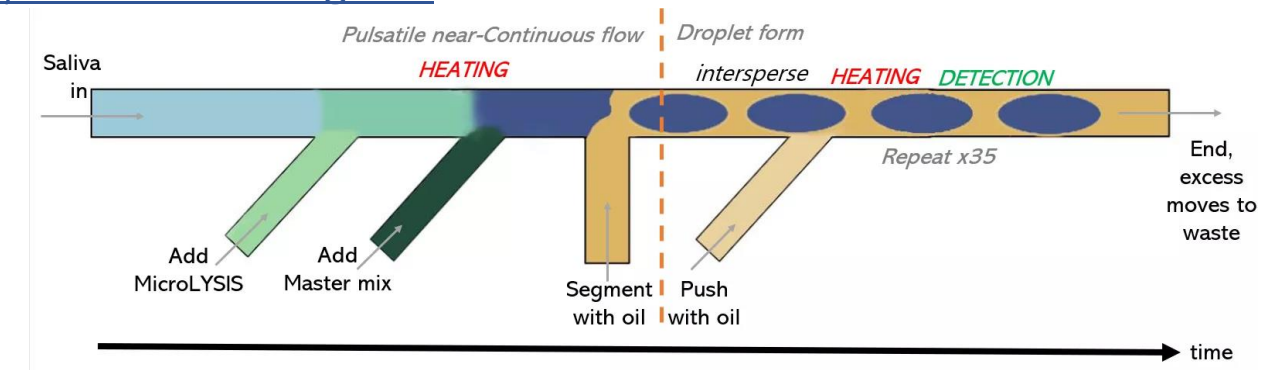


Figure 74: System flow diagram.

After the sample has been added to the cartridge, the sample and MicroLYSIS solution flow a junction where they meet up and flow through the micro mixer for mixing. The mixture then enters the thermocycler for heat treatment at 65°C and 95°C that aids in extraction of the DNA within the sample. The mixture then exits the thermocycler and enters another junction where it is made into droplets and combined with the PCR master mix. These droplets are then segmented by oil for even spacing between them. The oil then pushes the droplets

to re-enter the thermocycler for the heat treatment of the PCR process. The droplets move from the 95°C zone to the 55°C zone then finally to the 72°C zone where the fluorescent detection will detect the fluorescent levels of the droplets. This cycle then repeats for a maximum of 35 cycles and is achieved by utilizing oscillatory flow, moving the droplet back and forth between zones. After the PCR process, the droplets finally flow to a waste reservoir.

Project Review

The project outputs, aims and objectives were all achieved using a variety of skillsets to design, manufacture, prototype, analyse, and test different components that build the foundation of the project. The group conducted extensive research and literature reviews to identify and understand the what is needed in the scope of the project. Following this, designs for each subsystem of the device was conceptualized and critically reviewed to improve where possible making each design iteration better than the last. CAD models of the cartridge, casing, and the respective subsystems were made and thoroughly analysed. Simulations such as flow, mixing, both steady-state and transient thermal analyses were conducted to ensure the viability of these models. Although university restrictions were still in place, making manufacturing and further real-world testing of the subsystems considerably more difficult, the team however still managed to produce working prototypes with the help from the supervisors, lab technicians, and other academic staff. These prototypes were then used to run tests to gather data and information that is able to provide a better understanding for the functionality and viability of the device. Although the final assembly of the device could not be made and system integration was not conducted, the team nevertheless managed to provide sufficient evidence from the working subsystems for proof of concept of the device.

Innovation

A design for a fully integrated cartridge-in-a-box device that consists of sample collection, mixing, NA extraction, microfluidic droplet generation, thermal cycling and fluorescence detection was successfully created. This design is also relatively small in comparison to conventional PCR machines and considering that this device consists of other process such as extraction and detection. The small form factor of this final design enables the device to be portable and compact. The success of this design concept relied on innovative thinking to overcome issues that would normally prohibit these subsystems from working together in such a device. Designing a cartridge that is able to fit the chemical reservoirs and pump beds for means of driving the fluid further demonstrated the group's ability to apply theoretical knowledge and understanding to develop innovative solutions and ideas. By designing the pump beds and motor heads to peristaltically pump the fluid through the cartridge into the subsystems of the device, the group managed to achieve a cartridge that only requires downward force to work.

Process

Considering the scale of this project, it is absolutely crucial that a highly structured design process is not only made but followed throughout the design process of this project. This structure allows for the group to produce meaningful outputs at a reasonable rate allowing the project to run as smoothly as possible. Initially, the group was divided up into four sub-groups (fluidics, mixing/extraction, NA amplification, and fluorescence detection) based on skillsets, theoretical knowledge, and interests with each group consisting of one member with the exception of NA amplification. Overall design ideas were conceptualized as a group and each subsystem was tasked to build upon their respective system to satisfy the design criteria of the overall device. Critical deadlines were also set to ensure the team does not lag behind and everyone is on the same track. Each subgroup was also in charge of manufacturing and testing the viability of the subsystem. Following the end phase of the project, the subsystems were then joined together to form a fully integrated device.

Communication

Communication among the group members is crucial in any group project. Group members require the ability to effectively communicate ideas, designs, solutions and also problems throughout the entirety of the project. This communication was conducted via online meetings, text channels, and in person following the required social

distancing guidelines. The group also took advantage of cloud-based systems to not only store any info that can then be accessed by any other member at any time but to also work on documents such as presentations and reports at the same time. Communication to people outside the group such as the supervisors is also crucial in communicating the outputs and issues that the group faces to them. The supervisors can then provide guidance to the group for a way forward that ensures the group is always progressing. This communication can also be through media such as CAD models, renderings, schematics, figures, and tables to provide substantial information that allows both technical and non-technical audiences to fully comprehend what this project is able to produce throughout the process.

Pros and Cons of Current Design

Our current design uses the cartridge and the droplets approach so only micro-volumes of sample and reagents are required. All the necessary components such as thermocycler and pump are implemented on the device as well as reagents are prepared within the cartridge as well as the cartridge is disposable. Therefore, it is simple for the users to run the test. The overall size of the device is approximately 250x172x65mm which is smaller than an A4 paper, so the size is smaller than the normal PCR device and all step are integrated. However, only one test can be run at a time and the total test time has not been identified. The power source of the current design is a battery pack and the thermocycler consumes lots of power so it might need to be changed regularly. The thermocycler design is inefficient for thermal isolation. The manufacture of the cartridge would be 3D printing so the cost is relatively higher than the typical technique such as injection moulding and it can manufacture in a small amount at a time. As the cartridge is disposable, the problem might arise from how to manage the used cartridge. It contains chemicals inside and the waste should be managed properly so it cannot be in the general waste. Another concern is the sample collection. The syringe and the syringe filter was used to transfer the saliva into the cartridge. This is required an additional step from the user, and this may cause contamination.

Achievements

- Successfully designed a fully integrated cartridge-in-a-box concept for a point-of-care setting
- Successfully designed a small form factor device that is compact and portable
- Designed and evaluated a micro mixer that is able to fully mix two fluids together
- Designed and evaluated a thermocycler that is able to reach three distinct temperatures at any given time for PCR process
- Designed a microfluidic flow system that utilizes bidirectional flow
- Designed and evaluated a fluorescence detector that is able to accurately read fluorescent readings from droplet samples.

Limitations

- Due to university restrictions, the group was unable to fully assemble and test the overall device
- Comparison of accuracy and reliability to conventional diagnostic testing could not be conducted
- The times it takes for the entire diagnostic process could not be analysed

Future Work

Overall Device

The next step for this project is to fully manufacture every part and assemble the entire device to evaluate its design. Cost effective assembly will be a major challenge in creating a viable product. Assembly could not be done in time due to university restrictions and limited time. Although the programming for each individual section (pumps, thermocycler, and fluorescence detection) has already been completed, a fully integrated program is yet to be created. This code needs to be written to test the system's functionality as a whole and to ensure that it could work together. The electronics such as the motors, Peltier modules, LED, and sensors from each section as well has not had the chance to be fully integrated together. Due to this, an understanding of whether these components are able to work together cannot be achieved. Other components such as the LCD

screen and power supply has also not been taken into consideration when creating programs and CAD models. General work on the user-friendly interface should also be done to ensure that the steps taken by the user to use this device is as simple as possible and that the results are sent to the user's smartphone and direct to NHS.

Other possible modifications for future work of our device could be increasing the number of sample lines in the cartridge. Allowing for more than one sample to be tested at once. This could significantly increase the throughput of the device making it more viable in more scenarios in the real world. The results of the device should not only be displayed on the screen of the device but sent to the user's smartphone or even to hospitals/clinics/laboratories when used for contact tracing.

Sample collection, fluidics, and mixing

The method of sample collection at this stage is for the user to deposit their sputum in a container and use a syringe to transport the sample into the cartridge. This could cause contamination issues due to possibilities of user error when depositing the sample into the cartridge. Hence, this method of collection can be further refined into a much simpler process to reduce the risk of contamination.

A method or mechanism that can accurately measure the volume of the required sample needed for the entire process is also something that should be considered in the future. This would allow only the required amount of sample into the cartridge and device for processing. This allows for a more reliable set of data as the data gathered is a fixed amount and prevent pumping issues. This mechanism could also detect when insufficient sample volume is deposited and prevent the process from continuing. This would save any reagents from being wasted on an unsuccessful procedure.

The device should also be able to detect if there are leakages in the system as leaks from the cartridge could not only lead to contamination issues but also damaging the electronic components within the system. Pressure sensors could be used to detect the pressure in the flow channels and when there is a drop in pressure, it would show that a leak occurred somewhere throughout the system.

The reservoirs of the cartridge that contains the required reagents such as oil, MicroLYSIS solution, and the PCR master mix need to be redesigned better fitted for use. Air holes or another method need to be added to the reservoirs for an easy method to adding the reagents. Blister packs could be used in the future to accommodate all these issues. Further optimization of space on the cartridge by eliminate any unused space making the cartridge more compact.

Thermocycler

Future evaluations on the heat loss of the thermocycler needs to be conducted to understand how much heat loss to the surroundings and to calculate the thermocyclers efficiency. The measurements done in real life situations can be compared to thermal analysis conducted in software to see where these heat losses occur and potentially resolve them.

A full manufacturing of all components of the thermocycler is definitely needed to run tests in real world environments. These tests would allow us to understand how long it takes for the thermocycler to fully heat up from start to stable levels of temperature. Along with the calculations of heat loss previously mentioned, further iterations can be made to increase the efficiency of the thermocycler and reduce the ramp up time of the thermocycler. Different tests at different room temperatures should also be conducted to measure power consumption at different environments.

Effects of the heat radiating from the thermocycler on the other components of the device should be evaluated to ensure that other components are not affected or damaged. This evaluation would also provide information on how much insulation is needed around the thermocycler from the rest of the device.

Fluorescence Detection

Experimental results obtained from testing of the fluorescence detector should be replicated in a lab setting to avoid e.g. dilution errors and overcome certain limitations faced in tests run at home such as the inability to create very small dilutions accurately. Future testing needs to be done with smaller concentrations of fluorescein to simulate the expected concentration in a single droplet containing a DNA molecule. Regarding the detector itself, a lens should be placed before and after the long pass and short pass filters to focus the LED light beam and ensure the emission light hits the photodiode accurately, as currently only a limited range of the photodiode's full voltage range has been reached. Trials with high performance glass filters could also take place instead of using cheap acrylic filters, so long as the glass filters' shape can be optimized to use the least amount of material, reducing costs in the process. Finally, during testing the photodiode was only placed in parallel horizontally above the tube; in future iterations the angle of the photodetector could be varied by a small range (i.e. 5°, 10°, 15°) to determine if the sensitivity of the detector towards the emission light could be increased by doing so.

Conclusion

In conclusion, the point-of-care device designed incorporates fluidics, NA extraction and amplification (PCR) and fluorescence detection. Manufacture and testing of the overall system are still required, however the device has the potential to contribute in reducing the workload of laboratories in the early stages of future pandemics. Users with no-specialist knowledge will be able to test themselves in the comfort of their own home.

References

- [1] J. J. Speidel, "Environment and health: 1. Population, consumption and human health," (in eng), *CMAJ*, vol. 163, no. 5, pp. 551-556, 2000. [Online]. Available: <https://pubmed.ncbi.nlm.nih.gov/11006767/>.
- [2] N. Madhav, B. Oppenheim, M. Gallivan, P. Mulembakani, E. Rubin, and N. Wolfe, "Pandemics: Risks, Impacts, and Mitigation," 2017, pp. 315-345.
- [3] Y. M. Bar-On, A. Flamholz, R. Phillips, and R. Milo, "SARS-CoV-2 (COVID-19) by the numbers," (in eng), *eLife*, vol. 9, p. e57309, 2020, doi: 10.7554/eLife.57309.
- [4] J. S. Kutter, M. I. Spronken, P. L. Fraaij, R. A. M. Fouchier, and S. Herfst, "Transmission routes of respiratory viruses among humans," *Current Opinion in Virology*, vol. 28, pp. 142-151, 2018/02/01/ 2018, doi: <https://doi.org/10.1016/j.coviro.2018.01.001>.
- [5] R. Carrasco-Hernandez, R. Jácome, Y. López Vidal, and S. Ponce de León, "Are RNA Viruses Candidate Agents for the Next Global Pandemic? A Review," *ILAR Journal*, vol. 58, no. 3, pp. 343-358, 2017, doi: 10.1093/ilar/ilx026.
- [6] S. Durmuş and K. Ö. Ülgen, "Comparative interactomics for virus-human protein-protein interactions: DNA viruses versus RNA viruses," (in eng), *FEBS Open Bio*, vol. 7, no. 1, pp. 96-107, 2017, doi: 10.1002/2211-5463.12167.
- [7] J. K. Taubenberger and D. M. Morens, "1918 Influenza: the mother of all pandemics," (in eng), *Emerg Infect Dis*, vol. 12, no. 1, pp. 15-22, 2006, doi: 10.3201/eid1201.050979.
- [8] E. Petersen et al., "Comparing SARS-CoV-2 with SARS-CoV and influenza pandemics," (in eng), *Lancet Infect Dis*, vol. 20, no. 9, pp. e238-e244, 2020, doi: 10.1016/S1473-3099(20)30484-9.
- [9] B. J. Jester, T. M. Uyeki, and D. B. Jernigan, "Fifty Years of Influenza A(H3N2) Following the Pandemic of 1968," (in eng), *Am J Public Health*, vol. 110, no. 5, pp. 669-676, 2020, doi: 10.2105/AJPH.2019.305557.
- [10] S. Al Hajjar and K. McIntosh, "The first influenza pandemic of the 21st century," (in eng), *Ann Saudi Med*, vol. 30, no. 1, pp. 1-10, Jan-Feb 2010, doi: 10.4103/0256-4947.59365.
- [11] D. D. Hine, "The 2009 Influenza Pandemic: An independent review of the UK response to the 2009 influenza pandemic," 2010. [Online]. Available: https://assets.publishing.service.gov.uk/government/uploads/system/uploads/attachment_data/file/61252/the2009influenzapandemic-review.pdf.
- [12] WHO. "WHO Coronavirus (COVID-19) Dashboard." <https://covid19.who.int/> (accessed 6 May 2021).
- [13] L. Jafri, S. Ahmed, and I. Siddiqui, "Impact of COVID-19 on laboratory professionals-A descriptive cross sectional survey at a clinical chemistry laboratory in a developing country," *Annals of Medicine and Surgery*, vol. 57, pp. 70-75, 2020/09/01/ 2020, doi: 10.1016/j.amsu.2020.07.022.
- [14] F. Squazzoni et al., "Computational Models That Matter During a Global Pandemic Outbreak: A Call to Action," *Journal of Artificial Societies and Social Simulation*, vol. 23, 01/01 2020, doi: 10.18564/jasss.4298.
- [15] S. Griffin, "Covid-19: Lateral flow tests are better at identifying people with symptoms, finds Cochrane review," *BMJ*, vol. 372, p. n823, 2021, doi: 10.1136/bmj.n823.
- [16] M. Johnson-León et al., "Executive summary: It's wrong not to test: The case for universal, frequent rapid COVID-19 testing," *EClinicalMedicine*, vol. 33, p. 100759, 2021/03/01/ 2021, doi: <https://doi.org/10.1016/j.eclinm.2021.100759>.
- [17] C. Atchison et al., "Usability and Acceptability of Home-based Self-testing for Severe Acute Respiratory Syndrome Coronavirus 2 (SARS-CoV-2) Antibodies for Population Surveillance," *Clinical Infectious Diseases*, vol. 72, no. 9, pp. e384-e393, 2020, doi: 10.1093/cid/ciaa1178.
- [18] A. Krüttgen, C. G. Cornelissen, M. Dreher, M. W. Hornef, M. Imöhl, and M. Kleines, "Comparison of the SARS-CoV-2 Rapid antigen test to the real star Sars-CoV-2 RT PCR kit," *Journal of Virological Methods*, vol. 288, p. 114024, 2021/02/01/ 2021, doi: <https://doi.org/10.1016/j.jviromet.2020.114024>.
- [19] T. Notomi et al., "Loop-mediated isothermal amplification of DNA," (in eng), *Nucleic Acids Res*, vol. 28, no. 12, pp. E63-E63, 2000, doi: 10.1093/nar/28.12.e63.
- [20] M. Fakruddin et al., "Nucleic acid amplification: Alternative methods of polymerase chain reaction," (in eng), *J Pharm Bioallied Sci*, vol. 5, no. 4, pp. 245-252, 2013, doi: 10.4103/0975-7406.120066.
- [21] P. R. Sahoo, K. Sethy, S. Mohapatra, and D. Panda, "Loop mediated isothermal amplification: An innovative gene amplification technique for animal diseases," (in eng), *Vet World*, vol. 9, no. 5, pp. 465-9, May 2016, doi: 10.14202/vetworld.2016.465-469.
- [22] M. R. Watts et al., "A loop-mediated isothermal amplification (LAMP) assay for *Strongyloides stercoralis* in stool that uses a visual detection method with SYTO-82 fluorescent dye," (in eng), *Am J Trop Med Hyg*, vol. 90, no. 2, pp. 306-11, Feb 2014, doi: 10.4269/ajtmh.13-0583.
- [23] Roche, "What is PCR and why is it the "gold standard" in molecular diagnostics?," 2020. [Online]. Available: <https://diagnostics.roche.com/us/en/roche-blog/what-is-pcr-and-why-is-it-the--gold-standard--in-molecular-diagn.html>.
- [24] IAEA, "How is the COVID-19 virus detected using real time RT-PCR?," 2020. [Online]. Available: <https://www.iaea.org/bulletin/infectious-diseases/how-is-the-covid-19-virus-detected-using-real-time-rt-pcr>.
- [25] P. Shetty, "The Evolution of DNA Extraction Methods," *American Journal of Biomedical Science & Research*, vol. 8, pp. 39-45, 03/11 2020, doi: 10.34297/AJBSR.2020.08.001234.
- [26] S. Wang, M. A. Lifson, F. Inci, L. G. Liang, Y. F. Sheng, and U. Demirci, "Advances in addressing technical challenges of point-of-care diagnostics in resource-limited settings," (in eng), *Expert Rev Mol Diagn*, vol. 16, no. 4, pp. 449-59, 2016, doi: 10.1586/14737159.2016.1142877.
- [27] A. Ali-Cherif, S. Begolo, S. Descroix, J.-L. Viovy, and L. Malaquin, "Programmable Magnetic Tweezers and Droplet Microfluidic Device for High-Throughput Nanoliter Multi-Step Assays," *Angewandte Chemie International Edition*, vol. 51, no. 43, pp. 10765-10769, 2012, doi: 10.1002/anie.201203862.
- [28] B. Teste, A. Ali-Cherif, J. L. Viovy, and L. Malaquin, "A low cost and high throughput magnetic bead-based immuno-agglutination assay in confined droplets," *Lab on a Chip*, 10.1039/C3LC50353D vol. 13, no. 12, pp. 2344-2349, 2013, doi: 10.1039/C3LC50353D.
- [29] D. Ferraro et al., "Microfluidic platform combining droplets and magnetic tweezers: application to HER2 expression in cancer diagnosis," *Scientific Reports*, vol. 6, no. 1, p. 25540, 2016/05/09 2016, doi: 10.1038/srep25540.
- [30] S.-U. Hassan, X. Zhang, and X. Niu, "Droplet-Based Microfluidics: Formation, Detection and Analytical Characterization," *Research & Development in Material Science*, vol. 11, 09/27 2019, doi: 10.31031/RDMS.2019.11.000774.

- [31] K. C. Neuman and A. Nagy, "Single-molecule force spectroscopy: optical tweezers, magnetic tweezers and atomic force microscopy," *Nature Methods*, vol. 5, no. 6, pp. 491-505, 2008/06/01 2008, doi: 10.1038/nmeth.1218.
- [32] K. Ward and Z. H. Fan, "Mixing in microfluidic devices and enhancement methods," (in eng), *J Micromech Microeng*, vol. 25, no. 9, Sep 2015, doi: 10.1088/0960-1317/25/9/094001.
- [33] C. D. Tsai and X. Y. Lin, "Experimental Study on Microfluidic Mixing with Different Zigzag Angles," (in eng), *Micromachines (Basel)*, vol. 10, no. 9, Aug 31 2019, doi: 10.3390/mi10090583.
- [34] V. Mengeaud, J. Josserand, and H. H. Girault, "Mixing Processes in a Zigzag Microchannel: Finite Element Simulations and Optical Study," *Analytical Chemistry*, vol. 74, no. 16, pp. 4279-4286, 2002/08/01 2002, doi: 10.1021/ac025642e.
- [35] M. Khosravi Parsa, F. Hormozi, and D. Jafari, "Mixing enhancement in a passive micromixer with convergent-divergent sinusoidal microchannels and different ratio of amplitude to wave length," *Computers & Fluids*, vol. 105, pp. 82-90, 2014/12/10/ 2014, doi: <https://doi.org/10.1016/j.compfluid.2014.09.024>.
- [36] A. D. Stroock, S. K. W. Dertinger, A. Ajdari, I. Mezić, H. A. Stone, and G. M. Whitesides, "Chaotic Mixer for Microchannels," *Science*, vol. 295, no. 5555, pp. 647-651, 2002, doi: 10.1126/science.1066238.
- [37] C.-Y. Lee, W.-T. Wang, C.-C. Liu, and L.-M. Fu, "Passive mixers in microfluidic systems: A review," *Chemical Engineering Journal*, vol. 288, pp. 146-160, 2016/03/15/ 2016, doi: <https://doi.org/10.1016/j.cej.2015.10.122>.
- [38] A. Afzal and K.-Y. Kim, "Three-objective optimization of a staggered herringbone micromixer," *Sensors and Actuators B: Chemical*, vol. 192, pp. 350-360, 2014/03/01/ 2014, doi: <https://doi.org/10.1016/j.snb.2013.10.109>.
- [39] Y. Du, Z. Zhang, C. Yim, M. Lin, and X. Cao, "Evaluation of Floor-grooved Micromixers using Concentration-channel Length Profiles," *Micromachines*, vol. 1, no. 1, pp. 19-33, 2010. [Online]. Available: <https://www.mdpi.com/2072-666X/1/1/19>.
- [40] S. Hossain, M. A. Ansari, and K.-Y. Kim, "Evaluation of the mixing performance of three passive micromixers," *Chemical Engineering Journal*, vol. 150, no. 2, pp. 492-501, 2009/08/01/ 2009, doi: 10.1016/j.cej.2009.02.033.
- [41] A.-S. Yang *et al.*, "A high-performance micromixer using three-dimensional Tesla structures for bio-applications," *Chemical Engineering Journal*, vol. 263, pp. 444-451, 2015/03/01/ 2015, doi: <https://doi.org/10.1016/j.cej.2014.11.034>.
- [42] 3DGBIRE. "Ultimaker 3 Extended Tech Specs." <https://3dgbire.com/pages/ultimaker-3-extended-tech-specs> (accessed 6 May 2021).
- [43] A. Enders, I. G. Siller, K. Urmann, M. R. Hoffmann, and J. Bahnemann, "3D Printed Microfluidic Mixers—A Comparative Study on Mixing Unit Performances," *Small*, vol. 15, no. 2, p. 1804326, 2019, doi: 10.1002/smll.201804326.
- [44] A. J. Tudos, G. J. Besselink, and R. B. Schasfoort, "Trends in miniaturized total analysis systems for point-of-care testing in clinical chemistry," (in eng), *Lab on a chip*, vol. 1, no. 2, pp. 83-95, 2001/12// 2001, doi: 10.1039/b106958f.
- [45] A. M. Nightingale, G. W. Evans, P. Xu, B. J. Kim, S. U. Hassan, and X. Niu, "Phased peristaltic micropumping for continuous sampling and hardcoded droplet generation," (in eng), *Lab Chip*, vol. 17, no. 6, pp. 1149-1157, Mar 14 2017, doi: 10.1039/c6lc01479h.
- [46] IHP. "IHP Cartridge heaters 750°C." <https://www.ihpheating.com/cartridge-heaters-750c/> (accessed 6 May 2021).
- [47] RSComponents. "Peltier Module, 11.7W, 2.2A, 8.8V, 18 x 18mm." <https://no.rs-online.com/web/p/peltier-modules/4901323/> (accessed 6 May 2021).
- [48] "Technical Data Sheet: FluorX™ PVDF 3D Printing Filament." 3DXTECH Advanced Materials. https://www.3dxtech.com/wp-content/uploads/2021/03/Unfilled_PVDF_v03.pdf (accessed 6 May 2021).
- [49] DuPont. "Technical Data Sheet DuPont™ Nomex® 410." https://www.dupont.com/content/dam/dupont/amer/us/en/safety/public/documents/en/DPT16_216_68_Nomex_410_Tech_Data_Sheet_me03_REFERENCE.pdf (accessed 6 May 2021).
- [50] Ansys Granta EduPack. (2021). Granta Design Limited, Cambridge, UK. [Online]. Available: <https://www.ansys.com/en-gb/products/materials/granta-edupack>
- [51] H. Pohl. "What is the difference between fluorescence, phosphorescence and luminescence?" Enzo Life Sciences. <https://www.enzolifesciences.com/science-center/technotes/2019/december/what-is-the-difference-between-fluorescence-phosphorescence-and-luminescence?%5d> (accessed 6 May 2021).
- [52] S. Sohrabi, N. kassir, and M. K. Moraveji, "Droplet microfluidics: fundamentals and its advanced applications," *RSC Advances*, vol. 10, pp. 27560-27574, 2020.
- [53] Y.-H. Shin, M. Teresa Gutierrez-Wing, and J.-W. Choi, "Review—Recent Progress in Portable Fluorescence Sensors," *Journal of The Electrochemical Society*, vol. 168, no. 1, p. 017502, 2021/01/08 2021, doi: 10.1149/1945-7111/abd494.
- [54] W. Ockenga. "Fluorescence in Microscopy." Leica Microsystems. <https://www.leica-microsystems.com/science-lab/fluorescence-in-microscopy/> (accessed 6 May 2021).
- [55] J.-L. Fu, Q. Fang, T. Zhang, X.-H. Jin, and Z.-L. Fang, "Laser-Induced Fluorescence Detection System for Microfluidic Chips Based on an Orthogonal Optical Arrangement," *Analytical Chemistry*, vol. 78, no. 11, pp. 3827-3834, 2006/06/01 2006, doi: 10.1021/ac060153q.
- [56] K. Ishikawa, "Plasma Diagnostics," 2016, pp. 117-141.
- [57] C. Liu, D. Cui, and X. Chen, "Development of an integrated direct-contacting optical-fiber microchip with light-emitting diode-induced fluorescence detection," *Journal of Chromatography A*, vol. 1170, no. 1, pp. 101-106, 2007/11/02/ 2007, doi: <https://doi.org/10.1016/j.chroma.2007.08.087>.
- [58] C. Liu, Y.-y. Mo, Z.-g. Chen, X. Li, O.-l. Li, and X. Zhou, "Dual fluorescence/contactless conductivity detection for microfluidic chip," *Analytica Chimica Acta*, vol. 621, no. 2, pp. 171-177, 2008/07/28/ 2008, doi: 10.1016/j.aca.2008.05.040.
- [59] T. Scientific. "Fluorescein (FITC)." ThermoFisher Scientific. <https://www.thermofisher.com/uk/en/home/life-science/cell-analysis/fluorophores/fluorescein.html> (accessed 6 May 2021).
- [60] RSComponents. "3.2 V Blue LED 5mm Through Hole, Broadcom HLMP-AB65-TW0DD." <https://uk.rs-online.com/web/p/leds/8134845/> (accessed 6 May 2021).
- [61] a. AG. "TSL257LF by ams AG." Arrow. <https://www.arrow.com/en/products/tsl257-lf/ams-ag> (accessed 6 May 2021).
- [62] NinjaPCR. "NinjaPCR." <https://ninjaPCR.tori.st/en/index.html> (accessed 6 May 2021).
- [63] K. Morioka, A. Hemmi, H. Zeng, K. Uchiyama, and H. Nakajima, "OLED -INDUCED FLUORESCENCE DETECTION SYSTEM FOR COMPACT DISK-TYPE MICROFLUIDIC DEVICE," 2013.
- [64] T. Scientific. "Fluorescence SpectraViewer." ThermoFisher Scientific. <https://www.thermofisher.com/uk/en/home/life-science/cell-analysis/labeling-chemistry/fluorescence-spectraviewer.html#/!> (accessed 6 May 2021).
- [65] D. A. Armbruster and T. Pry, "Limit of blank, limit of detection and limit of quantitation," (in eng), *Clin Biochem Rev*, vol. 29 Suppl 1, no. Suppl 1, pp. S49-S52, 2008. [Online]. Available: <https://pubmed.ncbi.nlm.nih.gov/18852857>.
- [66] J. Xu, Y. Xiong, S. Chen, and Y. Guan, "A lamp light-emitting diode-induced fluorescence detector for capillary electrophoresis," (in eng), *Talanta*, vol. 76, no. 2, pp. 369-72, Jul 15 2008, doi: 10.1016/j.talanta.2008.03.027.
- [67] C.-f. Chen, "Fluorescence detection of fluorescein and SYBR green-stained DNA by reflective cavity-coupled fluorometer – A quantitative study," *Measurement*, vol. 163, p. 107946, 2020/10/15/ 2020, doi: <https://doi.org/10.1016/j.measurement.2020.107946>.
- [68] J. Wu, X. Liu, L. Wang, L. Dong, and Q. Pu, "An economical fluorescence detector for lab-on-a-chip devices with a light emitting photodiode and a low-cost avalanche photodiode," (in eng), *Analyst*, vol. 137, no. 2, pp. 519-25, Jan 21 2012, doi: 10.1039/c1an15867h.

Appendices

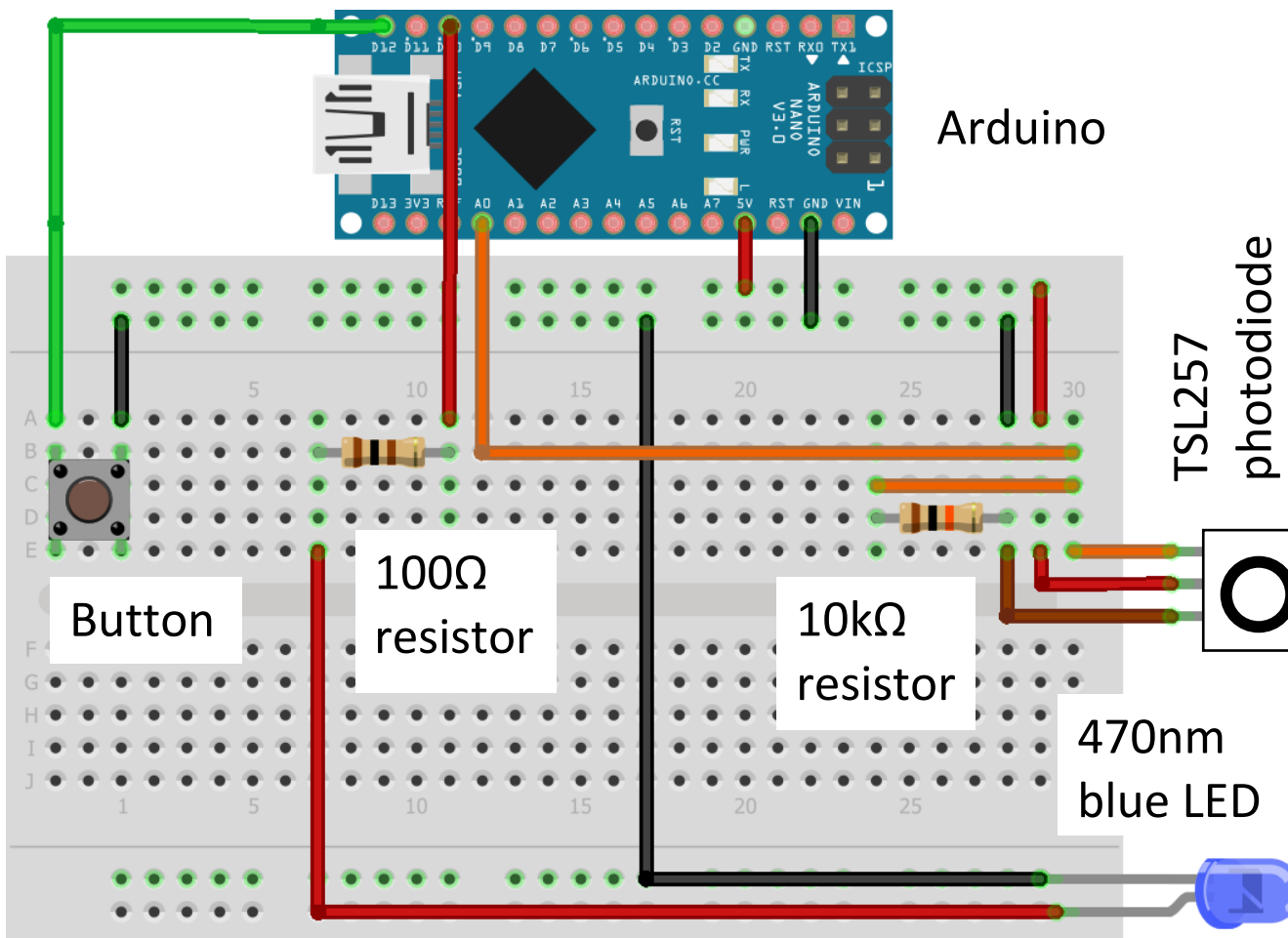
Appendix A: Gantt Chart

Month	Semester 1																		Semester 2																							
	Oct		Nov			Dec			Jan			Feb		Mar			Apr			May			Jun																			
Academic Week	1	2	3	4	5	6	7	8	9	10	11	12	13	14	15	16	17	18	19	20	21	22	23	24	25	26	27	28	29	30	31	32	33	34	35	36						
Research	●	●	●	●	●	●																																				
Initial Design				●	●	●	●	●	●																																	
Finalized Design								●																																		
System Integration																						●	●	●	●	●	●	●														
Materials Acquisition							●	●	●										●																							
Sponsorship					●	●	●	●	●																																	
Manufacturing																			●	●	●	●	●	●	●	●	●	●	●	●	●	●	●	●	●	●						
Testing and Iteration																																										
Analysis																			●	●																						
Report Writing																																										
Deliverables Submission																																								●		

Appendix B: Finance

Items	Price (£)
Peltier modules	97.02
Electronic parts (Sensors, wiring, etc.)	67.72
Microcontroller	9.49
Tubing	22.41
Materials (Heat sinks and Insulation)	44.55
Miscellaneous (other, delivery, tax)	94.67
TOTAL	335.86

Appendix C: Electronics circuit used for fluorescence detection testing



Appendix D: Sample Code (MATLAB) for Fluorescence Detector Testing

```

%% Acquire and analyze data live from a TSL257LF photodiode in MATLAB and save to a Microsoft Excel spreadsheet
clear variables; clc; close all;

%% Connect to Arduino
a = arduino('COM3','uno'); %Use the arduino command to connect to an Arduino device.
ledPin = 'D10';buttonPin = 'D12'; % Initialize pins
configurePin(a, buttonPin, 'pullup');
configurePin(a, ledPin, 'DigitalOutput');

%% Acquire and display live data
Figure; h = animatedline;
ax = gca; ax.YGrid = 'on';
startTime = datetime('now');
writeDigitalPin(a, ledPin, 1); %turn LED ON
while readDigitalPin(a, buttonPin)
    voltageReading = readVoltage(a,'A0'); % Read current voltage value
    t = datetime('now') - startTime; % Get current time
    addpoints(h,datenum(t),voltageReading) % Add points to animation
    ax.XLim = datenum([t-seconds(15) t]); % Update axes
    datetick('x','keeplimits')
    drawnow
    stop = readDigitalPin(a, buttonPin); % Check stop condition
end
writeDigitalPin(a, ledPin, 0); %turn LED off

%% Plot the recorded data
[timeLogs,VoltageLogs] = getpoints(h);
timeSecs = (timeLogs-timeLogs(1))*24*3600;
figure
plot(timeSecs,VoltageLogs)
xlabel('Elapsed time (seconds)'); ylabel('Voltage (V)');

%% Smooth out readings with moving average filter & plot!
smoothedVoltage = smooth(VoltageLogs,5); % Smoothed signal
figure;
plot(timeSecs,VoltageLogs,'k','LineWidth',1);hold on;
plot(timeSecs,smoothedVoltage,'r','LineWidth',2 );
xlabel('Elapsed time (seconds)');ylabel('Voltage (V)');

%% Save results to a file
t =
table(timeSecs',VoltageLogs',smoothedVoltage,'VariableNames',{'Time_sec','Voltage_V','SmoothedVoltage_V'});
dateString = datestr(datetime('now'));
filename = ['Voltage_Data_' strrep(dateString,':','-') '.xlsx'];

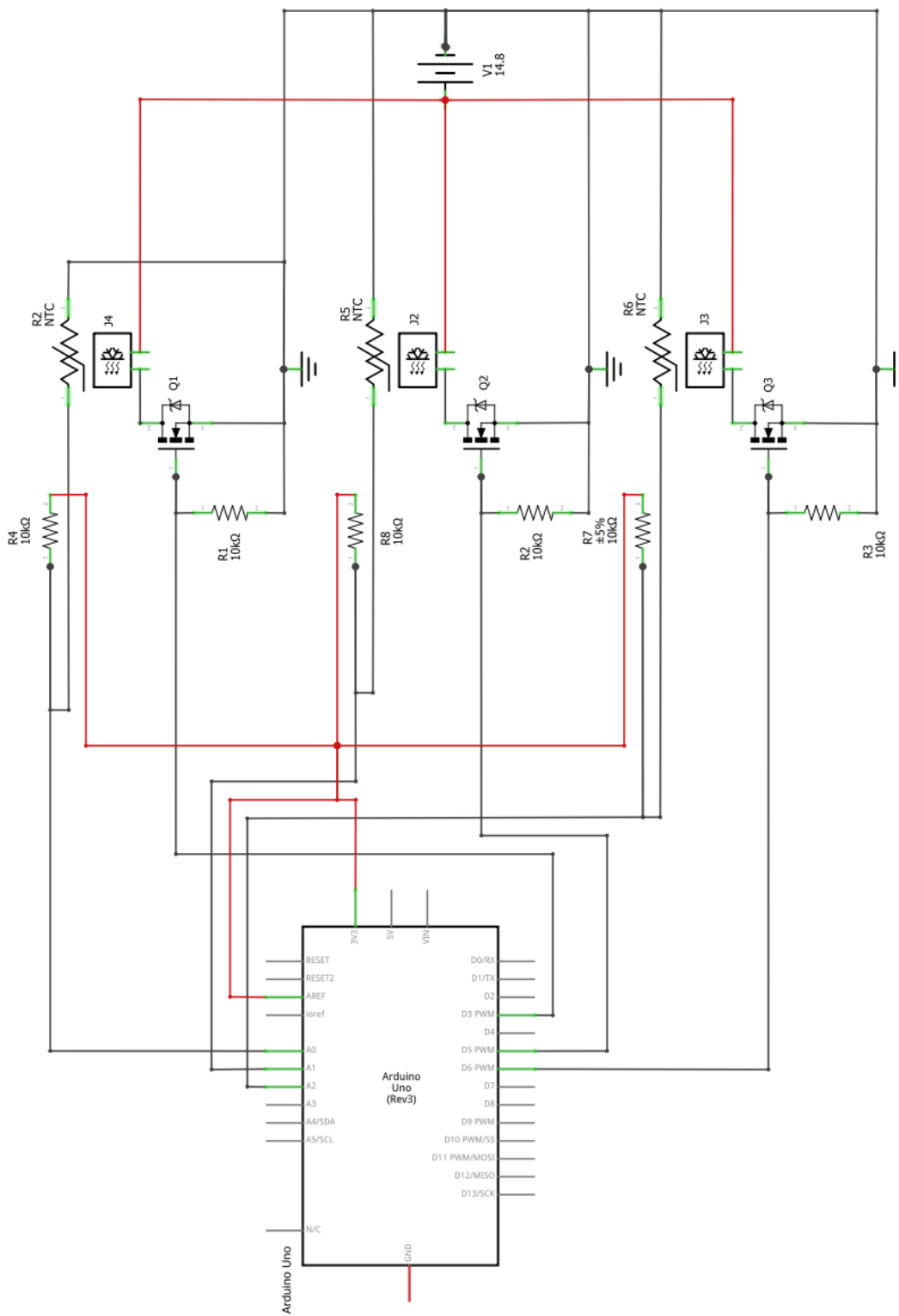
%% Write table to file
sheetname = strrep(dateString,':','-');writetable(t,filename,'Sheet',sheetname);

%% Print confirmation to command line
fprintf('Results: %g voltage measurements \nSaved to file: %s\n',length(timeSecs),filename)

```

Appendix E: Electronics Circuit Diagram for Thermocycler

The electronics circuit diagram for the thermocycler.



Appendix F: Sample Code (Arduino) for Thermocycler

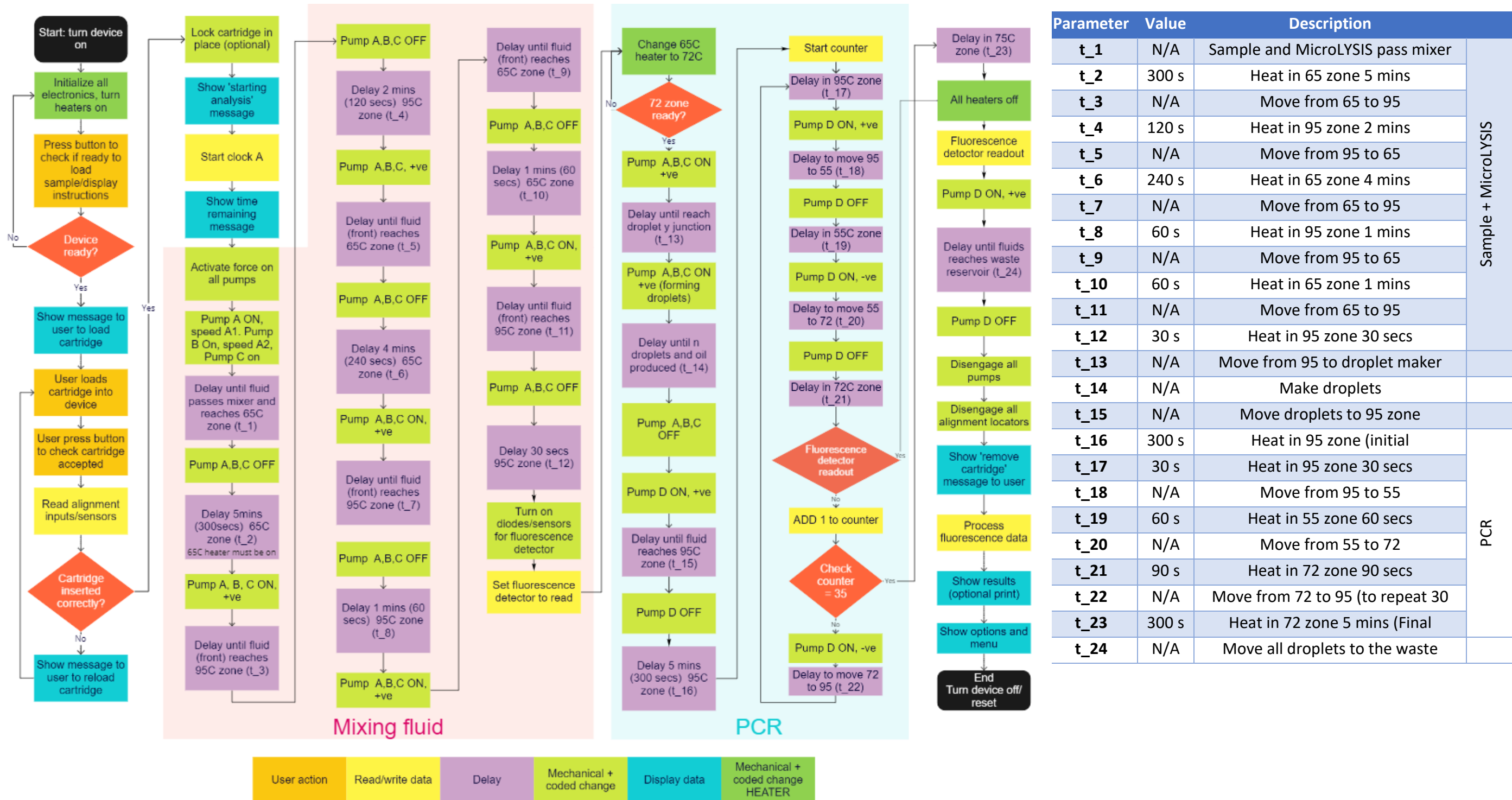
```

// The code was inspired by: https://learn.adafruit.com/thermistors/using-a-thermistor
// and https://ctms.engin.umich.edu/CTMS/index.php?example=Introduction§ion=ControlPID
//***** Define all variables and pins to use*****
#define thermistorPIN A0 //thermistor pin is A0
#define Res 10000 //the value of the resistor connected to the thermistor
#define n_temperature 25 //thermistor temp for nominal resistance (almost always 25 C)
#define n_thermistor 10000 //thermistor resistance at 25 degrees C (nominal thermistor)
#define Readings 5 //number of samples taken in order to control the temp readings
#define Bcoef 3625 //beta coefficient of the thermistor as shown in the datasheet
int peltier = 3;
int samples[Readings];
float temperature_read,average_temp;
float temp_error, temp_setpoint;
//set the PID parameters
float Kp = 22, Ki = 0.3, Kd = 0.5;
float sampling_time = 0, old_time = millis();
float error_old = 0, D_term = 0, I_term = 0;
void setup() {
  Serial.begin(9600);
  analogReference(EXTERNAL); //connection of AREF to Vcc=3.3V for less noisy sensor readings
  pinMode(peltier, OUTPUT); //pin for the Peltier module
  delay(1000);
}
void loop() {
  uint8_t i; //a type of unsigned integer of length 8 bits
  //take 5 sample readings in a row, with a slight delay in between
  for (i = 0; i < Readings; i++) {
    samples[i] = analogRead(thermistorPIN);
    delay(10);
  }
  for (i = 0; i < Readings; i++) {average_temp += samples[i];} //average the taken samples
  average_temp /= Readings
  //convert the average reading value to resistance
  average_temp = 1023 / average_temp - 1; //1023/ADC-1
  average_temp = Res / average_temp; //10kΩ/(1023/ADC-1)
  //convert the values into degrees C using a simplified Steinhart-Hart equation
  //((1/T = 1/T0 + 1/B*ln(R/R0))
  temperature_read = average_temp / n_thermistor; // (R/R0)
  temperature_read = log(temperature_read); // ln(R/R0)
  temperature_read = temperature_read/Bcoef; // 1/B * ln(R/R0)
  temperature_read += 1.0 / (n_temperature + 273.15); // + (1/T0)
  temperature_read = 1.0 / temperature_read; // invert
  temperature_read -= 273.15; // convert absolute temperature to degrees C
  //PID control
  sampling_time = millis()*0.001 - old_time; //sampling time
  float t_error = temp_setpoint - temperature_read; //temperature error
  float i_error = i_error + (t_error* sampling_time); //integration error
  float e_dot = t_error - error_old; //differentiation error
  if (sampling_time != 0) {D_term = e_dot / sampling_time;} //derivative term/kd
  else {D_term = 0;}
  I_term = i_error; //integral term/ki
  float Output = Kp*t_error + Ki*I_term+ Kd*D_term;
  if (Output > 255){Output = 255;} //setting the PWM maximum
  else if (Output<0) {Output = 0;} //setting the PWM minimum
  old_time = sampling_time; //save old timer value
  error_old = t_error; //save old temperature error value
  analogWrite(3,Output); //adjust the Peltier accordingly
  delay(500);
}

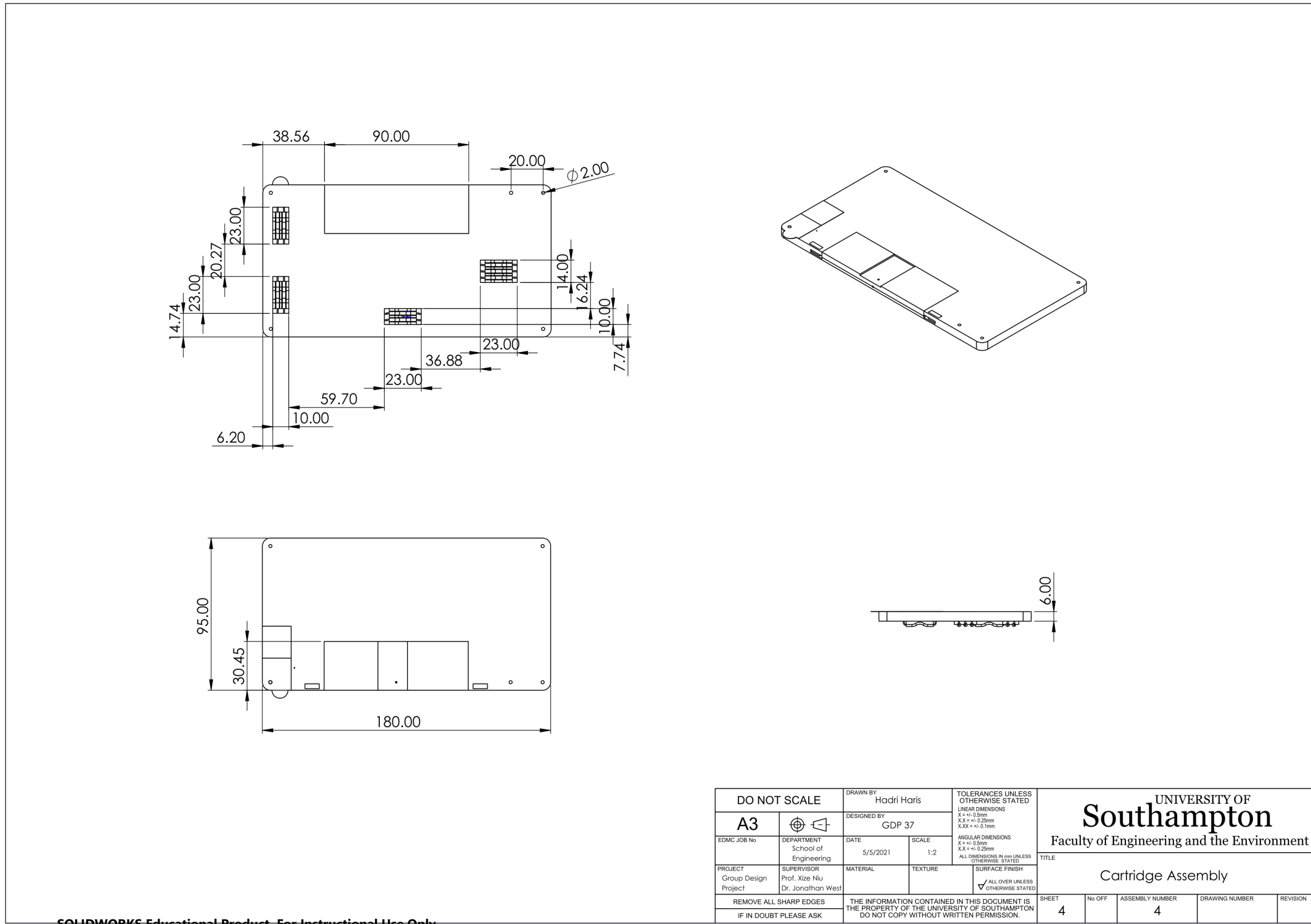
```

Appendix G: Software Flow Diagram

The software process starts when the device is on. It will initiate all electronics as well as the heaters then it will check whether the device and cartridge are ready or not. After that, the software will control the pump in order to control fluids to go to sequence sections in the device. It then deactivates all electronics and heaters when the test is finished. The software flow diagram and key parameter of the time are provided below.



Appendix H: Technical drawings – Cartridge

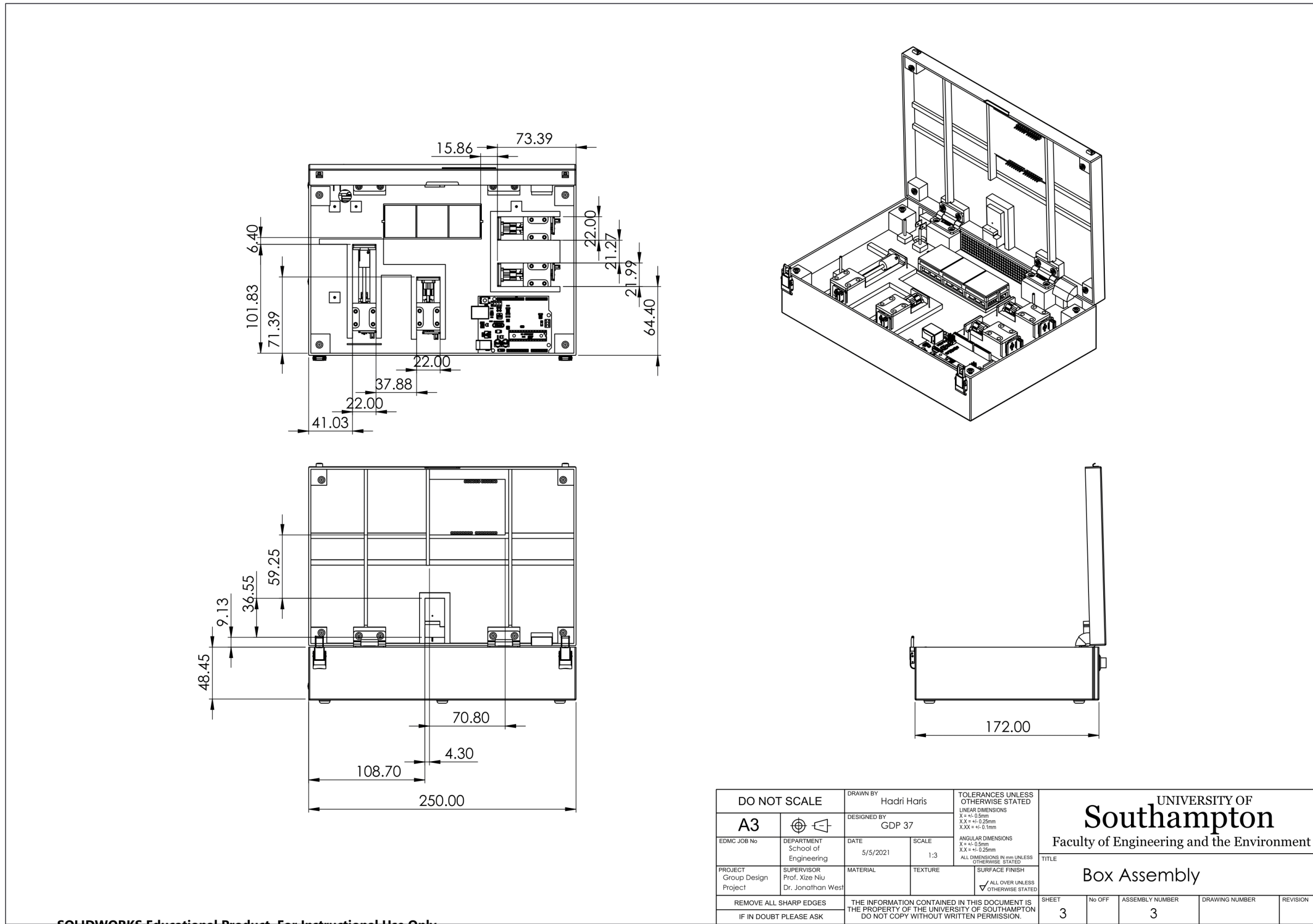


SOLIDWORKS Educational Product. For Instructional Use Only.

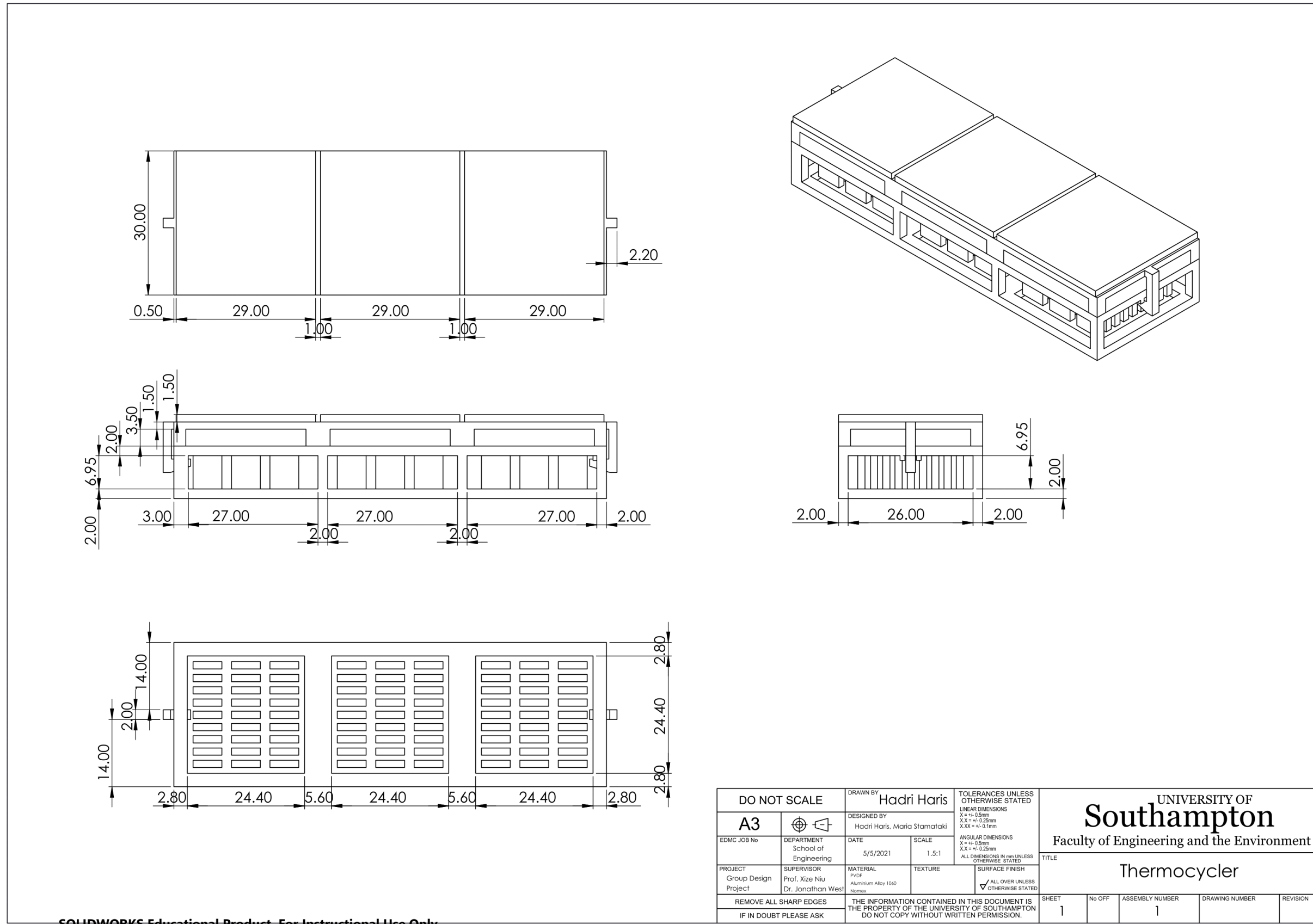
UNIVERSITY OF
Southampton
Faculty of Engineering and the Environment

Cartridge Assembly

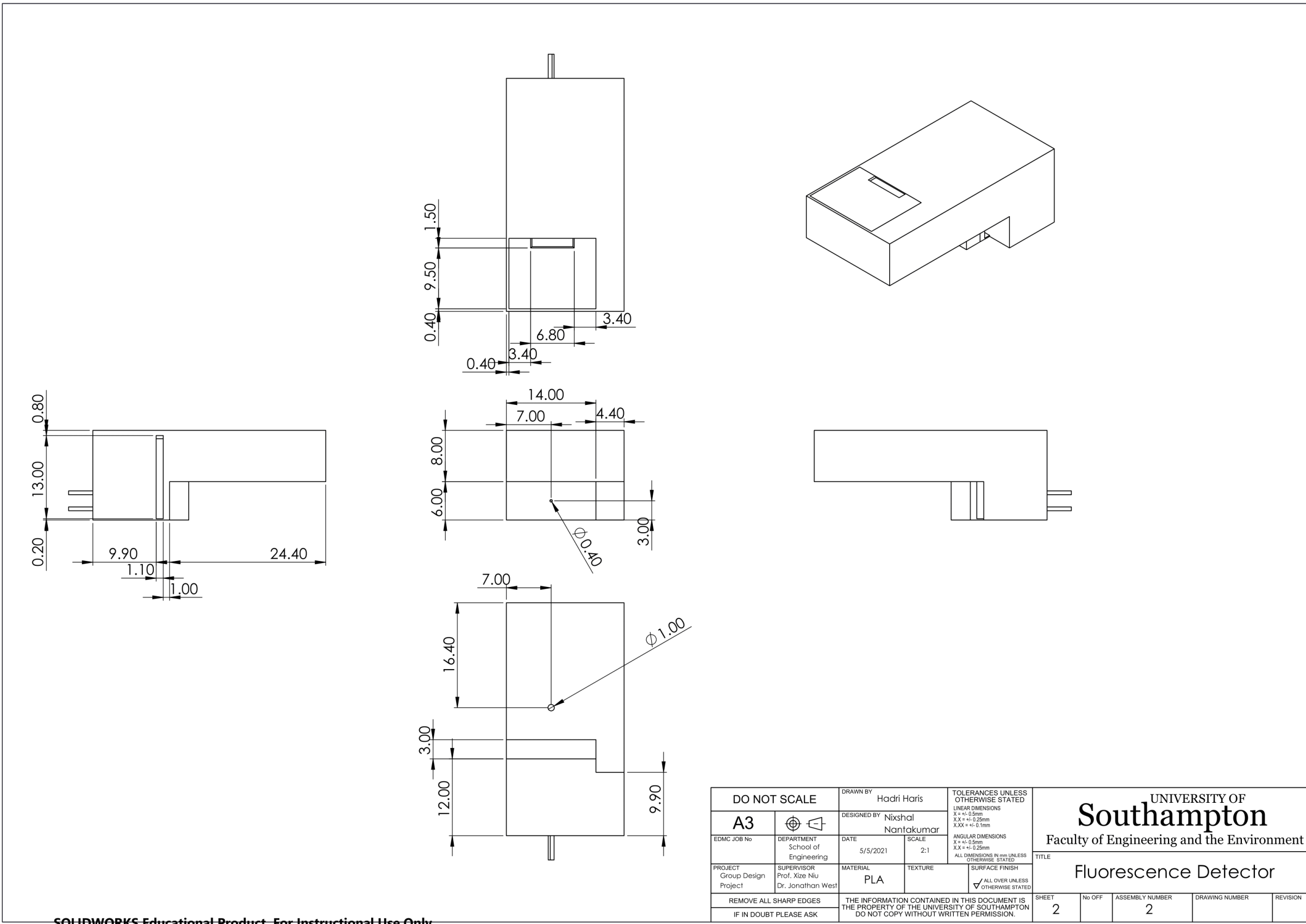
Appendix I: Technical drawings – Casing



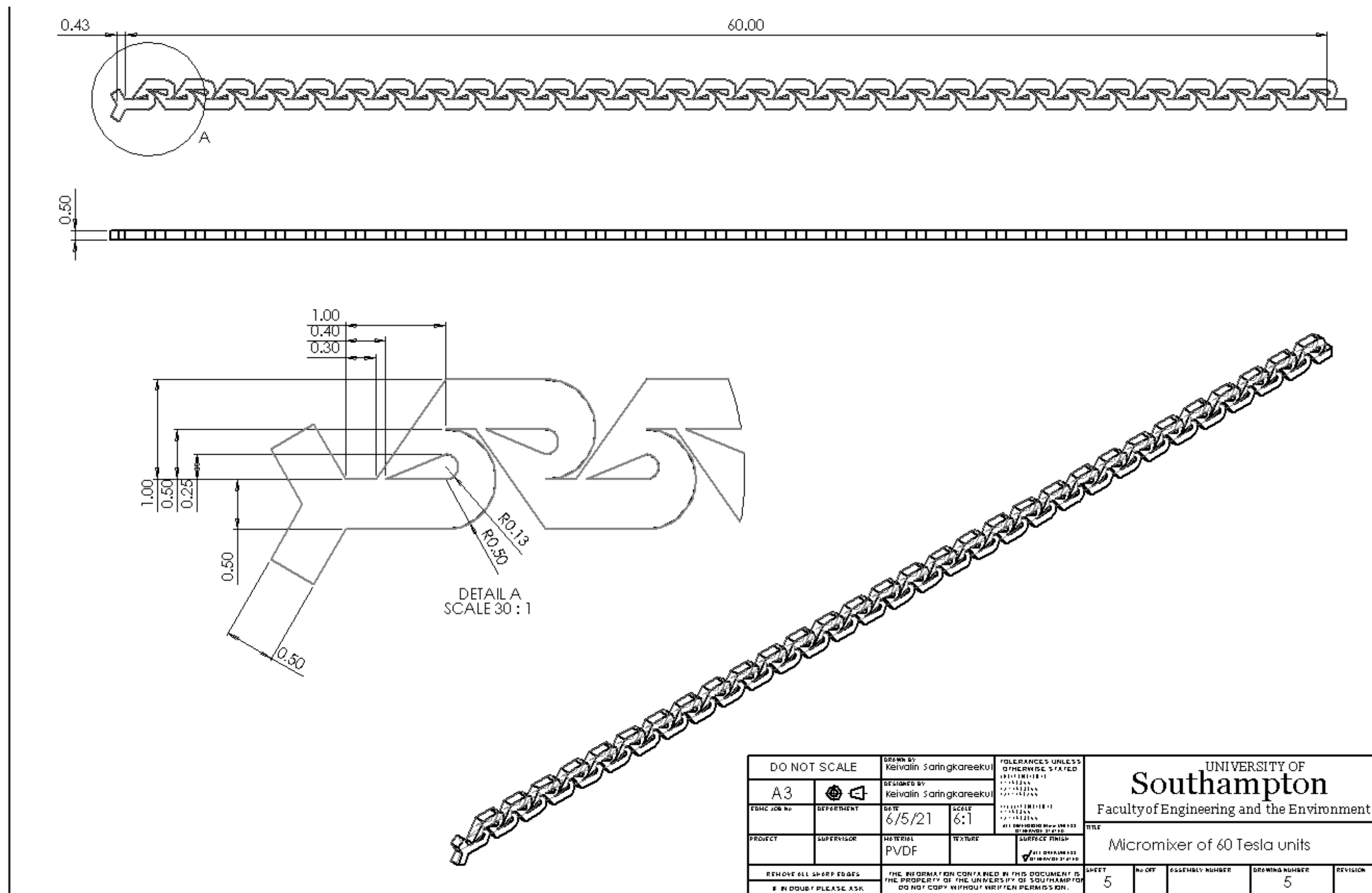
Appendix J: Technical drawings – Thermocycler



Appendix K: Technical drawings – Fluorescence Detector



Appendix L: Technical drawings – Mixing



Appendix M: Thermocycler – General Information – Components

Peltier modules information	
Sizes (from 10x10mm to 60x60mm)	https://uk.rs-online.com/web/c/hvac-fans-thermal-management/electronics-heating-cooling-components/peltier-modules/
Prices (£20-50)	https://uk.rs-online.com/web/c/hvac-fans-thermal-management/electronics-heating-cooling-components/peltier-modules/
Cartridge heaters information	
Sizes (from 8 mm diameter and length 38-660 mm to 25.0 mm diameter and length 200-1525 mm)	https://daltonelectric.com/product-data/cartridge-heater-sizes
Prices (£4-20)	https://uk.rs-online.com/web/c/?sra=oss&r=t&searchTerm=cartridge+heaters
Thermistors information	
Accuracy (0.1 – 1.5 °C)	https://docs.rs-online.com/96d5/0900766b815e5302.pdf
Thermal Response (0.05 to 2.5 sec)	
K-Type Thermocouple information	
Accuracy (0.5 to 5°C)	https://docs.rs-online.com/96d5/0900766b815e5302.pdf
Thermal Response (0.5 to 5°C)	
** Requires an Amplifier	https://datasheets.maximintegrated.com/en/ds/MAX31855.pdf